4. SEA ICE AND SNOW MEASUREMENTS

Gerit Birnbaum[1], Ruzica Dadic[2,3], Henna-Reetta Hannula[4], Nikolai Kolabutin[5], Felix Linhardt[6], Marcel Nicolaus[1], Roberta Pirazzini[4], Julia Regnery[1], Jan Rohde[1], Egor Shimanchuk[5], Gunnar Spreen[7], Linda Thielke[7], Melinda Webster[8]

(not onboard) Don Perovich[9]

[1]DE.AWI
[2]CH.WSL
[3]VUW.NZ
[4]FI.FMI
[5]RU.AARI
[6]DE.CAU
[7]DE.UNI-Bremen
[8]EDU.UAF
[9]EDU.DARTMOUTH

Grant-No. AWI_PS122_00

A comprehensive summary of the sea ice and snow measurements during all 5 cruise legs can be found in Nicolaus et al., 2022.

The sea ice and snow measurement program during PS122-5 MOSAiC leg 5 continues the work of the previous four legs. However, measurements are performed on a new floe after first floe disintegrated in the Fram Strait area. After suitable floe was found on 21 August 2020 the team ICE work was carried out for four weeks until 20 September 2020 and followed the weekly plan. Key objective for leg 5 was to capture the snow and ice transformation from melt to surface refreeze and further to ocean freeze-up. This is a key time of the year for ice mass balance development and energy fluxes and characterized by rapid change in surface albedo after melt pond refreeze and first snow fall. Thus, particular focus was on the optics and snow tasks. After leaving the leg 5 ice floe three more ice stations were conducted on our way back through the ice.

The sea ice and snow measurement program was carried out by a team of 13 scientists including the group leader Gunnar Spreen.

The following subchapters follow the task structure of the ice team. Chapter 4.1 incudes an overview of the changes in surface condition (Figure 4.1.3) and in Table 4.1.2 the development of surface, ice and weather conditions during leg 5.

References

Nicolaus, M, Perovich, DK, Spreen, G, Granskog, MA, Albedyll, LV, Angelopoulos, M, Anhaus, P, Arndt, S, Belter, HJ, Bessonov, V, Birnbaum, G, Brauchle, J, Calmer, R, Cardellach, E, Cheng, B, Clemens-Sewall, D, Dadic, R, Damm, E, de Boer, G, Demir, O, Dethloff, K, Divine, DV, Fong, AA, Fons, S, Frey, MM, Fuchs, N, Gabarró, C, Gerland, S, Goessling, HF, Gradinger, R, Haapala, J, Haas, C, Hamilton, J, Hannula, H-R, Hendricks, S, Herber, A, Heuzé, C, Hoppmann, M, Høyland, KV, Huntemann, M, Hutchings, JK, Hwang, B, Itkin, P, Jacobi, H-W, Jaggi, M, Jutila, A, Kaleschke, L, Katlein, C, Kolabutin, N, Krampe, D, Kristensen, SS, Krumpen, T, Kurtz, N, Lampert, A, Lange, BA, Lei, R, Light, B, Linhardt, F, Liston, GE, Loose, B, Macfarlane, AR, Mahmud, M, Matero, IO, Maus, S, Morgenstern, A, Naderpour, R, Nandan, V, Niubom, A, Oggier, M, Oppelt, N, Pätzold, F, Perron, C, Petrovsky, T, Pirazzini, R, Polashenski, C, Rabe, B, Raphael, IA, Regnery, J, Rex, M, Ricker, R, Riemann-Campe, K, Rinke, A, Rohde, J, Salganik, E, Scharien, RK, Schiller, M, Schneebeli, M, Semmling, M, Shimanchuk, E, Shupe, MD, Smith, MM, Smolyanitsky, V, Sokolov, V, Stanton, T, Stroeve, J, Thielke, L, Timofeeva, A, Tonboe, RT, Tavri, A, Tsamados, M, Wagner, DN, Watkins, D, Webster, M, Wendisch, M. 2022. Overview of the MOSAiC expedition: Snow and sea ice. *Elementa: Science of the Anthropocene* 10(1). DOI: https://doi.org/10.1525/elementa.2021.000046

4.1 Supporting observations

Melinda Webster[1], Marcel Nicolaus[2], Gunnar Spreen[3], Linda Thielke[3], Gerit Birnbaum[2], Jan Rohde[2], Julia Regnery[2], Ruzica Dadic[4,5], Henna-Reetta Hannula[6], Roberta Pirazzini[6], Egor Shimanchuk[7], Nikolai Kolabutin[7], Felix Linhardt[8], Steffen Graupner, Karl-Eugen Finkbeiner

(not on board:) Jennifer Hutchings[9]

[1]EDU.UAF
[2]DE.AWI
[3]DE.UNI-Bremen
[4]CH.WSL
[5]VUW.NZ
[6]FI.FMI
[7]RU.AARI
[8]DE.CAU
[9]EDU.OREGONSTATE

Objectives

In order to support the main tasks of the team ICE work of MOSAiC, several additional observations and activities were performed and continued from the earlier legs. Their common aim is to document the general snow and ice conditions and to support data interpretation afterwards. Also, most mapping activities of single measurements, installations, and operations on the ice were organized and documented in this task. In particular these activities include:

- Regular time laps photos of the surrounding of the vessel, the Panomax camera. Main objective during Leg 5 was to document ice, snow and weather conditions over freeze-up at the ice camp, but also along the transits through the ice.
- Standard sea ice observations from the bridge, ice observations. Main objective during Leg 5 was to document ice and snow conditions along the transects, but also during the drift with the ice camp.
- Visual observations of ice from airplane or ship are an integral part of sea ice monitoring for operational and research support [1]. These observations provide information about sea ice morphology that is not obtainable or ambiguous in remotely sensed data [1].
- Repeated mapping of the main floe using drone-based photography. Main objective during Leg 5 was to document the changing surface characteristics and to provide high-resolution images that were converted into visual floe maps and served as a base for the planning and mapping of the floe with all its installations and measurement sites.
- Mapping and documenting the ice floe and all measurements on the flow using the FloeNavi system. Main objective during Leg 5 was to test the latest updates (from Leg 4) of the new (since Leg 3) software package and to install and maintain the network on the floe. Furthermore, the FloeNavi system should be used for acquisition of device operations and recording of activities for the D-Ship and Sensor system (see Section DATA).

Background was that measurements and observations on sea ice have the particular challenge that the basis of all measurements, the ice floe(s), are in constant movement. Hence, commonly used position systems are not sufficient in order to describe the relative location of measurements and installations on the ice. Here we introduce a coordinate system (in meters x and y) that is fixed to the floe such that locations remain constant in relation to each other as long as the floe stays intact (no internal deformation or break up). In addition, also geographic (GPS) positions are recorded to allow reference to any other measurements, in particular airborne and satellites, that are not referenced to the floe. In order to overcome these challenges, the FloeNavi system was developed and used in different stages during the previous legs.

Work at sea

Panomax

The panorama camera (Panomax) was mounted above the crow's nest since departure in Tromsø, Norway, in September 2019. The camera worked without interruptions over the entire PS122 expedition. On Leg 5, the camera continued recordings of the 360° panorama photos without any changes to the earlier configuration. Each photo consists of 15680x2048 pixels. The recording of a single panorama took, depending on light conditions, up to 18 minutes. Therefore, the recording interval was kept constant at 20 minutes (72 photos per day).

Ice Observations

During MOSAiC, the ice observations are done hourly while RV Polarstern and the support vessels are moving through ice, in contrast to daily measurements while they are stationary. The aim of these observations is to describe the surrounding conditions over a 10-minute period within a radius of 1.5 nautical miles around the vessel. The list of conditions that are recorded is comprehensive, and includes for example ice concentration, floe size, fraction of ridged ice, ice thickness, amount of ice algae present and melt pond coverage. In addition, several parameters describing the weather conditions and macrofauna present are also included as part of the procedure. Due to the subjective nature of the observations, new observers were initially paired with people with more experience in order to ensure consistency throughout the MOSAiC drift.

Visual Floe Maps

Visual floe maps were created by stitching photographs from a drone (DJI Mavic Pro 2, camera Hasselblad) to a photo mosaic. Flight altitude varied for individual images between 100 and 300m (mostly 250m) and the grid covered approx. 2x1 km. Single images had a resolution of 5464x3640 pixels (12 bit). The complete grid consisted of some 130 photos. Postprocessing of the data involved developing all raw files in Adobe Lightroom, synchronizing picture parameters to adjust to the changing exposure conditions during the flight time of approx. 20 minutes, exporting the pictures as tiff files, stitching all files together then in PTGui with careful selection of key reference points and masking/demasking areas of critical interest. After several hours computing time, final visual floe maps were available with sizes of some 300 MP. Zooming in allows the identification of small installations and e.g. the thin fibre optics data cable at some points.

The final images were also geo-referenced to the local x/y coordinate system from the FloeNavi system (see below). This allowed to extract individual x/y coordinates from many sampling sites and installations to support the creation of the final table of x/y coordinates of all installations and sites (see Figure 4.1.4).

FloeNavi and Coordinate System

During Leg 5, we performed additional tests with the system to check the latest updates and configuration and also learned a few additional lessons on the operation of the system. This was in particular to have a close eye on the regular updates of the internal position streams (all icons need to be "green"). Finally, the system was used to provide the x/y grid through three permanent base stations

- Origin at Remote Sensing
- X-axis towards Ocean City (and y-axis towards *Polarstern*)
- Additional / backup base station at ROV Oasis

Based on this grid, most stations and installations on the ice were recorded with the system and contributed to the creation of the Leg 5 floe map. Obviously, the work with the system benefitted from the stable ice floe during the entire leg, where all base stations were installed.

Preliminary results

Ice Observations

Leg 5 covered a wide range of conditions going from above-freezing temperatures and advanced stages of ice melt to freeze-up and snow-covered ice (Figure 4.1.1). On average, sea ice concentrations were 79% ± 28%, with the lowest values mostly occurring during the transit into the pack ice and highest values at the Central Observatory. Sea ice thickness was 102 cm ± 72 cm on average, with the thickest ice being located in the vicinity of western Fram Strait and the North Pole. Melt pond coverage was highly variable with a 25% average and 21% standard deviation. The largest coverage occurred during the first half of Leg 5 when air temperatures ranged between -1°C and 1°C. Average temperatures were -3°C with a 4°C standard deviation for the entirety of the ice observation period of August 11 – October 1.

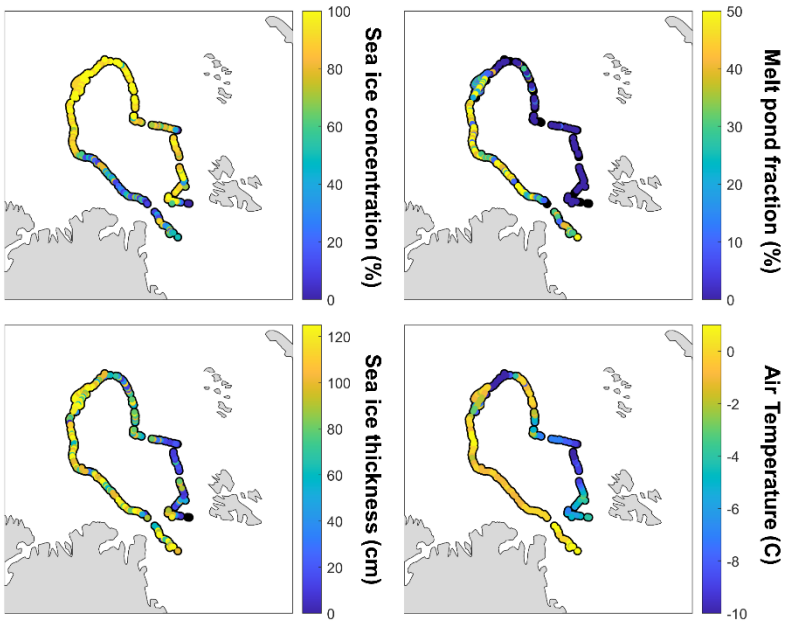

Fig. 4.1.1: Sea ice concentration, melt pond fraction (of ice area), sea ice thickness, and air temperature from ice observations during Leg 5 of the MOSAiC expedition.

Panomax

Using the panorama camera, we documented the sea ice, snow and weather conditions through the observation period. The camera recorded 72 photos per day. Figure 4.1.2 gives examples from different days of the ice station. The time series documents the changes in surface conditions from open ponds and early freeze-up to the snow covered and completely frozen surface. In addition, sea ice dynamics of and around the main ice camp becomes obvious with the shear and movements of parts of the ice pack beyond the ROV site (see also Map in Figure 4.1.4) and the opening of the port-side lead on 13/14 September (Figure 4.1.2E). A Time shift of the internal clock of the Panomax camera was noted during Leg 5. In the end it was 47 min ahead of time, e.g. at 12:00 UTC it was already 12:47 UTC for the recorded photos. This time shift was not corrected and the reasons for it are unknown, but it somehow accumulated / happened over the year of recordings.

Fig. 4.1.2: Exemplary photos from the panorama camera on the crow's nest (Panomax) from different dates: A) 23 August: Initial conditions, B) 31 August: after initial freeze-up, C) 04 September: after shear at the ROV lead, D) 10 September: frozen and snow covered surface, E) 14 September: after

opening of the lead on port side, F) 21 September: before departure from the floe. Note that images in this figure are reduced to the front view over the bow of RV Polarstern.

Visual Floe Maps

During Leg 5, 10 visual floe maps were created from the drone flights and 3 floe maps are available from the helicopter observations (Section 4.11). Table 4.1.1 summarizes all available floe maps. Altogether, 8 maps show the entire floe with some adjacent floes while the others focussed on parts of the floe, mostly the ROV area in order to support the under-ice optics of the new ice (see Section 4.7). Examples of these floe maps are shown in Figure 4.1.3.

Tab. 4.1.1: Visual floe maps recorded during Leg 5 by different platforms.

Date	Platform	Area
25 Aug	Drone	Entire floe
01 Sep	Drone	ROV area only
05 Sep	Drone	ROV area only
06 Sep	Drone	Entire floe
07 Sep	Helicopter	Entire floe
08 Sep	Drone	ROV area only
08 Sep	Drone	Entire floe
10 Sep	Drone	Entire floe
11 Sep	Helicopter	Entire floe
15 Sep	Helicopter	Entire floe
17 Sep	Drone	ROV area only
18 Sep	Drone	Entire floe
18 Sep	Drone	MET & RS area only

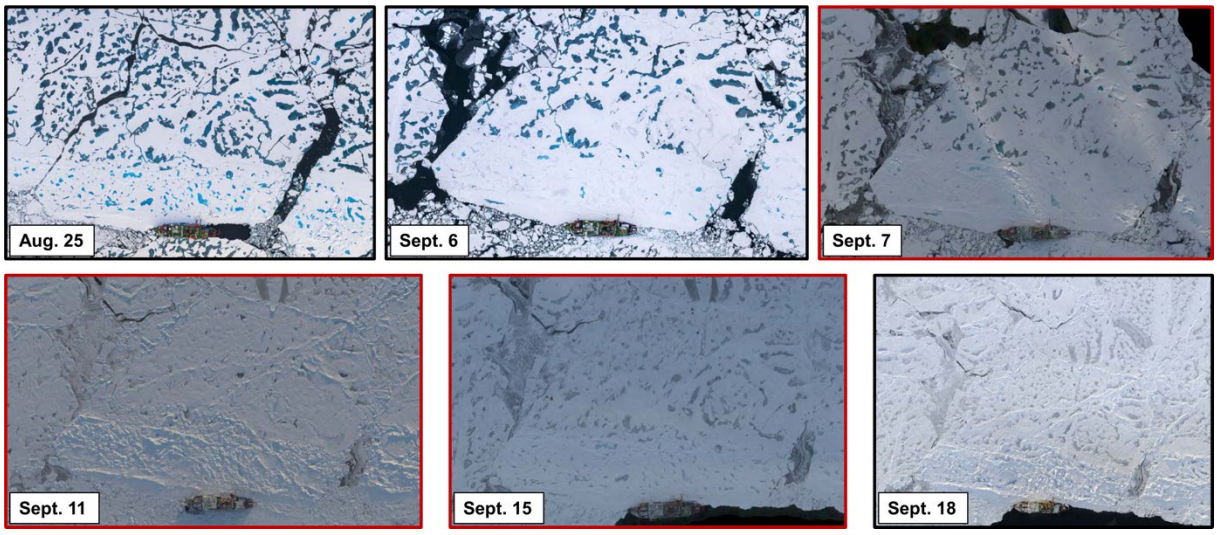

Fig. 4.1.3: Collection of floe maps showing the evolving surface conditions of the Leg 5 floe as observed by drone (black outline) and helicopter (red outline) imagery.

FloeNavi and Coordinate System

With the latest software update at the end of Leg 4, the FloeNavi system was available for a) receiving positions relative to the vessel, b) providing a static reference coordinate system on the floe (x/y coordinates), c) logging of device operations, and d) logging (logistical and scientific) installations on the ice. The main result of the FloeNavi system was the table of x/y positions of installations on the floe, which were (together with results from the visual floe maps) used to create the main floe map of Leg 5, as shown in Figure 4.1.4. For this map, also the x/y coordinates (in m) are available for all installations. This list (see Appendix A.5x/y-coordinates) also contains some additional points, which are not shown in the map. Close-ups of this map may be found in different sections of this report.

Fig. 4.1.4: Floe map of Leg 5. Dashed lines are x/y grid as defined by the FloeNavi System.

Time-series of Conditions

Below is a brief summary of weather and surface conditions that occurred at the Leg 5 floe (Table 4.1.2). Please see Figure 4.1.3 for visual comparison with the descriptions on select dates.

Tab. 4.1.2: Surface, ice and weather conditions during Leg 5

21 August	Arrival to the MOSAiC Leg 5 floe occurs. Approximately half of melt ponds are open while the other half have ~1-cm thick lid. The snow/surface scattering layer surface is soft.
23 August	Diurnal freeze-thaw occurs, with small melt ponds freezing and having less water volume, while the larger ponds lose their lids due to above-freezing temperatures during the day.
24 August	Ponds begin to refreeze and accumulate scant snowfall, but the ice surface remains soft. Melting snow and the surface scattering layer have an average depth of 10 cm ± 2 cm (see Transect Chapter 4.4).
25 August	Ponds are refrozen with scant dusting of snow.

27 August	Above-freezing temperatures cause melting conditions, and pond lids are barely intact.
28 August	Melting conditions ensue and pond lids are melting. The ice surface is soft.
31 August	Small ice pellets precipitate with slightly increasing intensity in the morning.
1 September	Freezing conditions prevail with dusting of snowfall and freezing mist; some ponds are still open.
2 September	Freezing conditions with light dusting of snow; snow ponds are still open, but the smallest and shallowest ponds are completely frozen and most extensively covered in snow. The snow/surface scattering layer reach their minimum depth of 2 cm ± 2 cm (Transect Chapter 4.4).
3 September	Freezing conditions with freezing mist; snow ponds are still open, but the smallest and shallowest ponds are completely frozen and most extensively covered in snow.
4 September	Freezing conditions with 1-2 cm dusting of snow, more ponds are becoming frozen with lids ranging in 1-4 cm thickness.
5 September	Freezing conditions with all ponds frozen with a 2-3 cm snow cover.
6 September	Windy with increasing snowfall and strengthening gusts. All ponds are frozen over with light drifting snow.
7 September	All ponds are frozen with small snow drifts; drifting snow is occurring and clouds are broken/scattered.
8 September	Ponds remain frozen with small snow drifts, with the new presence of saline frost flowers. Broken/scattered clouds are present.
9 September	Freezing conditions with light drifting snow.
10 September	Freezing conditions with light snow grains falling and freezing mist; some snow is drifting. Spectral and broadband albedo reach their peak values (see Optics Chapter 4.8) due to relatively thick snow cover (7 cm ± 4 cm).
11 September	1-2 cm feathery surface hoar crystals everywhere; clear sky, sun elevation ~5-6 degrees.
12 September	Freezing conditions with a snow cover averaging a 7-cm depth on Kinder Albedo Line (Transect Chapter 4.4).
13 September	Weather conditions transition from freezing to above-freezing; grauppel accumulated at first, following by sleet and then rain. Puddles of rain formed on the surface and melting surface conditions are pervasive.
14 September	Melting conditions with rain, mist, and strong gusts in the morning; rainwater accumulating on frozen ponds and producing wet slush on ponds that have a snow cover. Freezing mist and strong gusts occur in the evening, with ~4-5 mm of new ice accumulation on bamboo stick at end of the Kinder Albedo Line (Chapter 4.8).
15 September	Freezing conditions are present. Over bare ice, a frozen crust/glazing with light dusting of needle snow is present; nodules of ice are prominent with the grooves getting filled with needle snow crystals. Over larger ponds, slush with an upper snow layer is present. Precipitation is very light snowfall of needle crystals.
16 September	Ice nodules are still reaching the surface with snow filling in the grooves in between. The crust layer is up to 1 cm in thickness with <1 cm of snow on top, with deeper snow underneath in places. Light freezing mist intensified during the morning.

17 September	Snow drifts are now perpendicular to their previous orientation, resulting in some ponds suddenly becoming snow-covered. Slightly deeper snow (~2 cm) is on top of crust layer in places; noted specks of black soot in places, presumably due to the wind shift with the ship being windward.
19 September	Light freezing mist is occurring with broken clouds.

Data Management

All data are handled, documented, archived and published following the MOSAiC data policy (see APPENDIX). Data will be stored in the PANGAEA data repository: World Data Center PANGAEA Data Publisher for Earth & Environmental Science www.pangaea.de. DOIs will be communicated to PANGAEA for later access via the future MOSAiC Data Portal. The Panomax photos are all available online (http://www.mosaic-panorama.org).

References

[1] Hutchings, J., Delamere, J., Heil, P. (2018), The Ice Watch Manual (draft on board)

4.2 Snow

Ruzica Dadic[1,6], Henna Reeta-Hannula[2], Roberta Pirazzini[2], Julia Regnery[3], Marcel Nicolaus[3]

(not on board:) Stefanie Arndt[3], David Clemens-Sewall[4], Amy McFarlane[1], Polona Itkin[7], Matthias Jaggi[1], Glen Liston[8], Don Perovich[4], Chris Polashenski[4,5], Ian Raphael[4], Martin Schneebeli[1], David Wagner[1]

[1]CH.WSL
[2]FI.FMI
[3]DE.AWI
[4]EDU.DARTMOUTH
[5]USACE/CRREL
[6]VUW, NZ
[7]NO.UiT
[8]EDU.CU

Objectives

Snowpits

The overarching goal of the snow measurements is to characterize this spatial and temporal varying porous medium. This is conducted with the view of improving snow models and in support of all MOSAiC inquiries from ATMOS, BGC and ECO and Remote Sensing. We refer to the report of legs1-4 for details. Core parameters for snow are divided into physical; depth, temperature, snow water equivalent, density, specific surface area, snow microstructure, dielectric properties and chemical: see below subheading Chemical sampling.

TLS

Terrestrial Laser Scanning (TLS) is used to quantify changes in sea ice surface morphology to understand the evolution of the sea ice cover at cm precision. Changes in the surface occur due to thermodynamic processes (melt and refreeze) or dynamic processes (snow accumulation and redistribution). The major focus of Terrestrial Laser Scanning on Leg 5 was to map the surface roughness of the refrozen sea ice surface and observe and quantify the evolution of the surface with the first snowfall. The obtained data helps to connect the micro-scale surface characterization from snow pits and micro-CT measurements with the large-scale aerial observations (ALS) by helicopter. In coordination with the datasets of other Team

ICE tasks (e.g. Stakes, Snow, Transect, and ROV) an insights into the impact of snow processes on sea ice mass balance and thermodynamics is possible.

Work at sea

Conducted snow work can be structured in the following sub-tasks:

1. Snow pits and snow transects
2. Snow sampling
3. Terrestrial Laser Scanning (TLS) of the snow surface
4. Snow lab work

The set-up of the MCS raw data was continued with minimal changes from leg 4. SOPs and field tasks were updated for the handover to leg 5. Protocol sheets for the different snowpits were very useful and used throughout leg 5. All protocols and field note books were scanned and stored on MCS. Detailed documentation is all in the MCS/workspace/snowpits directory.

Snow pits and snow transects

We established 6 snow sampling sites on the new MOSAiC leg 5 floe. The sites were chosen to support major installations and measurements on the floe, namely: ROV, MET/OC, RS, Albedo Line, Coring and Atmospheric Flux measurements (only in the last 2 weeks of leg 5). Details of each individual pit can be found in Table 4.2.2. The location of the snow sites are shown in Figure 4.2.1 and 4.2.3. All events are documented in DSHIP as device "snowpit".

In total, we conducted 64 Snowpits during leg 5, 43 of which were A-pits (at least 1 A-pit a day throughout leg 5). Not all A-pits included chemical sampling, especially when only one person was conducting the measurements. The majority of the remaining 22 pits were mostly Transect pits, which were dug at beginning of co-located transects, mainly with RS (see transect action log and Chapter 4.12. Remote Sensing), but also as “mini-pits” at existing thermistor chains (see Chapter 4.3 Mass Balance Buoys and Stakes for details). Most snow sites were on FYI, except the ROV site, which was MYI and adjacent to a ridge. All drone-based albedo measurements and drone-based DEMs (FMI) were based on ROV and are relevant for our snowpit measurements (See Chapter 4.7).

For leg 5, we added a 25-80 m transect at snowpit location (except at the coring snow site, because of the space restrictions at the coring site) (Fig. 4.2.1). Along each transect, we conducted SMP measurements every 0.5 m or every 1 m, or NIR transects every 5 m. The ROV snow site had a “flat” as well as a “ridge” transect. The transects were generally conducted each time when an A-pit was made, although sometimes additional transects were conducted without an accompanying snowpit on that particular day or vice versa. One additional long S-transect (100 m) was conducted at ROV after a snowfall on 14.09.2020. We conducted 39 SMP (or NIR) transects at the regular snowpit locations.

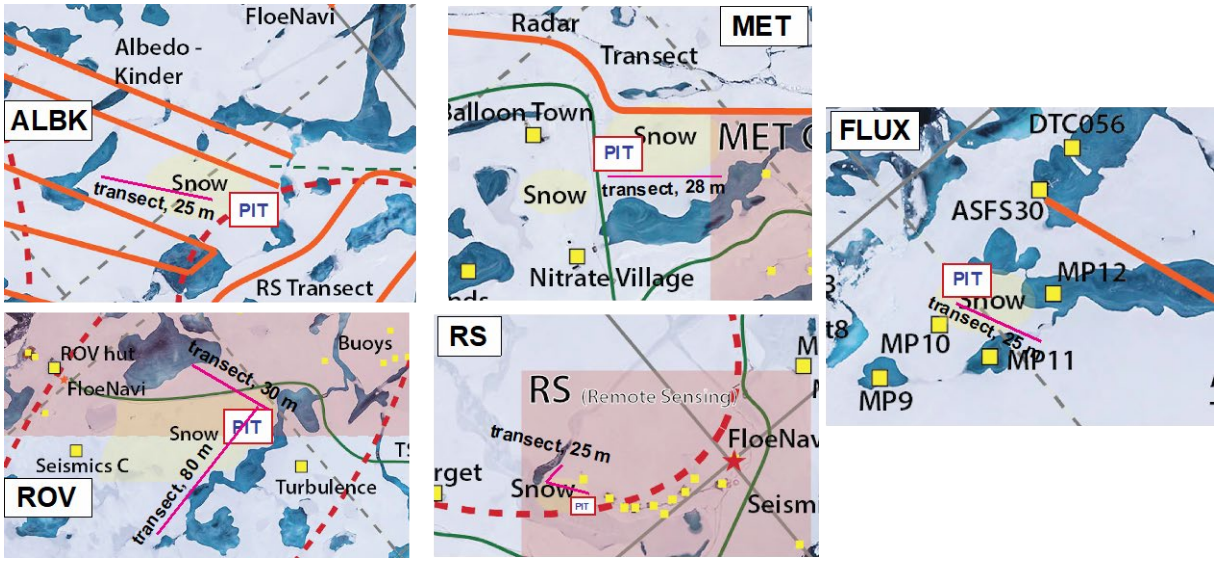

Fig. 4.2.1: Snowpit sites (except the coring site), with corresponding transects.

All but the coring site snowpits/transects were conducted at least twice weekly, except the coring site, which was only conducted once a week due to space restrictions at the coring site. Each snowpit measures about 1-1.5 m in width, plus the additional SMP measurements to the right and left of each pit. The spatial variability of the physical properties within a snowpit was often substantial, and we continued conducting A-pits with 5 additional SMP measurements every ~30 cm on each side, parallel to the profile, as suggested in the A-pit protocol sheets. We added dielectric permittivity profiles to all conducted snowpits during leg 5 to determine the liquid water content and to continue measurements that the RS team had started during leg 4.

Additional to the profile images with the NIR camera (when snow depth was sufficient to warrant a profile), we also took NIR images of the surface at all A-pits. Occasionally, when the variability was visually striking, we took multiple surface NIR images. We scanned 92 samples with the microCT, of which 80 were logged as “snowpits”, and also included platelet ice, frozen pond ice or leads (co-located with team ATMOS, BGC, BGC and RS). The sampling for the microCT is described in detail on the “Snow Lab” paragraph.

We regularly conducted co-located transects with the ARIEL microwave sensor (5x). The transects consisted of a Transect pit, and SMP or NIR (or both) measurements. On one occasion, we accompanied the radar KuKa transect with the SMP. Those transects were usually also accompanied by the Magna Probe and the GEM2. Occasionally, we also took additional NIR images of the surface to characterize the optical properties and spatial variability of individual ponds. We conducted one short NIR surface and SfM transect on day 1 on floe, at the albedo Kinder line.

Co-located with some of our measurements were direct and extensive surface and interface temperature measurements by and brightness temperature by the RS team using the IR camera. These measurements aim to address the variability of the longwave emissivity of different snow surface (See RS chapter for details). Measurements of surface temperature were carried out with the AARI probe thermometer simultaneously with and in the field of view of the FMI radiation station, the energy flux sledge in Hinterland, and the Infrared camera to derive the surface thermal emissivity and characterize its spatial variability. The measurements were co-located with snowpit observations, to relate the derived emissivity to the near-surface micro-structural properties. During the exit transit, the surface temperature measurements were carried out along the slow transect, simultaneously and co-located with the infrared camera and energy flux sledge measurements.

Table 4.2.1 lists the DSHIP numbers for the co-located snowpit, surface temperature, and infrared camera data according to location and date of the measurements. The surface

temperature measurements are in the mcs folders platforms/pack_ice/ice_ps/aari_thermometer/exdata/PS122/5_XXXXX.

The infrared camera measurements are in the mcs folders platforms/pack_ice/ice_ps/ir_variocam_01/exdata/PS122/5_XXXXX

Tab. 4.2.1: Table of DSHIP numbers for the co-located snowpit, surface temperature, and infrared camera measurements. The surface temperature measurements are located in the mcs folders platforms/pack_ice/ice_ps/aari_thermometer/exdata/PS122/5_XXXXX.The infrared camera measurements are located in the mcs folders platforms/pack_ice/ice_ps/ir_variocam_01/exdata/PS122/5_XXXXX

Location	Date	Snowpit	AARI thermometer	IR camera
Ice floe, ROV snow	14-Sept		PS122/5_62-261	
Ice floe, Met City	15-Sept		PS122/5_62-262	
	17-Sept		PS122/5_62-263	
	18-Sept	PS122/5_62-124	PS122/5_62-264	PS122/5_62-270
Ice floe, Hinterland	15-Sept	PS122/5_62-46	PS122/5_62-262	
	17-Sept		PS122/5_62-263	
	19-Sept	PS122/5_62-139	PS122/5_62-265	
Ice Station #1, slow transect	24-Sept	PS122/5_63-95 PS122/5_63-96	PS122/5_63-259	PS122/5_63-50
Ice Station #2, slow transect	26-Sept	PS122/5_63-97 PS122/5_63-98 PS122/5_63-99	PS122/5_63-260	PS122/5_63-71
Ice Station #3, slow transect	30-Sept	PS122/5_63-262 PS122/5_63-263	PS122/5_63-261	PS122/5_63-243

End of leg 5 sampling at the MOSAiC floe 2.0: At the end of leg 5, we conducted destructive measurements at existing sites during or after the removal of the fixed installations. We conducted snowpits, transects (SMP, NIR, SfM) and took samples for the microCT. These “end of leg” measurements were conducted at the

- RS site (A-pit, additional SMP profile)
- Albedo Kinder line (SMP, NIR surface, SfM) every 10 m along the albedo line
- Atmospheric Flux sled at Hinterland (SMP, NIR, SfM transect on pond under the instruments. MicroCT samples of snow and frozen pond ice + Transect-pit at the adjacent thermistor chain). Please refer to more details in the ATMOS Hinterland chapter. (Figure 4.2.2)
- A-pit at the Radiation Station over pond (stayed on the floe)
- A-pit at the Radiation Station over flat FYI (not quite finished because of Polar bear)
- ARIEL transect end measurements on original sampling points (NIR surface, SMP)
- FMI radiation station on pond (A-pit, NIR surface images for spatial variability, MicroCT sample of snow on top of pond)
- Transect-pits at some thermistor chains

Fig. 4.2.2: Flux sled pond at Hinterland during PS122/5_61-29 (left) and PS122/5_62-139 (right).

Tab. 4.2.2: Details of each unique snowpit ID from Leg 5.

	Snowpit ID	Comments
1	$SNOW5_ROV$	Snowpit at ROV snow site
2	$SNOW5_TRANS_ROV$	30 m transect at ROV, every 0.5 m
3	$SNOW5_TRANS_ROV_RIDGE$	80 m transect at ROV toward ridge, every 1 m
4	$SNOW5_TRANS_ROV_EXT$	Additional S-transect at ROV, one-off
5	$SNOW5_RS$	Snowpit at RS snow site (next to pond)
6	$SNOW5_TRANS_RS$	25 m transect at RS, every 0.5 m
7	$SNOW5_ALBK$	Snowpit at Albedo Kinder line
8	$SNOW5_TRANS_ALBK$	25 m transect at Albedo Kinder line, every 1 m (0.5 m once)
9	$SNOW5_MET$	Snowpit at Met city snow site
10	$SNOW5_TRANS_MET$	28 m transect at MET city snow site
11	$SNOW5_CORING$	Snowpit at Coring site
12	$SNOW5_FLUX$	Snowpit at Hinterland snow site, set up on 06.09.2020
13	$SNOW5_TRANS_FLUX$	25 m transect at Hinterland snow site
14	$POND_ICE_RS$	Pond ice from RS pond
15	$POND_ICE_BGC$	Pond ice from BGC pond
16	$FLUX_SLED_POND$	Pond ice + other measurements at FLUX sled pond in Hinterland
17	$LEAD_ICE_RS$	Lead ice from RS/seismic lead
18	$LEAD_ICE_OC$	Lead ice from OC city lead
19	$LEAD_ICE_LUNA$	Lead ice from LUNA lead
20	$FLUX_CHAMBER$	Co-located sampling (snow/lead) with gas flux chamber
21	$SNOW5_TRANS_ARIEL_PIT$	Transect pit at RS ARIEL transect
22	$SNOW5_TRANS_ARIEL$	Transect with RS ARIEL
23	$SNOW5_TRANS_KuKa_PIT$	Transect pit at RS KuKa radar transect
24	$SNOW5_TRANS_KuKa$	SMP transect at RS KuKa radar transect
25	$ALBK$	Short one-off transect at Albedo Kinder on day 1
26	$SNOW5_OC$	Snowpit at OC snow site. Was right next to MET and got annexed by Miss Piggy.
27	$PLATELET_ICE$	Platelet ice samples, collected on two occations for MicroCT scanning
28	$FRONT_OF_SHIP$	Snow samples for microCT infront of ship, collected on two occations

29	$SNOW5_TCHAIN_FLUX_RS056$	Transect pit at thermistor chain at Flux sled in Hinterland, DTC_RS056
30	$SNOW5_TCHAIN_RS053$	Transect pit at thermistor chain at ROV ridge, DTC_RS053, top one in ridge
31	$SNOW5_TCHAIN_RS054$	Transect pit at thermistor chain at ROV ridge, DTC_RS054, lower one on pond
32	$SNOW5_TCHAIN_2020T78$	Transect pit at thermistor chain at ROV flat, 2020T78
33	$SNOW5_RADST_POND$	Snowpit at Radiation station over pond at main buoy site at ROV
34	$SNOW5_RADST_FLAT$	Snowpit at Radiation station over flat ice at main buoy site at ROV
35	$SNOW5_FMI_RADST$	Snowpit at FMI radiation station over pond after removing the station
36	$SNOW5_ALBK_ENDTRANSECT$	Destructive sampling transect at albedo Kinder line
37	$SNOW5_ICESTATION1$	Snowpit at Ice Station 1
38	$SNOW5_ICESTATION1_TRANS$	Transect at Ice Station 1
39	$SNOW5_ICESTATION2$	Snowpit at Ice Station 2
40	$SNOW5_ICESTATION2_TRANS$	Transect at Ice Station 2
41	$SNOW5_ICESTATION3$	Snowpit at Ice Station3
42	$SNOW5_ICESTATION3_TRANS$	Transect at Ice Station3

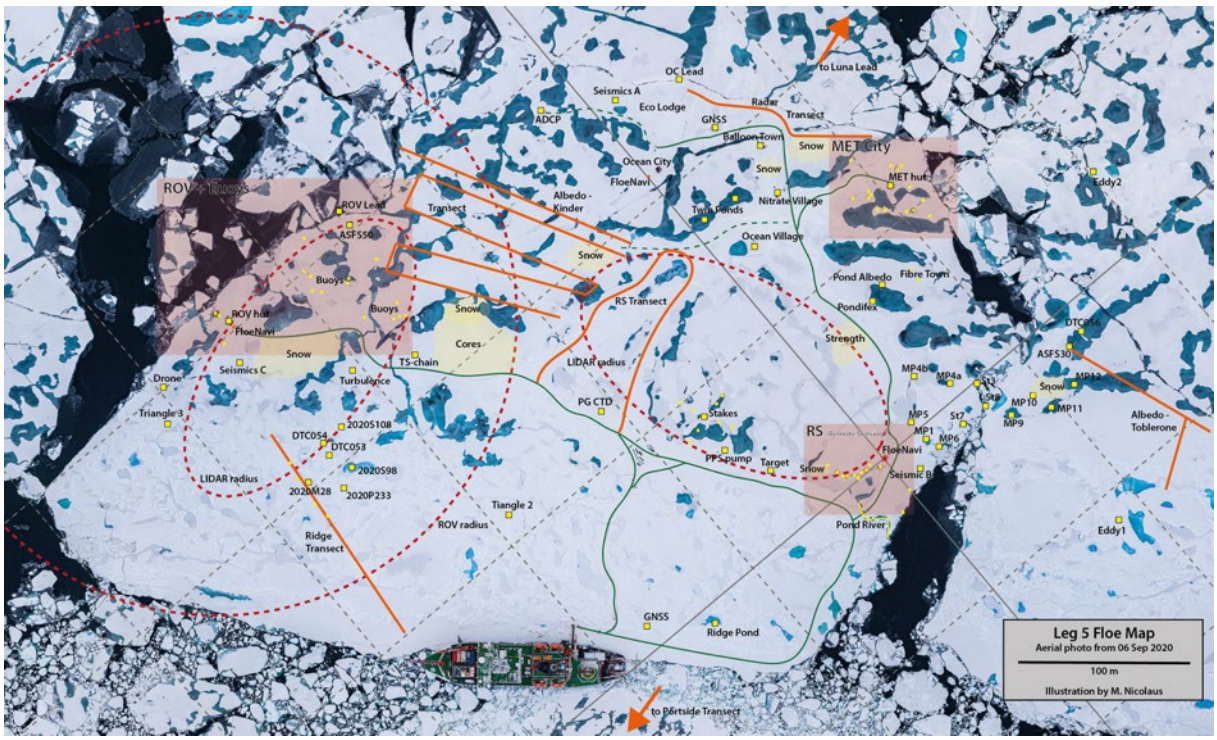

Fig. 4.2.3: Floe map (06.09.2020) with locations of the snow sites.

Ice Stations work 1-3 on the way back to the ice edge: On the way back to the ice edge, the snow team conducted measurements with the Remote Sensing and ATMOS teams to address the spatial variability of snow at different scales, and its influence on turbulent fluxes, surface temperatures and microwave emissivity. The "field experiment" at ICE Stations 1-3 consisted of a transect that was headed by the RS team using the IR camera and the ARIEL microwave sensor (aka "fast transect"), followed by the ATMOS team with the mobile flux sled (slow transect), and the snow team following with snow measurements (even slower transect). Along the fast transect, snow surface and bottom temperatures at all RS points was measured using a handheld thermometer address the influence of snow surface variability on longwave

emissivity, as well as using the opportunity to get more information on temperature gradients in snow. See Chapter 4.4 for more details on these transects.

The snow team followed the FLUX sled and made NIR images, Snow MicroPen measurements and SfM pictures (1 per site) covering the footprint (stations 2 and 3) of the sled and the RS instruments. We also conducted 1 A-pit at Ice Station 1, 2 A-pits at Ice Station 2, and 1 A-pit at Ice Station 3 (the second snowpit at Ice Station 3 was shortcut by a polar bear visit). Also, we did not take microCT samples at Ice Station 3, because we could not scan when the ship was not stationary.

At Ice Station 1, we measured at 15 different points along the transect, taking 1-3 sets of NIR surface images, 1 set of SfM images and 5 SMP measurements where snow was present. After Ice Station 1 and discussion with our colleagues from the ATMOS team, we decided to have fewer points, but with more measurements at each points, so we can better address the m-scale spatial variability in the field of view of the instruments. We decided on a 5x3 m grid, with 9 NIR surface images, 18 SMP measurements and 1 set of SfM images per transect point (Figure 4.2.4). Following this setup, we measured 1 A-pit and 4 points along the slow transect, and 1 A-pit and 1 point at the stationary flux sled for Ice Stations 2 and 3.

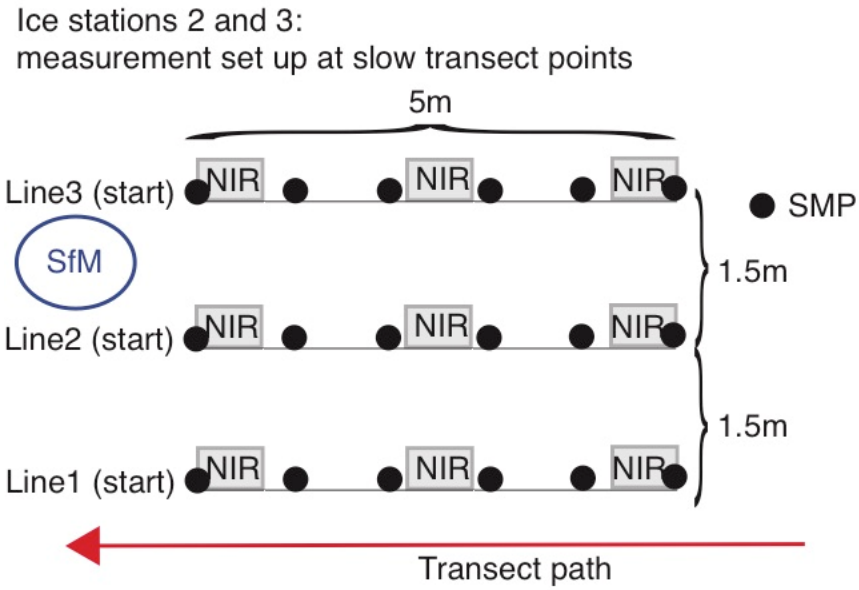

Fig. 4.2.4: Measurements setup for the slow snow transect on Ice Stations 2 and 3.

Chemical Snow Sampling: Each week, at an A-Pit location, we conducted several sampling tasks. Due to time, personnel and weather/ice constraints we could not fulfil all requests as listed. Furthermore, some sampling was requested only for e.g. 2-weekly, monthly ore only after snowfall. The SSL/snow depth during leg 5 was shallow so we ended up collecting mostly surface samples. However, we took snow samples for the following purposes (in parentheses: sample coordinator)

- Black Carbon (AWI/Daniela Krampe)
- Ice Nucleating Particles (INPs) (Jessie Creamean)
- Iodide (Uni Grenoble/Hans-Werner Jacobi)
- Major Ions and Water Isotopes (AWI Glaciology/Maria Hörhold)
- Major Ions, Bromide, INPs, 34S (SO4), Salinity, S-Isotopes (BAS/Markus Frey)
- Major Organic Compounds (PSI/Julia Schmale)
- Microplastics (AWI/SLF)
- Salinity (ICE)

- micro-CT samples
- The melted snow for salinity measurements was also used for d18O samples (NPI)

Unlabelled sample vials were pre-labelled by us before going into the field and for each sample the corresponding snow pit and location within the profile has been documented.

After sampling, the bags and vials were stored either in the -20°C freezer in the F-Deck or in the -20° AWI sea ice physics freezer at the bow - either in prepared boxes by the institutes who conducted the sampling requests or in one of the WSL skufa boxes.

The number of samples collected on leg 5 can be found in Table 4.2.3.

Tab. 4.2.3: Total number of chemical samples collected over leg 5.

Sample ID	***Leg5***
BAB	7
BAS	15
BC surface	7
BC profile	18
IDA	12
IDB	9
INP	18
ION	9
ORG	6
PLA	1
dO18	119 (including MicroCT samples)
salinity	119 (including MicroCT samples)
SUM	340

Terrestrial LiDAR Surveys (TLS)

On Leg 5 we established two scan fields in the central observatory (CO) area. One included the Remote Sensing site and the Stakes site, and the second one parts of the ROV measurement area, the buoy site, one snow measurement area close to the ROV site and the edges of the ridge site (see Figure 4.2.5.). A fixed grid of bamboo sticks was installed at both sites and the reflectors were put up for each measurement. Those fixed reference points allowed us to register the individual scans together to create daily scan sets, and to be able to compare the scan sets from multiple days.

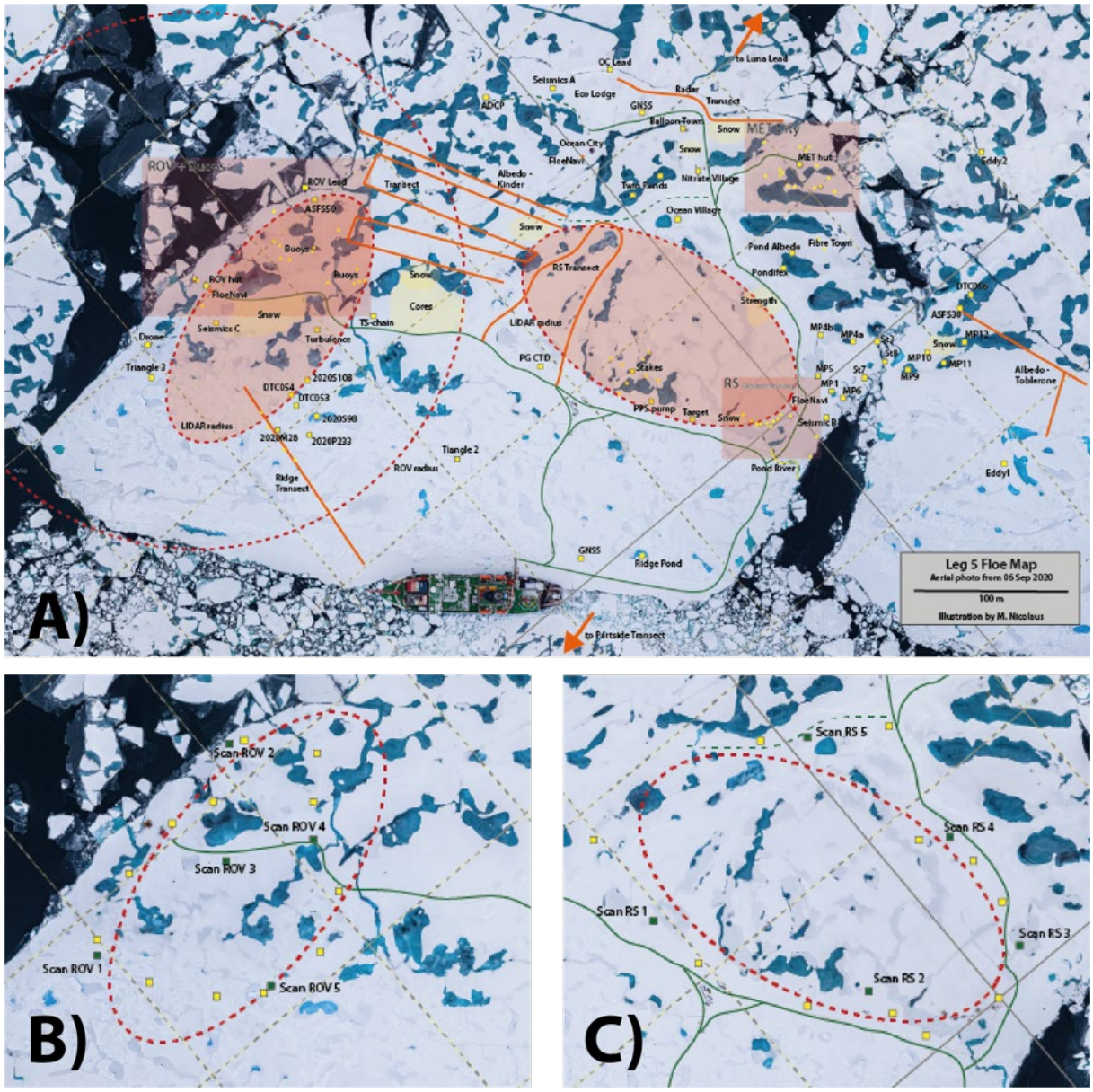

Fig. 4.2.5.: A) Leg 5 floe map with both scan areas marked as red ovals. B) close-up of the ROV area, C) close-up of the Remote Sensing area. Scan positions are marked in green, reflector poles in yellow.

Shortly after our arrival and setup of the Leg 5 floe, there was a warm air event, which caused the already frozen surface to melt and most ponds to open again. Due to those ice and weather conditions the first scanning attempt resulted in poor signals with the VZ-1000 Lidar and was aborted. The first full scans with 4 different scan positions of the Remote Sensing and the ROV field were accomplished at the beginning of September after a cooler refreezing period. In the following weeks we tried to obtain a weekly scanning routine of both scan fields with regard to some weather events (e.g. snowfall, warm air). However, permanently changing weather conditions like moist air, fog, rain, snowfall and a warm air with melt interfered frequently with the measurements and made the scanning a challenge. Eventually we collected 4 data sets of 4 to 5 scan positions for each site. Table 4.2.4 lists the TLS scans from Leg 5.

Tab. 4.2.4.: Overview of Leg 5 Lidar scans

Date (dd.mm.yyyy)	Site	Comment	Device Operation
03.09.2020	Remote Sensing	4 scan positions after refreezing; no new snow; ponds are mostly open	PS122/5_60-80
05.09.2020	ROV	4 scan positions with a little bit of new snow on the refrozen surface	PS122/5_60-173
06.09.2020	Remote Sensing	5 scan positions; first snow; before strong winds event	PS122/5_60-172
08.09.2020	ROV	5 scan positions after strong wind event and some new snow	PS122/5_61-26
09.09.2020	Remote Sensing	5 scan positions after snowfall event	PS122/5_61-68
11.09.2020	ROV	5 scan positions after intensive snowfall	PS122/5_61-163
15.09.2020	ROV	Final scan with 5 positions; after warm air event	PS122/5_62-48
18.09.2020	Remote Sensing	Final scan with 5 scan positions; after warm air event and little snowfall	PS122/5_62-127

Snow Lab

We scanned 92 samples with the microCT, of which 80 were logged as “snowpits”, and also included platelet ice, frozen pond ice or lead ice (co-located with team ATMOS, BGC, BGC and RS). 12 samples were logged as “ice cores”, and include the lowest part of the ice cores from two coring events, as well as a special core of a top and bottom of a pond, which was requested by BGC (see BGC chapter). For details on the coring procedure refer to the SOP ‘snow coring’ and the SOP / cheat sheet for the micro-CT 90 on the MCS.

As suggested by the leg 4 team, we mostly used to 88 mm diameter Micro-CT sample holder. Occasionally, when we had new snow or surface hoar deposition, or when we had difficulties extracting larger samples due to stubborn surface crusts, we used the smaller diameter samples. Ice samples (frozen pond surface or lead samples) were often taken with the 68 mm sample holder, because 88 mm samples did not fir into the centrifuge. We often had difficulties using the drill, as we found that the snow often rotated in the drill, thereby compromising the sample. Therefore many samples were taken without using the drill. The sampling of “crusty” snow was performed by pre-cutting the surface crust with the tiny saws from the orange sample drilling box.

The only problems with reconstructions we had was when the computer cable in the Trockelabor 3 was unplugged by accident, and we had to restart the Windows machine. Other than that, there were no problems with partial reconstruction or missing slices. Special attention was taken to scan the interface between snow and ice, this included re-frozen ‘snow-ice’ interfaces from melt or flooding events and clear snow to ice transitions. The majority of these interface scans were taken using the 88mm diameter holder.

No samples were cast in the field or in the laboratory, as there was no time left for this time-consuming task, and due to the excellent performance of the micro-CT.

Data is stored on MCS semi-automatically in the correct folder using a script developed on Leg 2 (see 4.2.4 Data management).

Salinity and dO18: We measured snow salinity in Trockenlabor 3, with the salinity sensor provided by U. Fairbanks, the same as used for the physical measurements of the ice cores.

The 20 ml sample vials for d18O from NPI were suitable for the melted volumes of snow from salinity measurements.

In the second part of leg 5, we additionally cut and melted 19 microCT samples, after they were scanned. The samples were cut in approximately 2 cm pieces (depending on the condition of the snow/ice) with the aim to get **higher resolution dO18** measurements at the snow/ice interface in particular. We also measured salinity of those samples. The samples are stored in same vials and with the same labelling as the snow dO18 samples. Details can be found in platforms/pack_ice/snowpit/exdata/dO18IceSnowMicroCT.xls and in Table 4.2.5.

Tab. 4.2.5: Overview of microCT samples that were cut for salinity and dO18 after scanning.

Event ID	Sample holder MicroCT	#samples
PS122/5_59-250	K	1
PS122/5_61-210	S	3
PS122/5_61-210	M	3
PS122/5_62-10	X	4
PS122/5_62-44	Z	3
PS122/5_62-69	AC	3
PS122/5_62-89	W	3
PS122/5_62-99	Y	4
PS122/5_62-119	AE	3
PS122/5_62-124	AA	4
PS122/5_62-125	AB	3
PS122/5_62-139	AD (snow)	1
PS122/5_62-139	X	4
PS122/5_62-139	AD	4
PS122/5_62-140	AF	3
PS122/5_63-96	Z	3
PS122/5_61-97	Y	3
PS122/5_63-99	AD	2

Frozen samples: From the many frozen ponds and lead ice samples that we scanned, we had planned to make some thin sections during leg 5 to study the grain size evolution of the freeze-up. Unfortunately, there was not enough time to make the thin sections, and a selection of 8 samples was sent back to SLF together with the cast samples from previous legs (in refrigerated box SLF35). See Table 4.2.6. for sample event-IDs.

Tab. 4.2.6: Overview of ice samples (frozen pond or lead) that are shipped as refrigerated storage in SLF35.

Event ID	Sample holder microCT	description
PS122/5_60-49	AA	BGC pond, 2 samples (Flux chamber co-located)
PS122/5_60-171	AD	Flux sled pond
PS122/5_61-29	AE	Flux sled pond
PS122/5_61-107	AA	Lead ice from RS lead (CTD)
PS122/5_61-155	V	Lead ice from OC lead (Flux chamber co-located)

PS122/5_61-157	V	Lead ice from RS lead (CTD)
PS122/5_61-209	AE	Flux sled pond
PS122/5_61-249	M	Lead ice from Luna lead (ECO co-located)

Preliminary results

Snowpits

We measured all core parameters for snow regularly, at least bi-weekly per snow site. Over the entire ice floe, we have at least daily A-pits, including snow microstructure measured by the microCT. All key devices for measurements of snow on the ground such as SMP, NIR worked without major issues, although SMP31 got a bit slow starting the measurement towards the end. The air temperature was seldom below -10C, and caused no issues with any instruments. The usually reliable measurement of snow density with the density cutter was difficult or impossible when the surface crust was hard or very fragile depth hoar layers.

In the first 10 days, the prevalent surface was the SSL, with one snowfall on day two after our arrival. This gave us the opportunity to study new snow deposition on the existing SSL on several occasions (Figure 4.2.6). We were also able to observe relatively fast changes in microstructural snow properties. Figure 4.2.7, for example, shows the difference between the scan in the morning after a snowfall, and six hours later, when a prominent crust had developed at the surface, likely affecting the energy balance of the sea ice system.

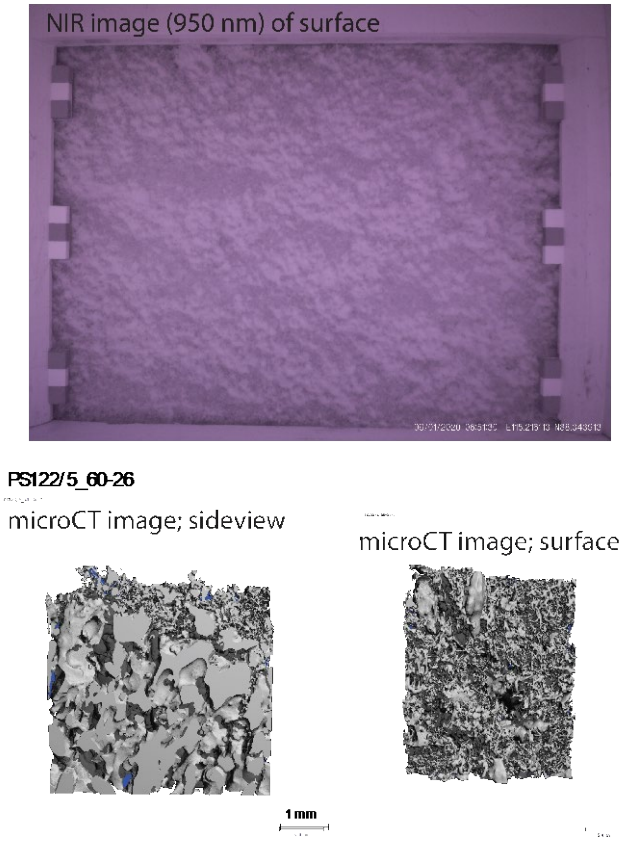

Fig. 4.2.6: Deposition of snow on top of the SSL. The image on the top shows the reflected radiation in the near infrared (NIR) at 950 nm. The two microCT images below are from the same sample, which was taken below the NIR image. The images show the surface view (on the right), and a 5 cm profile view (on the left).

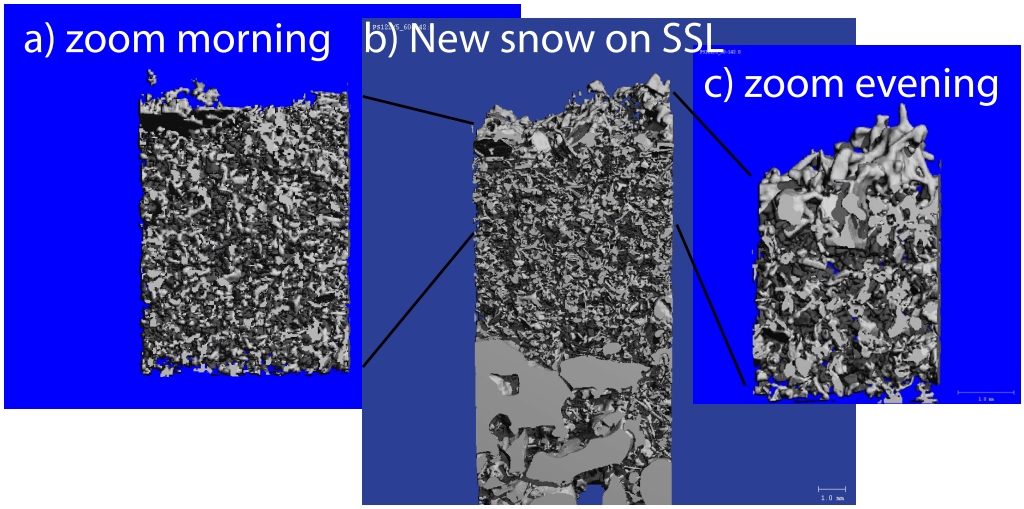

Fig. 4.2.7: Image b) (PS122/5_60-128), shows the new snow with the SSL below images a) (PS122/5_60-128), and c) (PS122/5_60-128) zoom in on the top cm. We can see the delicate structure of the new snow and how it fills the spaces within the topmost mm of the SSL, but we can also observe the changes in the microstructure of the top few mm at the snow surface.

We were further able to observe several snowfalls, surface deposition events (Figures 4.2.8., 4.2.9.) as well as rain-on-snow events, which were followed by freezing and more melting. The resulting snow structure, as well as the spatial variability was really exciting, and demonstrated the complexity of the snow cover build up over the Arctic sea ice.

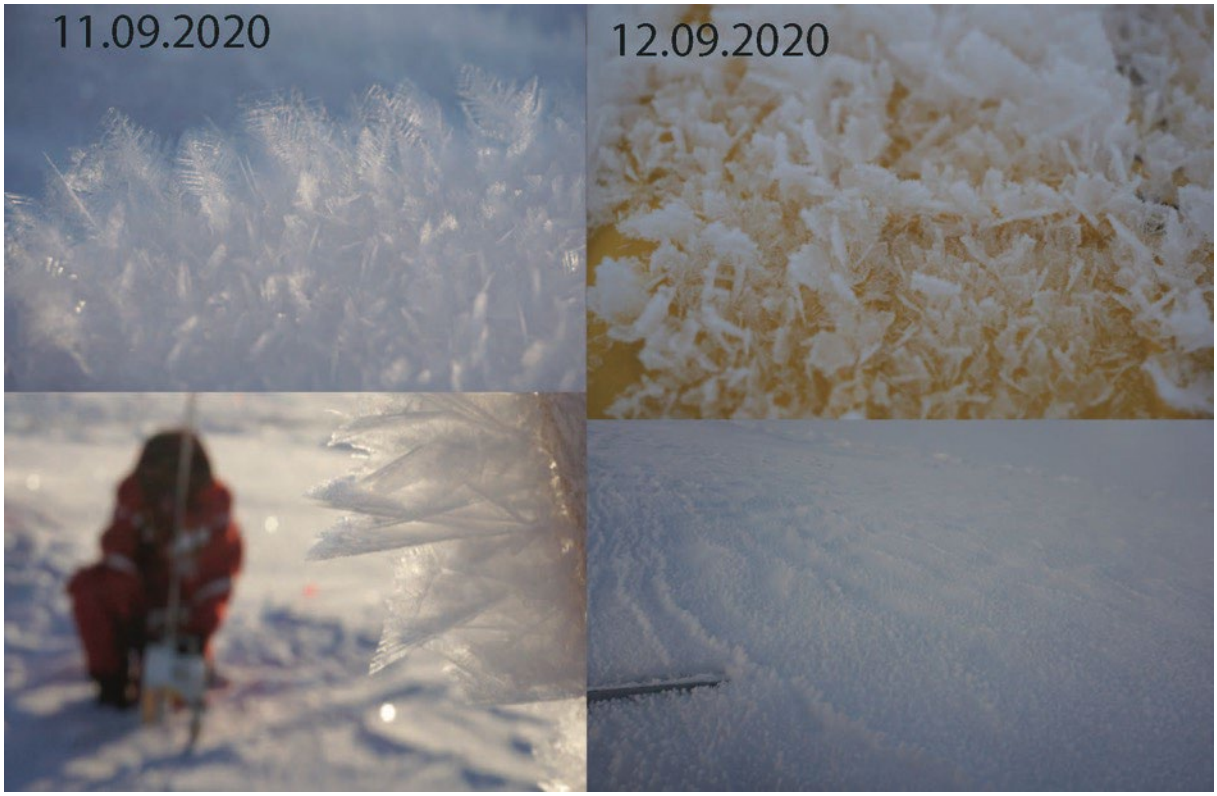

Fig. 4.2.8: Different surface deposition on 11.09.2020 (left) and 12.09.2020 (right). The pictures correspond to microCT images in Figure 4.2.9.

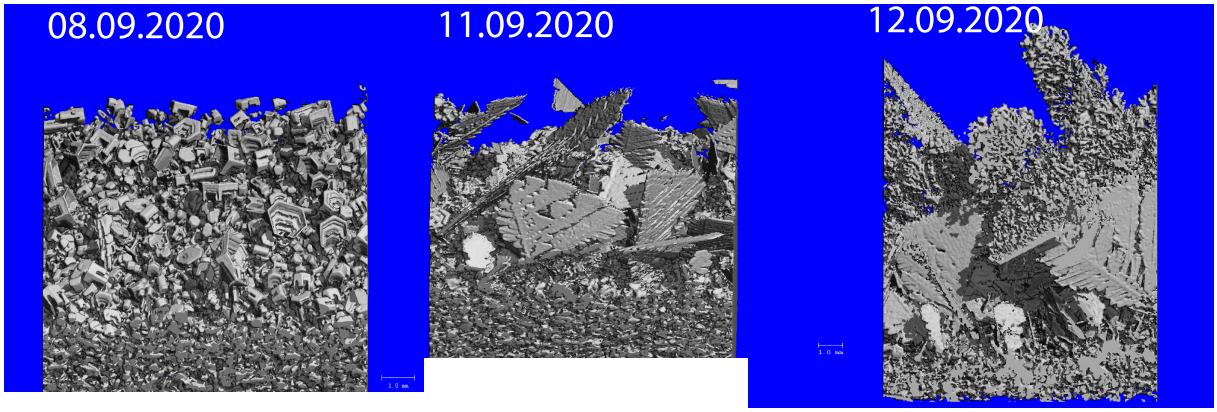

Fig. 4.2.9: Depending on atmospheric conditions and temperature gradients, we observed different types of surface depositions on the snow surface. The microCT images correspond to pictures from Fig. 4.2.8.

Salinity was zero for the majority of our samples. Towards the end, when we were able to sample snow over frozen ponds, salinity values of snow increased slightly. The largest snow salinity, aside from our measurements of lead ice and pond ice, was measured on the Ice Stations 1 and 3 before we reached the ice edge.

TLS

We were able to capture the first surface scan without (Remote Sensing site) or with only little snow (ROV site) after the initial freeze-up. These scans represent the surface (roughness) at the end of melt season when ponds were distinct from the white ice and had obvious edges. Figure 4.2.10 shows the ROV scan area on 5 September where all ponds are clearly visible as smooth black areas within the ice. All the following scan sets document the evolution of the surface with the influence of different events like intensive snowfall or warm air intrusion with melting conditions. Figure 4.2.11 shows the same ROV area on 11 September, only 6 days later, when the surface conditions had changed significantly and melt pond areas are much smoother and less visible after re-freezing and new snow accumulation.

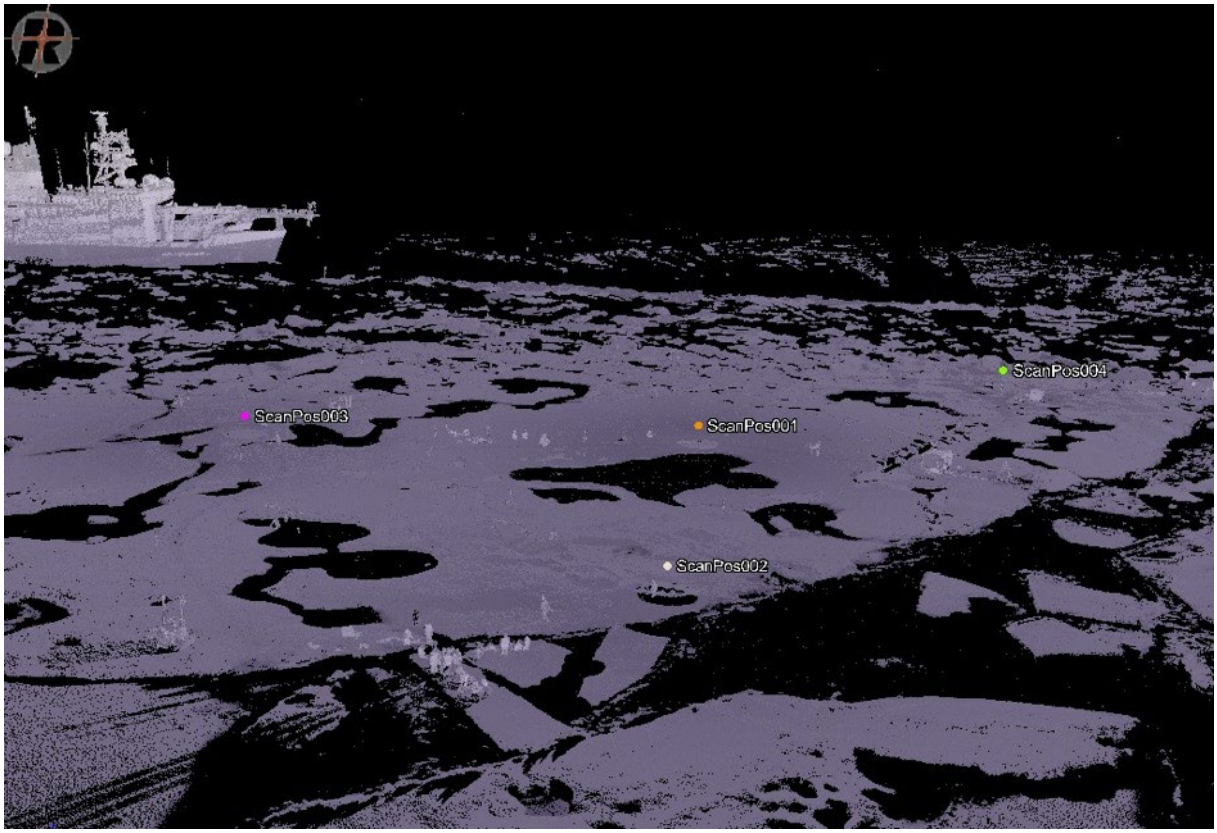

Fig. 4.2.10.: Scan of the ROV area with 4 different scan positions on 5 September. Ponds are not frozen or covered with snow.

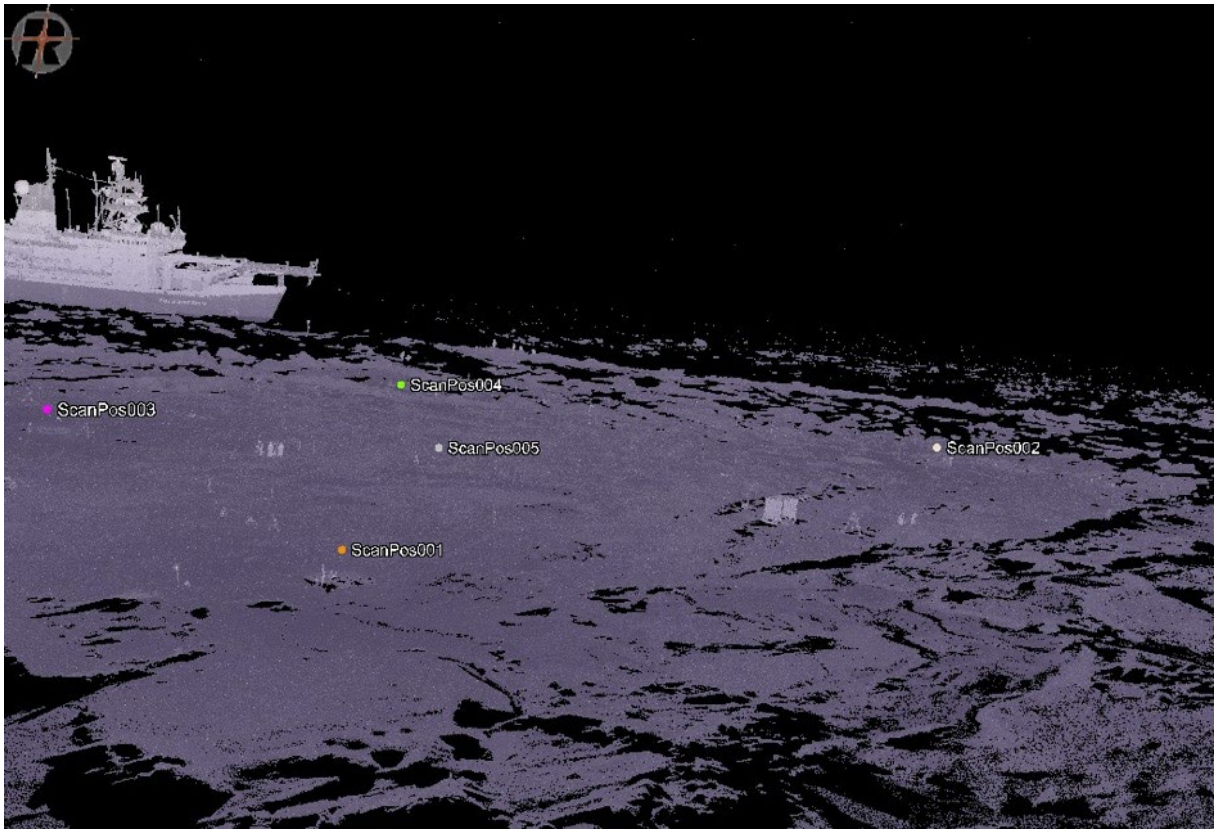

Fig. 4.2.11.: Scan of the ROV area with 5 different scans on 11 September. Ponds are refrozen and covered with snow.

Data management

All data are handled, documented, archived and published following the MOSAiC data policy (see APPENDIX). All device operations were logged in the AWI sensorweb portal and all sensor raw data files are stored in platform section of MCS. Snowpit raw data files are available through platforms/packice/ in MCS. Final geophysical parameters will be made available via the workspace section of MCS. Final data products will be stored at the PANGAEA data repository (World Data Center PANGAEA Data Publisher for Earth & Environmental Science (www.pangaea.de)).

Tab. 4.2.7: Overview on all measured parameters for the three defined snow pit types during leg 3.

Type A: Parent snow pit	Type B: Quick snow pit	Type C: SnowMicroPen or NIR (and sometimes SfM)
Complete sampling of physical and chemical properties	Complete physical sampling	Super quick measurements
• 1.5 m - SMP transect, 0.3 m spacing • MicroCT sampling • Density (volumetric) • Temperature • Salinity • Snow samples for chemical and physical properties (not in all A-pits) **All Type B measurements**	• SnowMicroPen (SMP) • NIR photography (SSA), at surface and pit wall if there was enough snow • SWE (ETH tube) • MicroCT sampling • Site overview photos • Permittivity • Pictures for snow surface and ice surface roughness (SfM)	• SnowMicroPen (SMP) • NIR • SfM

See the DSHIP action log extract file for an overview of the snowpits conducted for legs 1, 2, and 3

References

Proksch, M., Lowe, H., and Schneebeli, M.: Density, specific surface area, and correlation length of snow measured by high-resolution penetrometry, J Geophys Res-Earth, 120, 346-362, 10.1002/2014jf003266, 2015.

4.3 Mass Balance Buoys and Stakes

Marcel Nicolaus[1], Mario Hoppmann[1], Julia Regnery[1]

(not on board:) Ian Raphael[2], Don Perovich[2], Bin Cheng[3], Ruibo Lei[4], Giulia Castellani[1]

[1]DE.AWI

[2]EDU.DARTMOUTH

[3]FI.FMI

[4]CN.PRIC

Objectives

Sea ice and snow mass balance vary on large range of scales in space and time. The aims for the deployments of snow and ice mass balance stations and stakes are to obtain the annual cycle of snow and sea ice mass balance, to identify the importance of the various processes that affect the seasonal evolution of ice mass balance, and to characterize the role of summer heat storage in the upper ocean and snow over the ice on sea ice mass balance. Important changes in the seasonal evolution of an ice cover can be detected. All units together provide a good opportunity for ice mass balance observations in clusters or transects measuring local spatial variability over time. The stakes measurements are manual ice mass-balance measurements.

On Leg 5, the deployments aimed for detailed studies of surface re-freezing and new ice formation to characterize the transition from summer melt season into freeze-up, including snow thickness changes after initial freeze-up. We installed the devices across different surface types, e.g. ponds or white ice. As a particular focus, we deployed several units into the ridged ice, which will then allow to study differences of level ice (as most previous deployments were done) and deformed ice.

Work at sea

Deployment of SIMBA/Bruncin IMBs

A total of 5 Ice Mass balance Buoys with Iridium capabilities were deployed within the main ice camp during the Leg 5 drift (see Table 4.3.1). The 4 SIMBA-type and one Bruncin-type IMBs were deployed on different ice types, and mostly co-deployed with other buoys. The SIMBA-type buoys (SRSL, Oban Scotland) were standard-configuration buoys equipped with 5 m long thermistor chains at 0.02 m sensor spacing, and with heating capability. The Bruncin-type buoy was equipped with a 5.12 m long chain, also at 0.02 m sensor spacing and heating capability. Along with standard simple meteorological sensors, the unit was additionally equipped with a snow pinger right next to the chain, a Solumetrix BKIN50 conductivity cell (installed directly under the ice) and a camera facing the iBOB/AZFP buoys.

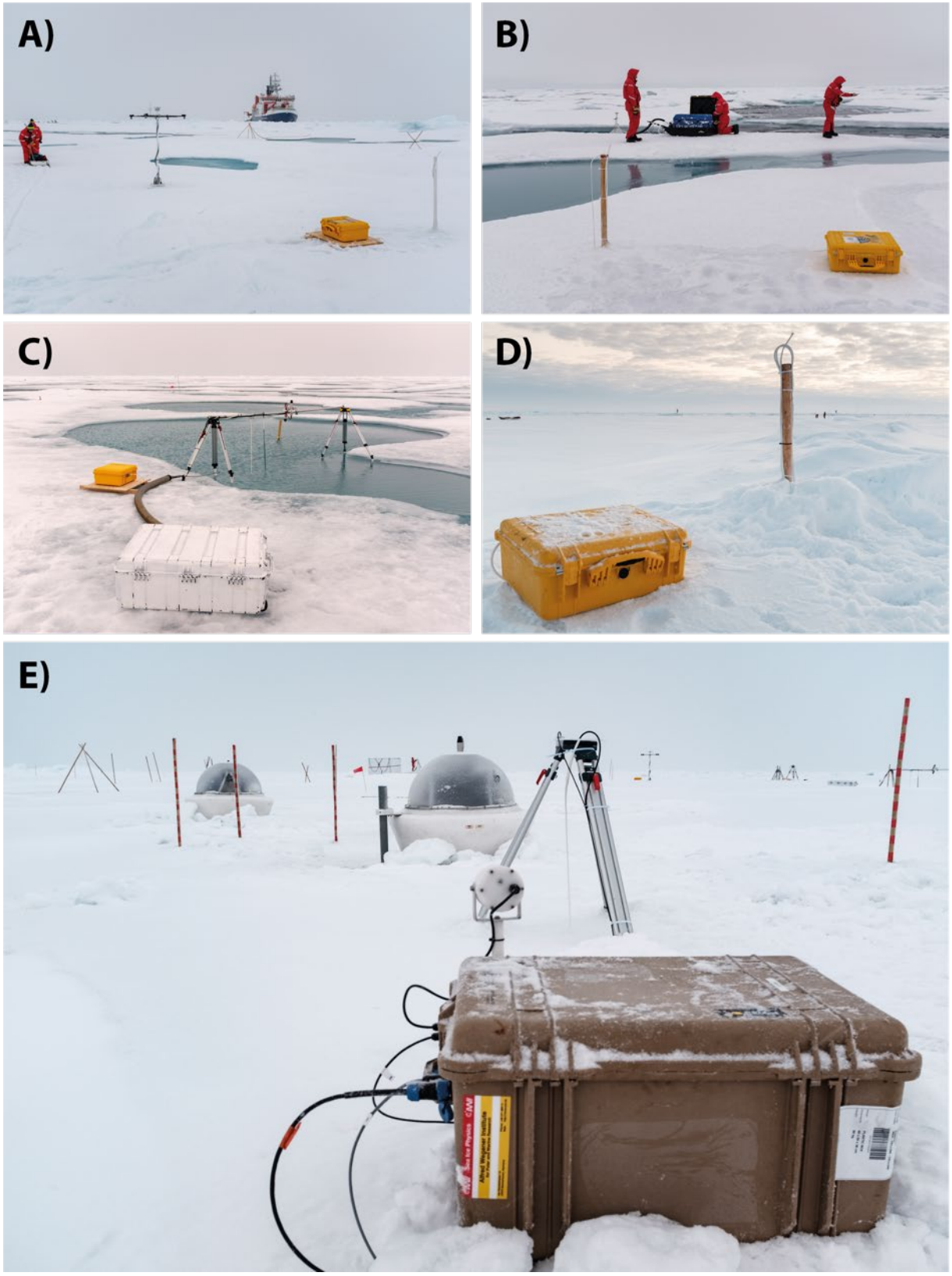

Fig.4.3.1: SIMBA-type IMBs A) 2020T78 at the main buoy site, B) 2020T84 in Met City, C) 2020T81 in melt pond next to 2020R21, D) 2020T85 in a small ridge close to the iBOB/AZFP buoys, E) Bruncin-type IMB 2020M23 right next to the iBOB/AZFP buoys.

Tab.4.3.1: Overview of IMBs deployed in the main camp during the Leg 5 drift

Buoy ID	Internal ID	IMEI	Depl. date	Location	Ice type	Dship log
2020T78	PRIC 1006	300234068529570	20200823	Buoy site	Level FYI	5_58-56
2020T81	FMI 0608	300234068708320	20200830	2020R21	Meltpond	5_58-67
2020M23	IMB051	300025060609430	20200918	iBOB/AZFP	Level FYI	5_58-105
2020T85	PRIC 0906	300234068704730	20200919	iBOB/AZFP	Ridge	5_58-170
2020T84	FMI 0607	300234068707340	20200826	Met City	Level FYI	5_58-101

Tab.4.3.2: IMB deployment parameters

Buoy ID	Ice thickness (m)	Snow/SL depth (m)	Freeboard/pond depth* (m)	Sensor interface	@air/ice
2020T78	1.52	0	0.17	33	
2020T81	1.14/0.88	0	0.26*	32/33	
2020M23	1.55	0.05	0.18	29	
2020T85	4.00	0.05	0.76	12	
2020T84	1.14	0.03	0.14	26	

Deployment of Digital Thermistor Chains

A total of 6 digital thermistor chains (sensor spacing 0.02 m) were deployed at different sites within the main ice camp between 23 August and 04 September 2020 (Table 4.3.1). The instruments consisted of an Arduino data logger and standard Bruncin digital thermistor chains of variable lengths and with a 0.02 m sensor spacing. They were mounted on a standard photo tripod. Upon deployment, standard parameters were documented. The units measured temperature and heating profiles throughout air, snow, ice and ocean at 1-hourly and 6-hourly intervals, respectively. The heating cycle was set to 20s, and temperature values during the heating cycle were recorded every second for one minute. During their operation time, the thermistor chains were often covered by substantial riming, which was sometimes cleaned off. The instruments were recovered on 19/20 September 2020.

Fig.4.3.2: Locations of the 6 digital thermistor chains and 5 Iridium IMBs.

Table 4.3.3: Overview of DTC deployments.

Instrument	Location	Depl. Date	Dship	Chain length	Ice	Snow /SL	FB / pond depth	T_sur
DTC_RS051	Buoy site	20200823	PS122/5_58-157	4.16 m	1.52	0.02	0.16	37
DTC_RS052	Remote Sensing	20200827	PS122/5_58-159	2.36 m	1.32	0.05	0.17	29
DTC_RS053	Main ridge	20200901	PS122/5_58-160	7.18 m	4.92	0.00	0.75	41
DTC_RS054	Ridge meltpond	20200901	PS122/5_58-161	5.12 m	1.76	0.00	0.18	40
DTC_RS055	Met City	20200826	PS122/5_58-158	5.12 m	1.14	0.03	0.17	36
DTC_RS056	Hinterland	20200904	PS122/5_58-162	2.36 m	1.09	0.00	0.43	30

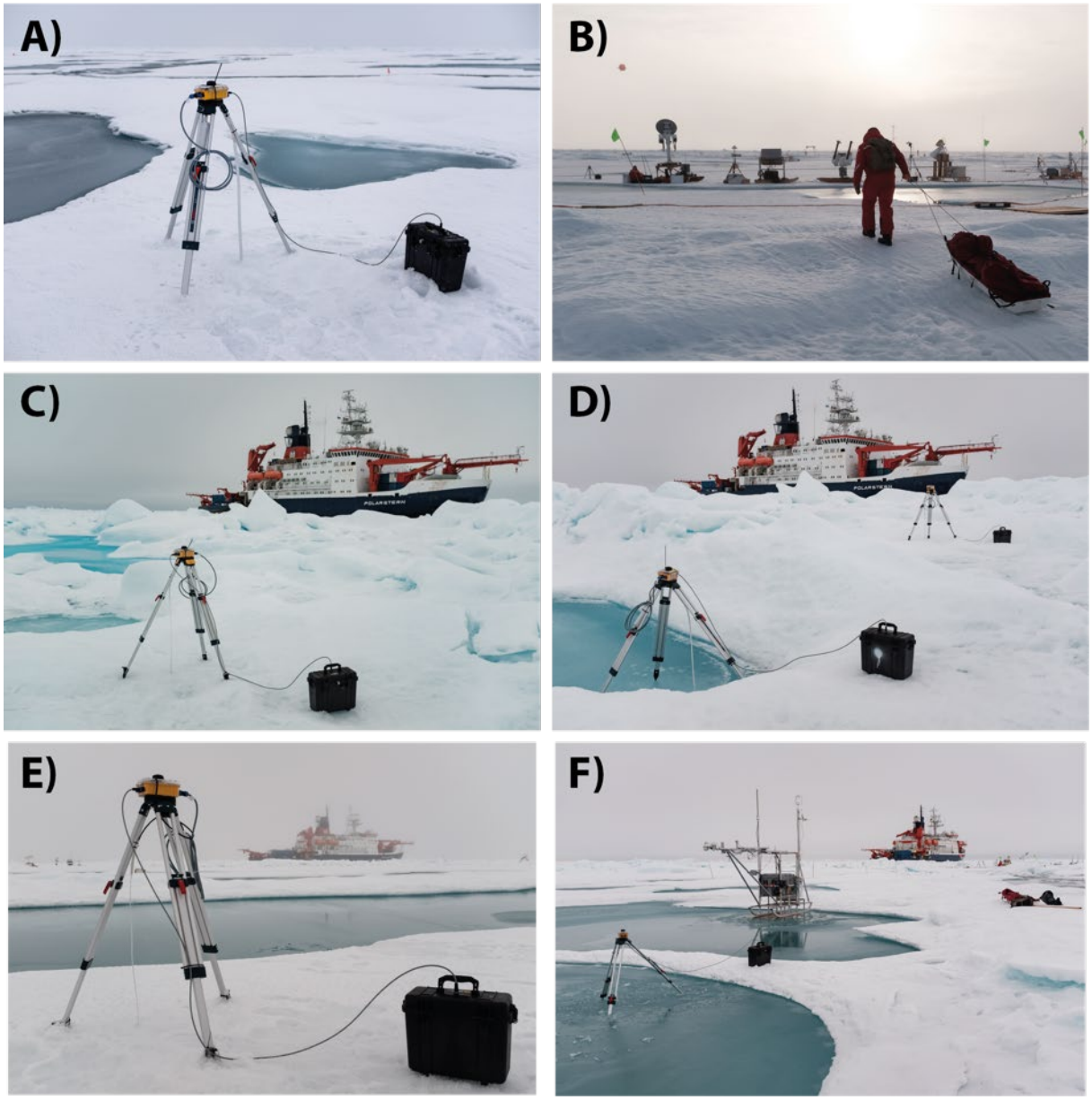

Fig.4.3.3: Photos of initial digital thermistor chain deployments: A) DTC_RS051, B) DTC_RS052 (far left corner on the photo), C) DTC_RS053, D) DTC_RS054, E) DTC_RS055, F) DTC_RS056.

Ridge thermistor chains (HAVOC IMB081)

On 04 September 2020, an Ice Mass balance Buoy equipped with four 7 m long thermistor chains (shortname: 2020M28, Dship action log PS122/5_28-95), each with a sensor spacing of 0.02 m, was deployed along the ridge transect in the main ridge as part of the HAVOC project (see Team ICE chapter). Temperature data along the chains was recorded at hourly intervals. The instrument was recovered on 20 September 2020.

Table 4.3.4: Ridge IMB deployment details (snow was absent at all chain sites)

Chain ID	Ridge transect point	Ice thickness	Freeboard	Surface thermistor
1	#4	5.60 m	-	26
2	Between #2 and #3	5.52 m	0.45 m	29
3	#6	5.04 m	0.5 m	30

4	#7	6.04 m	0.6 m	32

Fig.4.3.4: Deployment of HAVOC ridge IMB081 (2020M28) along the ridge transect.

Deployment of Snow Buoys

On Leg 5, we deployed 6 Snow Buoys: 4 buoys were deployed on the main floe with two of them on level ice (2020S106 at Met City and 2020S107 at the buoy site) and two of them in ridged ice (2020S98 and 2020S108). They can also be found on the main floe map (Figure 4.1.4). The two other buoys were deployed on the way from the ice camp towards the ice edge on 21 September (2020S105 and 2020S109, Figure 4.3.5a and b).

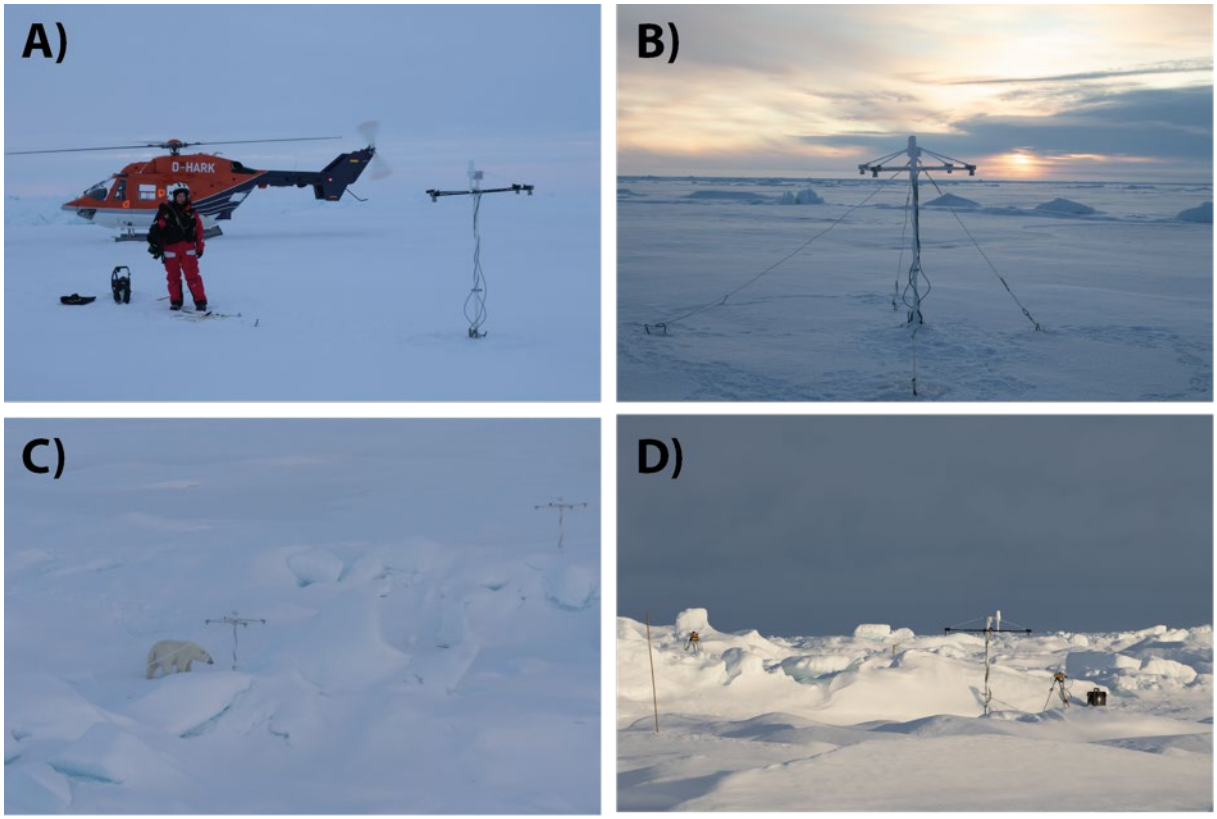

Fig.4.3.5: Snow Buoys deployed during Leg 5: A) Buoy 2020S105, B) 2020S109, C) 2020S98 and 2020S108 in the ridge, D) 2020S108 together with 2 DTC.

Stakes

A 'stake' is a combination of an ablation stake together with a hotwire thickness gauge. The ablation stake gives the position of the ice and snow surfaces, while the thickness gauge shows the position of the ice bottom.

On 26 August. we installed one stakes site with 9 stakes. As the ice floe consisted only from one ice type connected to a big ridge the 9 stakes were arranged in a cross grid (see Figure 4.3.6). Within the grid, we tried to cover measurement points in ponds (4 stakes) and on white ice (5 stakes). The ponds were covered already with a thin layer of fresh ice. However, the warm air at the end of August caused the melt of this fresh ice cover on the ponds of the stakes site and even made one stake melt through. Therefore, we had to setup one stake new and replace a second one, which broke on 30 August. Two stakes placed on the edge of a pond were frozen in by 4 September (see Figure 4.3.7). The other two "pond" stakes were frozen in on the reading on 9 September. We conducted the stakes readings every 4-6 days which added up to 6 stake readings (including the setup) during leg 5.

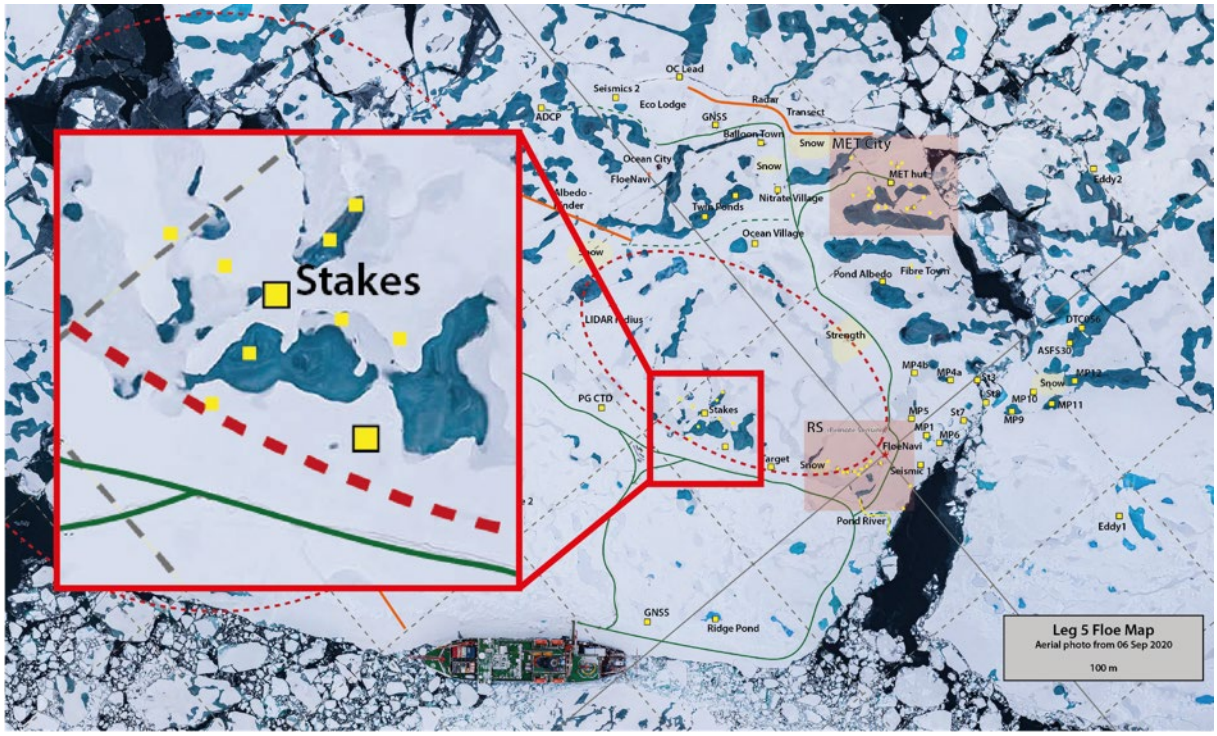

Fig.4.3.6: Setup of the stakes grid on Leg 5.

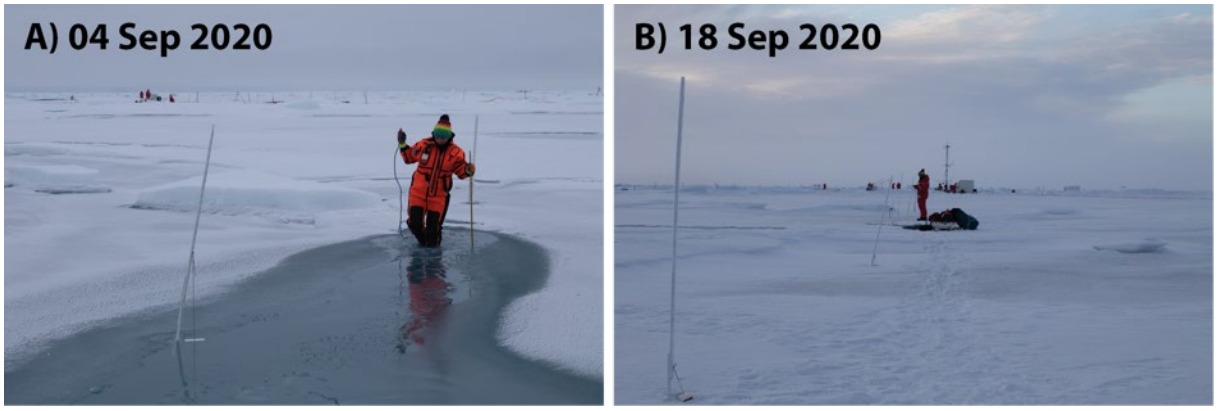

Fig.4.3.7: A) Stake readings on 4 September. Some pond stakes are frozen in already but not all. B) Stake readings on 18 September. All ponds are frozen.

Preliminary results

Buoys

All buoys were operational when leaving the floe on 21 September. Beyond this, no results are available yet, but data are currently recorded and archived for later analyses

Stakes

The readings from the stakes grid show ice thicknesses of the white ice between 110cm to 145cm. The lowest ice thickness in one of the ponds was around 70cm. After the freeze-up of the ponds, these stakes showed similar ice thicknesses as the ones initially installed on the white ice. Figure 4.3.8 shows the ice thickness of the “white ice” stakes over the measurement period. However, in general the ice thickness did not change over the Leg 5 period. We could not detect any significant melt or freezing on the bottom of the predominant ice. The surface

did go through many changes but did not increase significantly. Surface measurements were between 0 to 10cm of surface scattering layer, snow or slush. Pond depth was at a maximum of 47cm, which was frozen over, that walking over was possible by September 9.

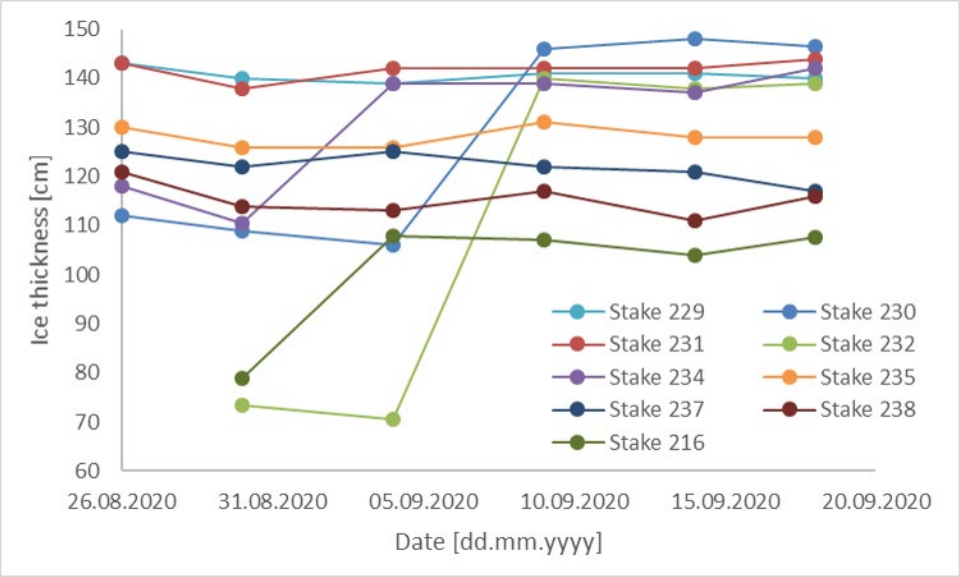

Fig.4.3.8: Ice thickness measurements of the stake readings of Leg 5.

Data Management

All data are handled, documented, archived and published following the MOSAiC data policy (see APPENDIX). All device operations were logged in the AWI sensorweb portal and all sensor raw data files are stored in platform section of MCS. Final geophysical parameters will be made available via the workspace section of MCS. Final data products will be stored at the PANGAEA data repository (World Data Center PANGAEA Data Publisher for Earth & Environmental Science (www.pangaea.de)).

References

No references

4.4 Transect

Melinda Webster[1], Jan Rohde[2], Linda Thielke[3], Gunnar Spreen[3], Ruzica Dadic[4,5],
(not on board:) Polona Itkin[6], Stefan Hendricks[2]

[1]EDU.UAF
[2]DE.AWI
[3]DE.UNI-Bremen
[4]CH.WSL
[5]VUW, NZ
[6]University or Tromsø

Objectives

A new transect route was established on Leg 5 for monitoring the changes in snow depth, sea ice thickness, and melt pond depth during the freeze-up season. Surveys began when melt ponds were still present and ended shortly after continuous freeze-up, when melt ponds refroze and the surface became snow-covered. The data from the nearly month-long time-series from Leg 5 will be valuable for better understanding the:

- Mass balance of snow and sea ice during sea-ice freeze-up.
- Widespread transition of a ponded ice surface to a snow-covered state.
- Short-term changes in surface conditions in relation to variable weather conditions.

Work at sea

The Leg 5 transect work consisted of four types of surveys: (1) a ~100 m by ~200 m grid (referred to as "Kinder grid") comprised of four parallel survey lines and, at times, coordinated with snow sampling (Chapter 4.2), (2) two remote sensing transects less than 100 m in length (Chapter 4.12), (3) ridge transects in conjunction with the ridge measurement program (Chapter 4.10), and (4) off-site transects on nearby floes, encompassing larger (~1+ km) spatial coverage. The transect grid was established by the Kinder albedo line and was the primary time-series for the transect program, being surveyed once per week. The following list reflects the number of visits per survey type between August 24 and September 19:

- Kinder grid survey: 6.
- (a) Remote sensing survey with coincident ARIEL measurements: 7.
- (b) Remote sensing survey with coincident KuKa band radar measurements: 5.
- Ridge survey: 3.
- Port side: 3; Starboard side: 1; Bow side: 1.
- Gem-2 calibrations: 4.

Before arriving to the floe, an initial survey was carried out on August 21 to determine the sea ice thickness. During camp de-installation on September 19, the Remote Sensing site was surveyed after remote sensing instruments were removed. During the discrete measurement sampling on the transit to Bremerhaven, three ice stations were carried out and included each of the following transect work:

- Multi-kilometer long transect surveys with the GEM-2 and Magnaprobe.
- Short (<500 m) surveys in conjunction with the ARIEL and infrared camera data collection.
- GEM-2 calibrations.

Instrumentation

On Leg 5, the transect work involved measuring both snow and melt pond depths as the surface conditions transitioned from a melting state to frozen, snow-covered sea ice during freeze-up. To accommodate both types of measurements when snow and melt ponds were both present, the snow basket of the Magnaprobe was outfitted with foam on its upper portion to provide buoyancy in melt ponds. The bias associated with this addition was ~0.25 cm.

Magnaprobe-anja was the primary instrument for all transect surveys. For total (snow + ice + pond) thickness surveys, Geophex GEM-2 Broadband Electromagnetic Induction Sensor 512 was used (Table 4.4.1). For the corresponding instruments and device operation identifications, please see Table 4.4.2.

Tab. 4.4.1: An overview of instruments used on the Leg 5 transects.

Instrument	Description	Device URN	Geophysical Parameter
GEM-2	Geophex GEM-2 Broadband Electromagnetic Induction Sensor	pack_ice:ice_ps:gem2-512	Total (sea ice + snow) thickness

Magnaprobe	GPS snow depth probe	pack_ice:ice_ps:magnaprobe-anja	Snow depth and melt pond depth

Tab. 4.4.2: An overview of device operations of the sea-ice transect and related data.

Date (MM/DD/YYYY)	Survey Type	GEM-2	Magnaprobe
8/21/2020	Initial floe survey	PS122/5_59-194	N/A
8/21/2020	Calibration	PS122/5_59-273	N/A
8/24/2020	Transect by Kinder albedo line	PS122/5_59-276	PS122-5_59-256
8/27/2020	Off-site transect on port side	PS122/5_59-316	PS122/5_59-411
8/28/2020	Ridge survey	PS122/5_59-428	PS122/5_59-412
8/30/2020	Transect by Kinder albedo line; Remote Sensing Transect with ARIEL	PS122/5_59-427	PS122/5_59-413
8/31/2020	Remote Sensing Transect with ARIEL		
9/2/2020	Off-site transect on starboard side	PS122/5_60-52	PS122/5_60-58
9/3/2020	Transect by Kinder albedo line; Remote Sensing Transect with ARIEL	PS122/5_60-222	PS122/5_60-163
9/3/2020	Calibration	PS122/5_60-225	N/A
9/3/2020	Off-site transect on port side	PS122/5_60-226	PS122/5_60-164
9/4/2020	Ridge survey	PS122/5_60-162	N/A - see spreadsheet titled: "RidgeSurvey_SnowDepth _Sept04_2020"
9/5/2020	KuKa Radar Transect	N/A	N/A
9/7/2020	Transect by Kinder albedo line; Remote Sensing Transect with ARIEL and KuKa Radar Transect	PS122/5_61-290	PS122/5_61-110
9/9/2020	Off-site transect beyond ship's bow	PS122/5_61-292	PS122/5_61-111
09/10/20	Transect by Kinder albedo line; Remote Sensing Transect with ARIEL and KuKa Radar Transect	PS122/5_61-258	PS122/5_61-216
9/10/2020	Off-site transect on port side	PS122/5_61-260	PS122/5_61-217
9/14/2020	Radar transect	N/A	N/A
9/14/2020	Remote Sensing Transect with ARIEL	N/A	PS122/5_62-17
9/17/2020	Remote Sensing Transect with ARIEL	PS122/5_62-190	PS122/5_62-239
9/17/2020	Calibration	PS122/5_62-191	N/A
9/17/2020	KuKa Radar Transect	PS122/5_62-192	PS122/5_62-241

9/18/2020	Ridge survey	PS122/5_62-198	PS122/5_62-242
9/18/2020	Transect by Kinder albedo line	PS122/5_62-199	PS122/5_62-243
9/19/2020	Calibration	PS122/5_62-193	N/A
9/19/2020	Remote Sensing Site	PS122/5_62-194	PS122/5_62-244
9/24/2020	Ice Station 1: short & long transects	PS122/5_63-33	PS122/5_63-37
9/24/2020	Ice Station 1: Calibration	PS122/5_63-34	N/A
9/26/2020	Ice Station 2: short & long transects	PS122/5_63-68	PS122/5_63-80
9/26/2020	Ice Station 2: Calibration	PS122/5_63-69	N/A
9/30/2020	Ice Station 3: short & long transects	PS122/5_63-257	PS122/5_63-145
9/30/2020	Ice Station 3: Calibration	PS122/5_63-258	N/A

Challenges

Ice dynamics created cracks, leads, and shearing from the onset of the camp installation on Leg 5. The initial staking of the transect loop drifted away and a new grid survey was established a few days later on August 24 in parallel to the Kinder albedo line. The Leg 5 floe was constrained to an area of ~500 m by 500 m due to new cracks and leads. To balance to the need for a transect time-series, large-scale sampling, and the limited working area of the Leg 5 floe, the Leg 5 transect program focused on a comparatively smaller grid survey (~100 m by ~200 m) for time-series measurements and off-site visits for larger-scale characterization of the surface and ice conditions.

Preliminary results

The sea ice thickness remained somewhat constant throughout the duration of Leg 5. Average sea ice thicknesses on the Kinder grid survey ranged from 1.4 ± 0.7 m to 1.5 ± 0.5 m from August 24 to September 18, respectively. Given the uncertainty of 0.1 m over level ice and derivations using different calibrations (Figure 4.4.1), the results suggest that no detectable changes in sea ice thickness occurred during Leg 5; however, a deeper analysis of the data is warranted, especially with regard to applying different calibration data in the thickness derivations. Further analysis of data between the survey types may also reveal insightful information regarding spatial sampling (Figure 4.4.2).

The time-series of snow/surface scattering layer (SSL) depth and melt pond depth correspond with the weekly trend in atmospheric conditions. From August 21 to August 30, above-freezing temperatures and intermittent rainfall persisted and the average snow/SSL depth decreased from 10 cm to 4 cm, while melt pond depths remained relatively the same at ~27 ± 9 cm (Figure 4.4.3). From September 1 to September 3, air temperatures were below freezing, allowing the SSL to solidify, subsequently causing shallower penetration of the Magnaprobe into the surface. The resulting snow/SSL depth average and standard deviation were 2 ± 1 cm. Related, melt ponds on the surveys became sufficiently frozen with 5+ cm lids to withstand the weight of the transect surveyors after September 3. Between August 24 and September 3, no notable difference was found in melt pond depths. From September 5 to September 10, incremental snowfall (~1 cm per day at times) and drifting snow ensued, leading a 4 cm average snow depth with a notable increase of 3 cm in standard deviation. By September 18, a mixture of drizzle, freezing drizzle, and snowfall produced an average snow depth of 6 ± 3 cm.

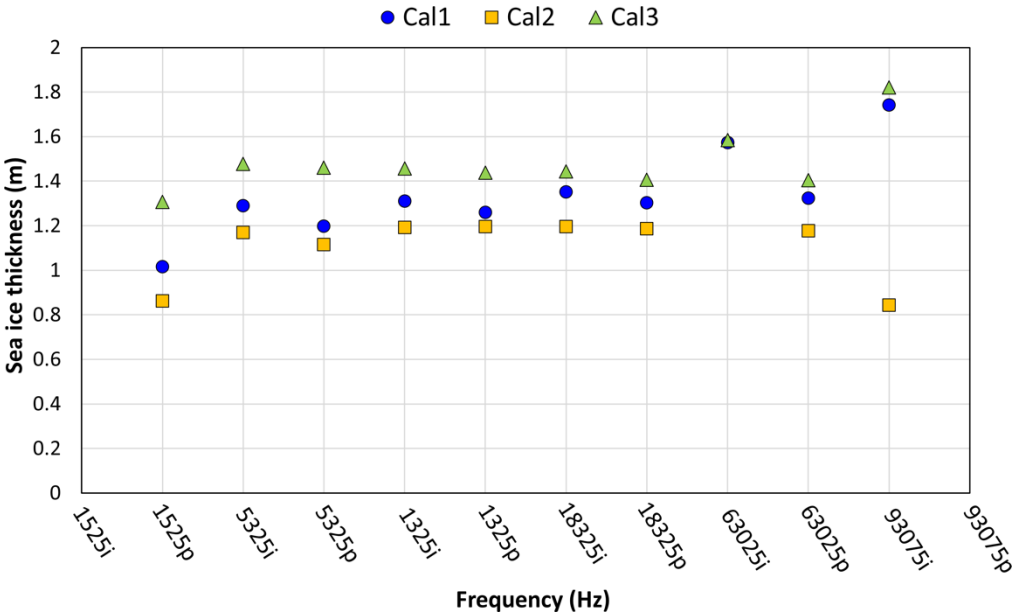

Fig. 4.4.1: An example of sea ice thickness derivations using three different calibration models for the range of GEM-2 frequencies.

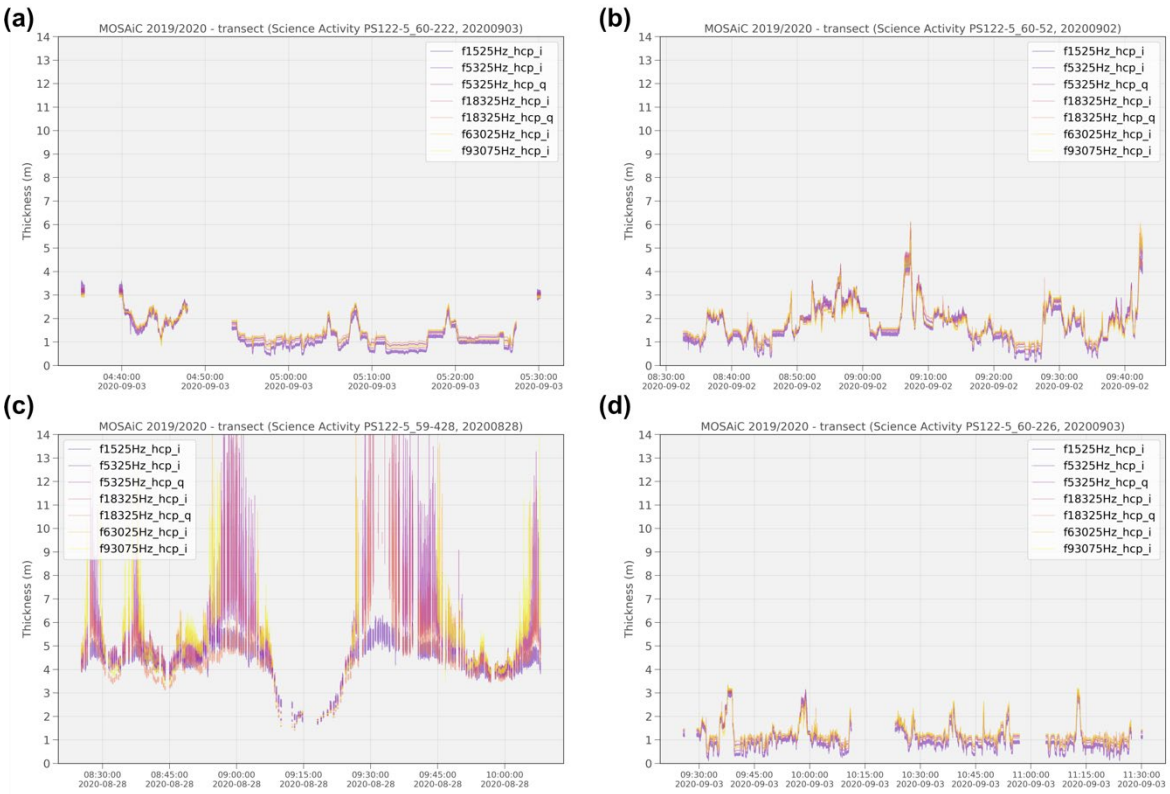

Fig. 4.4.2: Quicklooks of sea ice thickness derivations from the variety of survey types during Leg 5. (a) the Kinder grid survey, characterized by level, first-year ice; (b) an off-site survey on the starboard side of the RV Polarstern, which was characterized by deformed first-year sea ice; (c) one of the ridge surveys conducted in conjunction with drill-hole thickness measurements; and (d) an off-site survey on the port side of the RV Polarstern, which was characteristic of smooth, first-year sea ice.

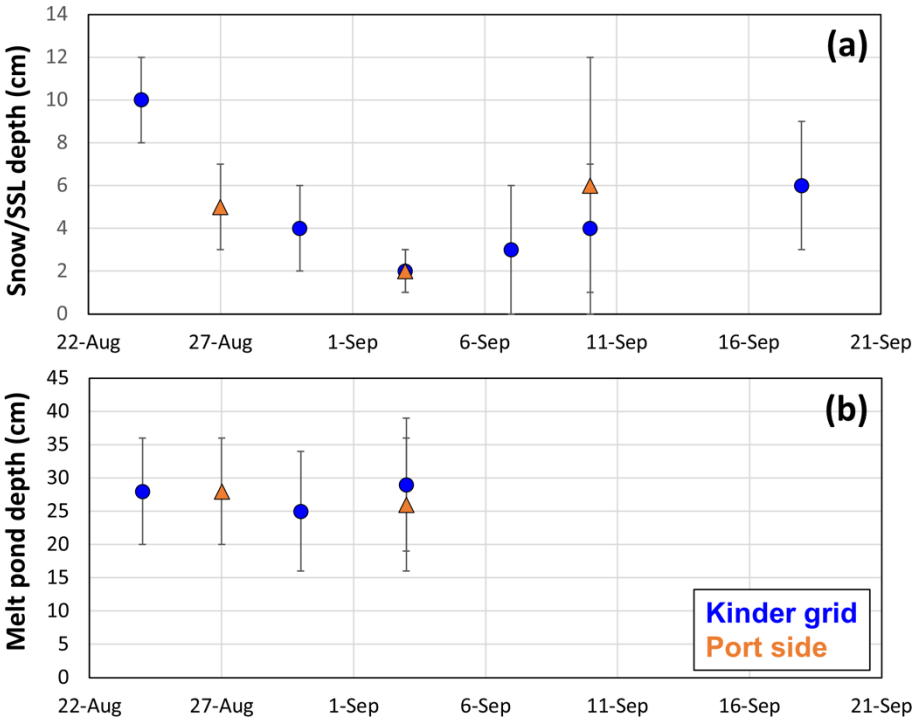

Fig. 4.4.3: Time-series of the average and standard deviation in (a) snow depth and (b) melt pond depth on the kinder grid transect (blue) and port side transect (orange). Even though both transects encompassed different floes and spatial coverage, their surface conditions were comparable. Snow depth continued to melt during the first two weeks despite scant snowfall events. From the second week onward, freezing conditions led to frozen-over melt ponds (note, the lack of data for pond depth after September 3) and a persistent snow cover, which thickened over time.

Data management

All data are handled, documented, archived and published following the MOSAiC data policy (see APPENDIX). All device operations were logged in the AWI sensorweb portal and all sensor raw data files are stored in platform section of MCS. Final geophysical parameters will be made available via the workspace section of MCS and archived in the PANGAEA data repository according the MOSAiC data policy. Metadata and device operation associations are also recorded in **/mcs.fs-polarstern.de/workspace/teams/ice/transects/mosaic-transect-actionlog.xlsx**

4.5 Ice Coring

Nikolai Kolabutin[1], Egor Shimanchuk[1], Linda Thielke[2], Marcel Nicolaus[3]

(not on-board:) Marc Oggier[5], Ruibo Lei[6], Mats Granskog[7], Sonke Maus[8], Martin Schneebeli[9], Benjamin A. Lange[7], Evgenii Salganik[8], Igor Sheykin[1], Sergey Kovalev[1]

[1]RU.AARI
[2]DE.UNI-Bremen
[3]DE.AWI
[5]EDU.UAF
[6]CN.PRIC
[7]NO.NPOLAR
[8]NO.NTNU
[9]CH.WS

Objectives

Within the general coring objectives (8.2 Objectives for General Coring.), the ICE team is responsible for the ice physics properties analysis (salinity, density, texture, microstructure, optics, sediments, ISO).

Work at sea

The main coring works were carried out at Mondays on the level ice area roughly 180 meters from the vessel behind the ridge. The coring team included 5 people from Ice, Eco and BGC teams. There were taken samples for ice physics properties analysis, for eco and chemical analysis. Some cores were sectioned in the tent on the area, the rest were sealed in plastic sleeves. Then samples were brought on the vessel cold storages for further analysis and measurements.

Following the general coring event, upon return from the field, the CT samples were centrifuged, and imaged using x-ray computed tomography (CT) technique within half a week. Cores for archive, backup, plastic, ISO, texture, optics and the upper part of the CT core were sealed in plastic sleeves and stored at -20 °C. Density was measured at -15 °C by densitometry in paraffin in the freezer lab using a Kern EMB-V scale. Then salinity was measured on the melted samples with a conductivity probe Voltcraft LWT-100 from team ICE. Within 1 day, melted salinity samples were bottled for future isotope measurement, before bulk salinity was measured on the remaining water using a conductivity probe YSI 30 from team ECO. Each week, one ice core was processed into horizontal and vertical thick texture sections. Following additional coring events, similar approach was used to process collected cores with respect to its type.

In addition to coring on main coring area there were also carried out coring on other areas for main ice physical properties analysis: at the ridge area, at the area of ice strength measurements (Strength area), at melt ponds (together with BGC team), at lead. Also after leaving the main ice floe there were coring works on three ice stations.

The overview of device operation for coring is presented in the table 4.5.1. The devices are SI_corer_9cm Kovacs Mark II, 9cm, SI_corer_7cm Kovacs Mark III, 7cm and SI_corer_14cm Kovacs Mark V, 14cm

Dates of coring works:

Main coring area – 31.08, 07.09, 14.09, all cores for physical properties (temperature, salinity, density, texture, microstructure, optics, sediments, ISO + repository, backup, plastic) + ECO and BGC cores together ECO and BGC teams;

Strength area – 29.08, 10.09, basic physical properties (temperature, salinity, density, texture);

Ridge area – 11.09 basic physical properties (temperature, salinity, density, texture) together with BGC team.

Melt ponds – 14.09, 18.09, temperature, salinity, density, texture, optics, microCT + BGC cores together with BGC team.

Lead – 18.09, temperature, salinity, density, texture

First ice station – 24.09, old and new ice, temperature, salinity, texture, density, microCT, optics + ECO and BGC cores at new ice together ECO and BGC teams;

Second ice station – 26.09, temperature, salinity, density, texture, optics;

Third ice station – 30.09, temperature, salinity, density, texture.

Tab. 4.5.1: An overview of device operations of the ridge thickness measurements using the drill and ice gauge.

Date (DD.MM.YYYY)	Area	SI_corer_9cm	SI_corer_7cm	SI_corer_14cm
29.08.2020	Strength Area	PSS122/5_59_492	PSS122/5_59_493	
31.08.2020	Main coring Area	PSS122/5_60_3	PSS122/5_60_4	
07.09.2020	Main coring Area	PSS122/5_61_6	PSS122/5_61_7	
10.09.2020	Strength Area			PSS122/5_61_188
11.09.2020	Ridge survey	PSS122/5_61_185	PSS122/5_61_186	
14.09.2020	Main coring Area	PSS122/5_62_16	PSS122/5_62_15	
14.09.2020	Melt Pond 4a (RS)	PSS122/5_62_35	PSS122/5_62_282	
18.09.2020	Melt Pond 1 (RS)			PSS122/5_62_135
18.09.2020	Lead RS			PSS122/5_62_136
24.09.2020	Ice Station 1 (Old Ice)	PSS122/5_63_29	PSS122/5_63_28	
24.09.2020	Ice Station 1 (New Ice)	PSS122/5_63_31	PSS122/5_63_30	
26.09.2020	Ice Station 2	PSS122/5_63_325		
30.09.2020	Ice Station 3	PSS122/5_63_326		

Preliminary Results

At the Main coring area, ice consists of an upper layer of granular ice, about 15 to 20 cm thick, then layer of columnar ice about 20 to 30 cm, then about 35 cm of rotten ice with many saline inclusions and then columnar layer underneath (Figure 4.5.2). The ice thickness is variated from 145 to 170 cm because of heterogeneous bottom (Figure 4.5.1). There were rafts at some points. Over 3 weeks the ice thickness wasn't changed significantly.

At the strength area ice has the similar structure: the upper layer of granular ice about 20 to 25 cm, then layer of columnar ice about 35 cm then about 6 cm of destructed ice filled water then about 40 to 45 cm of rotten ice then columnar ice underneath (Figure 4.5.2). The main ice thickness was grew from 130 cm to 140 cm over 4 weeks.

Fig. 4.5.1: The bottom layer of ice cover at Main coring area

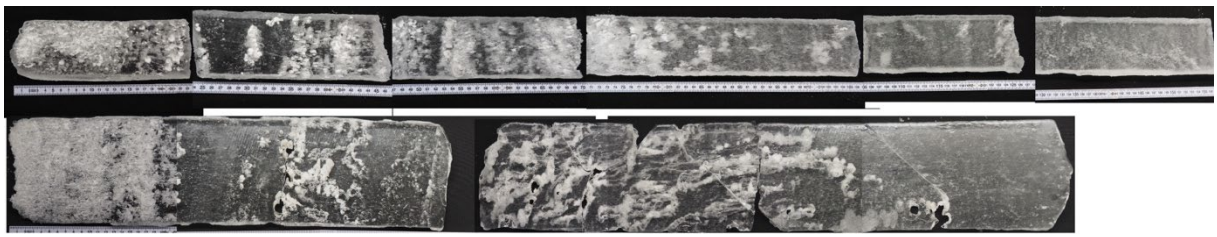

Fig. 4.5.2: Vertical texture sections for FYI from Main coring area (top) and Strength area (bottom) core collected at the middle of leg 5 (5_61). The ice surface is on the left. The ice from Main coring area consists of 15 cm of granular ice then 30 cm of columnar ice, then about 35 cm of rotten ice with many saline inclusions and then columnar layer underneath. Total thickness is 157 cm. The ice from Strength area consists the upper layer of granular ice about 20 cm, then 35 cm of columnar ice then layer of water about 6 cm then about 45 cm of rotten ice with many saline channels then columnar ice underneath. The total thickness is 135 cm.

Figure 4.5.3 below shows the evolution of the salinity, temperature and density profiles for sea-ice from Main coring. Ice was warm, temperature was changed only on top levels staying stable at the rest. Salinity displays the expected profiles: low salinity in upper levels then high increasing at level of rotten ice and then decreasing at low levels with new increasing at bottom.

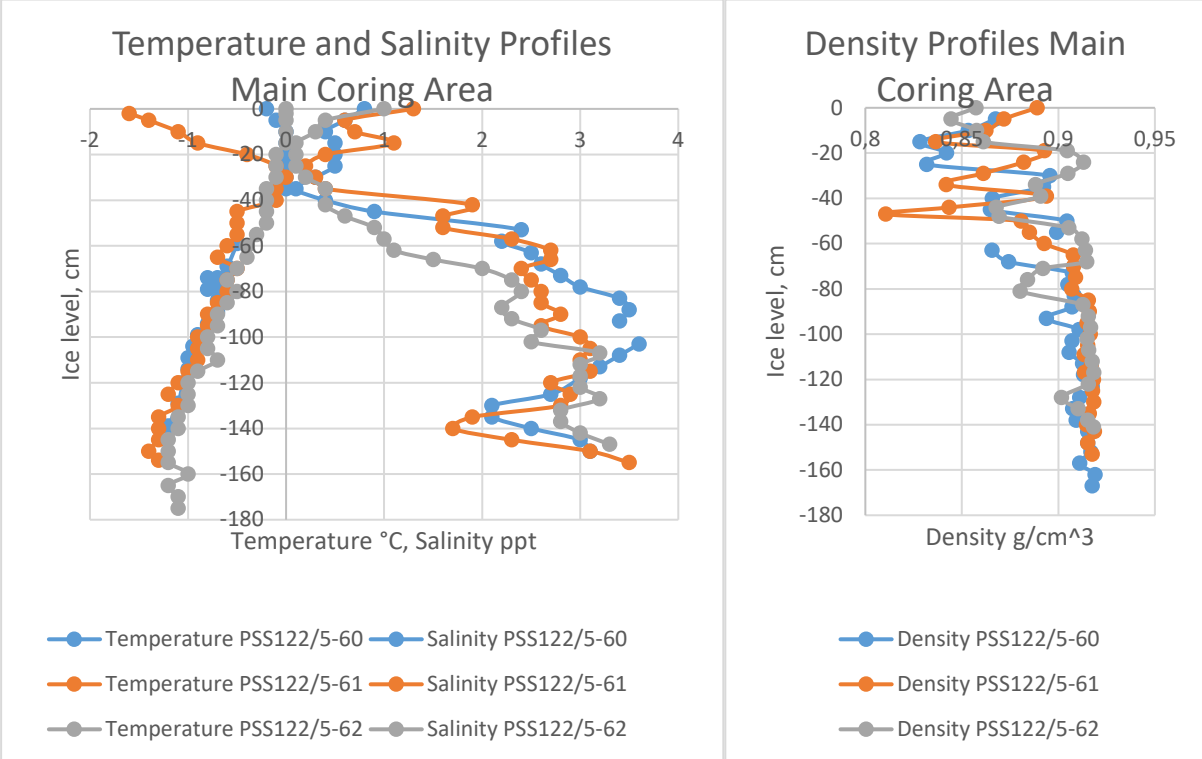

Fig. 4.5.3: Evolution of salinity, temperature and density profiles over a 3-week period for first-year ice at Main coring area.

The ridge ice consists of upper layer of granular ice, about 25 cm, then about 40 cm of columnar with many bubbles, then about 40 cm of columnar ice and after that there was 5 cm of destructed ice filled water. Then there was 25 cm of columnar ice then another destructed layer about 2 to 5 cm and then few meters of columnar ice to the end.

Figure 4.5.4 below shows the salinity, temperature and density profiles for sea-ice from Ridge. Ice was warm, temperature was changed only on top levels staying stable at the rest. Salinity displays the following profiles: high salinity on the top, then low salinity in levels from 20 to 40 cm (0,1 – 0,4 ppt) then high increasing to the level of destructed ice (100 cm) and then stable level of salinity (4 - 5 ppt).

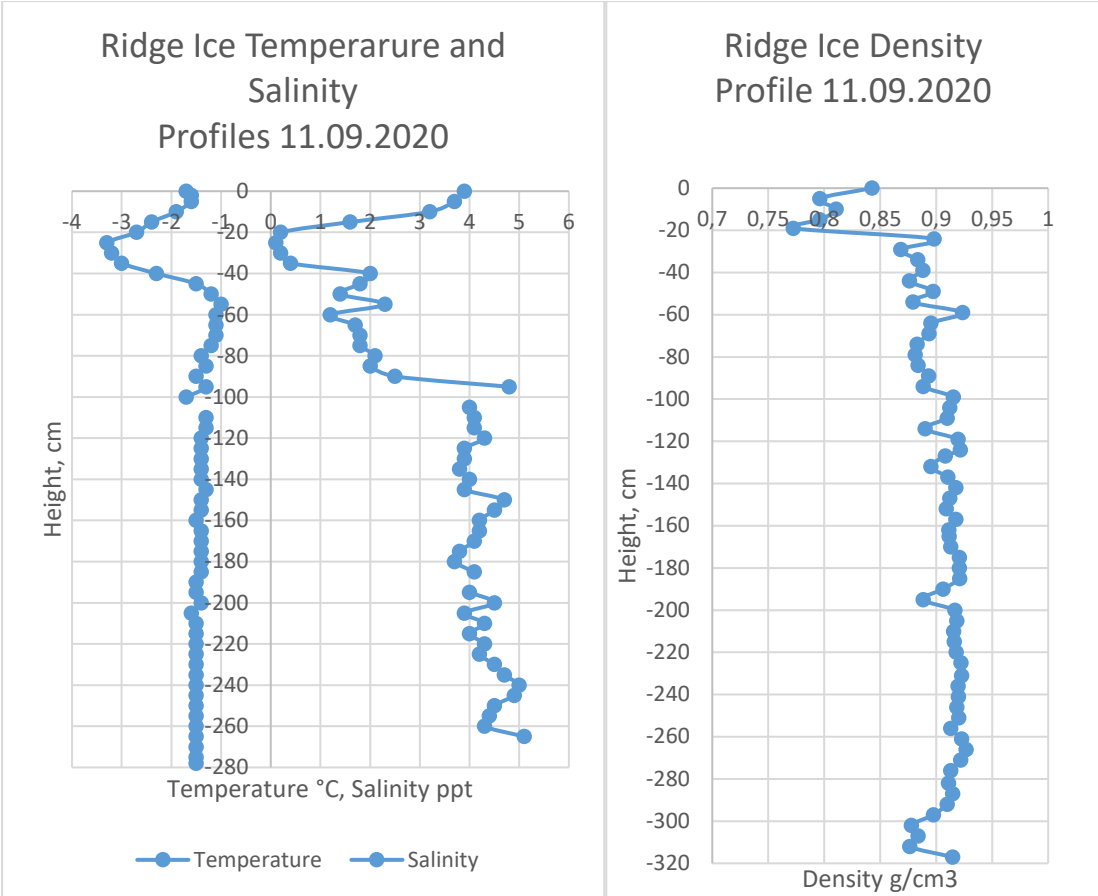

Fig. 4.5.4: Salinity, temperature and density profiles for ice at Ridge area.

The melt ponds have ice on the bottom with upper layer of rotten ice about 40 to 60 cm and then columnar layer underneath. Over three weeks the new ice on the surface grew from 0 to 20 cm.

The lead has new ice on the surface which grew to 20 cm during measurements period.

The ice at first ice station (24.09) has opaque upper level about 10-18 cm and columnar structure underneath. The ice at second and third ice stations (26.09 and 30.09) has layer of destructed and rotten ice in the middle. Figure 4.5.5 below shows the salinity, temperature and density profiles for three ice stations.

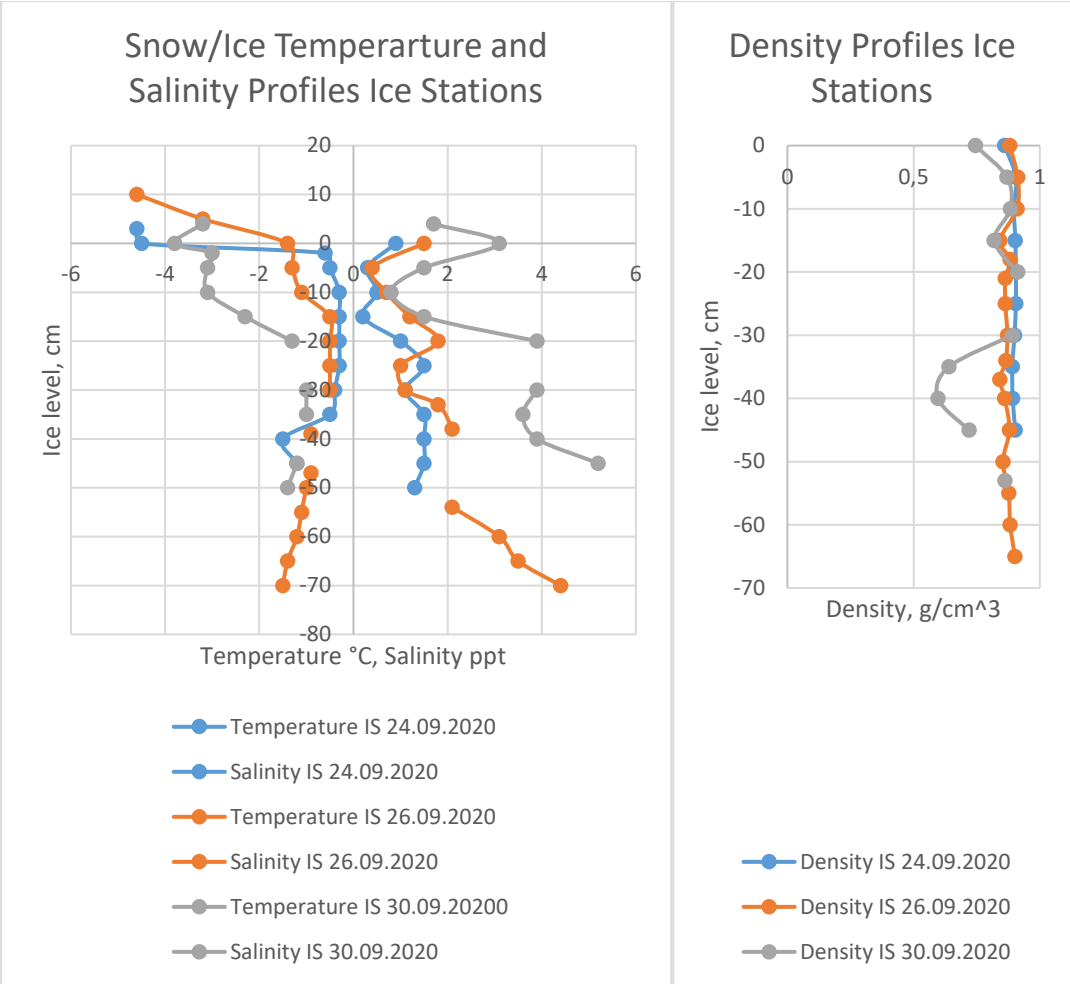

Fig. 4.5.5: Salinity, temperature and density profiles for ice at three ice stations (24.09, 26.09 and 30.09).

Data Management

All data are handled, documented, archived and published following the MOSAiC data policy (see APPENDIX). All data related to a coring event are collocated on the MCS within the folder of the device operation corresponding to the profile end of the corer Kovacs Mark II, 9cm, Kovacs Mark III, 7cm and Kovacs Mark V, 14cm. A scanned copy of the field note and laboratory book will be uploaded. The exhaustive list includes:

Primary data for each ICE, ECO and BGC core transcribes into a spreadsheet (section depths, ice thickness, ice draft, weather, date and time…)

Salinity and density measured on board within 2 days of the coring

Vertical and horizontal texture sections photographed on board during the leg

Tomographic imagery is available on the MCS within a separate subfolder contained in the folder of the X-ray tomographer Scanco90.

Final data products will be stored at the PANGAEA data repository (World Data Center PANGAEA Data Publisher for Earth & Environmental Science (www.pangaea.de)).

4.6 Ice Dynamics

Nikolay Kolabutin[1], Egor Shimanchuk[1], Gunnar Spreen[2], Marcel Nicolaus[3]

(not onboard:) Jari Haapala[4], Andrea Haase[5], Jennifer Hutchings[6], Phil Hwang[7], Victor Smirnov[1]

[1]RU.AARI
[2]DE.UNI-Bremen
[3]DE.AWI
[4]FI.FMI
[5]DE.HSVA
[6]EDU.OREGONSTATE
[7]UK.AC.HUD

Objectives

An overall objective of ice dynamics research at MOSAiC is to deepen the understanding on how pack ice moves and deforms over a full annual cycle. In particular, we are examining spatial and temporal scales of motion and deformation and how those vary regionally and seasonally. We also aim to establish a relationship between deformation scales and physical characteristics of pack ice (in connection with data from IMB buoys, DTC, ice cores etc). The seismic stations obtain data on waves on ice and fracturing of the pack ice for a development of forecast methods for sea ice breaking.

Overview of measurement system

Ice dynamics research is based on the local measurements at the Central Observatory, ice drift observations from the Distributed Network and large scale satellite products.

- GNSS stations (U Hud)
- Seismic stations (AARI)
- Ice radar (FMI)
- Stress panels (HSVA)
- Ice drifters (U Hud)
- Sea ice strength measurements (AARI)

Work at sea

GNSS stations

The GNSS stations measure ice motion on high precision and high sampling rate (1 and 2 s) as well as a constant reference frame for floe-relative coordinate transformations. Four GNSS stations were deployed in the CO on the MOSAiC leg 5 floe: at the Remote Sensing Site (S2), on the way to Ocean City (S6), at the ROV Oasis (S5), and in the ridged area close to Polarstern (S3). The locations are marked with “GNSS” in the floe map in Figure 4.1.4. The GNSS stations were operational between 28 August and 18 September. There are some gaps in the measurement time series because some stations turned off for unknown reasons. Likely this was not due to empty batteries. Stations with only one battery or all batteries exchanged the same time seem to run most stable. Table 4.6.1 gives an overview of the device operations, operation periods of the four stations, and when data was downloaded.

The long name for all buoys in sensor web unfortunately is identical: “GNSS buoy”. The short name, however, provides the GNSS station identification: “GNSS_UoH_SP_S1” to “GNSS_UoH_SP_S6”.

Tab. 4.6.1: List of deployment and operation periods for the four GNSS stations.

Activity - Device Operation	*Timestamp*	*Location*	*Action*	*Comment*

PS122/5_58-59 GNSS_UoH_SP_S2	28.08.20 04:37	Remote Sensing	recording start	Start of GNSS measurements. GNSS RS
PS122/5_58-60 GNSS_UoH_SP_S6	28.08.20 06:07	Ocean City	recording start	Start of GNSS measurements. GNSS OC
PS122/5_58-61 GNSS_UoH_SP_S5	28.08.20 06:28	ROV Oasis	recording start	Start of GNSS measurements at ROV site. GNSS ROV
PS122/5_58-64 GNSS_UoH_SP_S3	01.09.20 08:27	Polarstern	recording start	GNSS PS
PS122/5_58-61 GNSS_UoH_SP_S5	01.09.20 08:57	ROV Oasis	information	Downloaded data and exchanged battery (now 2 at site).
PS122/5_58-60 GNSS_UoH_SP_S6	01.09.20 09:43	Ocean City	information	Downloaded data and exchanged battery (now 2 at site). The GNSS station was off and had only recorded a small amount of data.
PS122/5_58-59 GNSS_UoH_SP_S2	01.09.20 09:53	Remote Sensing	information	downloaded data. Two more batteries (now 3) were added the day before 31.8.2020.
PS122/5_58-60 GNSS_UoH_SP_S6	09.09.20 05:05	Ocean City	information	Station was again off and recorded only 3 days of data. Station broken? Brought the 2 empty batteries back and left 1 new one.
PS122/5_58-61 GNSS_UoH_SP_S5	09.09.20 07:00	ROV Oasis	information	Downloaded data and exchanged 1 of the 2 batteries.
PS122/5_58-59 GNSS_UoH_SP_S2	09.09.20 09:00	Remote Sensing	information	Downloaded data and exchanged batteries. Now two batteries at site.
PS122/5_58-59 GNSS_UoH_SP_S2	10.09.20 10:21	Remote Sensing	information	GNSS station was out of battery for unknown reason (one battery exchanged just yesterday). Exchanged the two batteries with two new ones. Back online 11:04
PS122/5_58-64 GNSS_UoH_SP_S3	12.09.20 09:00	Polarstern	information	Exchanged the two batteries and downloaded data.
PS122/5_58-60 GNSS_UoH_SP_S6	18.09.20 09:34	Ocean City	recording end	End of recording during MOSAiC. Brought GNSS station back onboard.
PS122/5_58-59 GNSS_UoH_SP_S2	18.09.20 09:40	Remote Sensing	recording end	End of measurements during leg 5. GNSS station brought back onboard.
PS122/5_58-61 GNSS_UoH_SP_S5	18.09.20 10:04	ROV Oasis	recording end	End of measurement during MOSAiC leg 5. Brought GNSS station back onboard.
PS122/5_58-64 GNSS_UoH_SP_S3	18.09.20 10:18	Polarstern	recording end	End of measurement during leg 5. Brought GNSS onto the ship.

Seismic stations

Objectives of the seismic observations is to obtain data on waves on ice and fracturing of the pack ice for a development of forecast methods for sea ice breaking. The seismic monitoring method has been developed in the AARI.

For continuous measurements of waves in ice, three seismic stations (Alfa, Beta, Gamma) were deployed close to the Remote Sensing area. The seismic stations have been operational since 23th August 2020. Each station includes seismometer CME 4311, tiltmeter ИН-Д3-360, autonomous recorder “Baykal-8” for logging signals, GPS-antenna, antenna for signal transmission to the base and battery for powering station. Initially all three stations were deployed at one place, then at September 1th Alfa was redeployed at Ocean City Area and Gamma was near to the ROV-City.

Measurements were recorder to the “Baykal-8” data logger with 100 Hz frequency. Data of the seismic stations were also transmitted by the wireless connection to a laptop deployed on-board the Polarstern for a continuous visual monitoring of seismic observations.

Seismic stations have been operationally most of the time. Together, three seismic stations have been recorded 5,38 GByte of data (1,93 GByte from Alfa, 1,47 GByte from Beta, 1,97 GByte from Gamma) during 23th August 2020 to 18th September 2020.

The overview of device operation for seismic is presented in the Table 4.6.2. The devices are pss_alfa, pss_beta and pss_gamma.

Tab. *4.6.2*: An overview of device operations for seismic.

Date (DD.MM.YYYY)	**Area**	**Pss_alfa**	**Pss_beta**	**Pss_gamma**
23.08.2020	Seismic Area RS	PS122/5_59-238		
25.08.2020	Seismic Area RS		PS122/5_59-239	
26.08.2020	Seismic Area RS			PS122/5_59-240
01.09.2020	Ocean City	PS122/5_60-291		
11.09.2020	ROV City			PS122/5_60-290

Ice radar

In order to obtain data of local ice dynamics in high temporal and spatial scale, we used a system which digitizes the raw analogical ship radar data in a manner that echoes from the sea ice features, which normally are considered as a noise in marine applications, are digitized in high resolution. The radar signal digitizing unit, developed by the Imagesoft ltd., was connected to the antenna of the Rutter WAMOS radar. The set-up of the system is similar than used for the N-ICE2015 campaign (Oikkonen et al, 2017).

During the MOSAiC leg 5, processed images of every radar loop have been stored. Interval of those images is about 2 seconds. Digitizing area covers 20 x 20 kilometres area with 8.3 meters horizontal resolution. Continuous recordings during leg 5 began on 15th August 2020 shortly after the start of leg 5 and when we were traveling through the ice. Data collection stopped on 30th September after we left the sea ice. The device operation is “PS122/5_58-84 FMI_Ice_Radar” and all data is stored as daily tar files.

The same data is also digitised by the Rutter WAMOS system in 5-minute intervals and recorded as ship data (not on the MCS).

The CO of the leg 5 ice floe remained stable throughout the one-month drift. However, in the surroundings a lot of ice dynamics was observed and cracks opened and closed on regular basis around the floe. Notes were maintained of all the deformation events observable in the RADAR. These notes are summarized in the preliminary results section below.

There was one glitch in data collection on 2nd September 2020 from about 11:26 to 12:19. About 50 minutes of data files are missing. This 50 minute gap happened also at other instances but always could be recovered from the original data on the server besides in this one case.

Stress panels (HSVA)

No stress panels were deployed in the sea ice during leg 5. However, the stress and temperature sensors deployed in the ship hull in void 92 were all operational during leg 5. The measurements were running unattended during leg 5. Data were downloaded on 10th October 2020 and copied to the MCS. Most of the time the ship had to hold its position relative to the leg 5 ice floe by using thrusters.

The device operation is “PS122/5_58-156 DMS_Logger_HSVA” and contains data of all sensors.

Ice drifters

Around the new ice floe MOSAiC leg 5 a small Distributed Network (DN) of ice drifters was deployed. In total 22 drifters were brought out. 20 of them were PacificGyre Ice Tracker provided by U Huddersfield plus two additional MetOcean SVPs by AWI. Figure 4.6.1 shows the leg 5 DN on 8th October 2020, about 2.5 weeks after *Polarstern* has left the floe. Table 4.6.3 gives an overview of the drifter names, device operations, and deployment dates.

10 of the drifters were deployed on foot within 1 km of the ship on 2nd September 2020. On 6th September one drifter was brought out by helicopter about 9 km north of *Polarstern.* Two more helicopter flights on 7th and 12th September followed when 11 additional drifters were deployed. With that the leg 5 DN consists of 4 drifters at about 4.5 km, 4 at 9 km, and 4 at 28 km distance to the ship. Plus the 10 within the 1 km vicinity of the ship.

This ice dynamic DN will be used to follow the drift of the leg 5 ice floe and its surrounding, and will allow to calculate sea ice deformation at different spatial scales. These are then compared and combined with sea ice deformation obtained by the ship radar (see above) and from SAR satellite images.

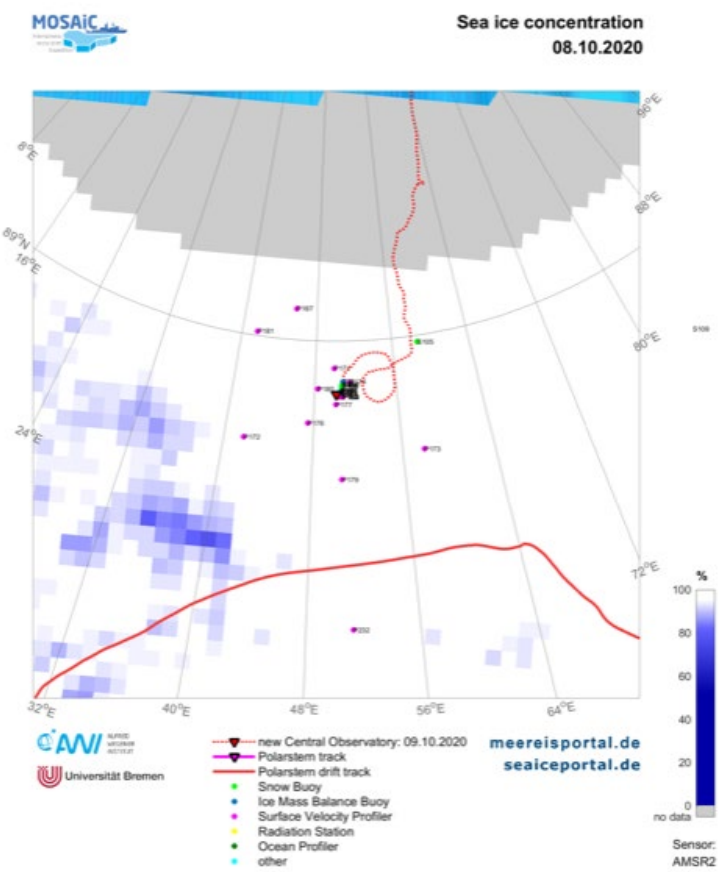

Fig. 4.6.1: During leg 5 a small distributed network (DN) for sea ice dynamics studies was deployed. The map shows the layout of the DN on 8th October 2020, 2.5 weeks after Polarstern had left the floe.

Tab. 4.6.3: Names, device operations, and deployment dates of the ice drifters in the leg 5 DN.

Name	*Original Name*	*IMEI*	*Device Operation*	*Deployment*
2020P162	TUOH-IT-0002	300534061800900	PS122/5_58-82 2020P162	02.09.20 11:35
2020P163	TUOH-IT-0003	300534061801880	PS122/5_58-81 2020P163	02.09.20 11:11
2020P164	TUOH-IT-0004	300534061805870	PS122/5_58-80 2020P164	02.09.20 10:40
2020P165	TUOH-IT-0005	300534061805890	PS122/5_58-76 2020P165	02.09.20 08:49
2020P166	TUOH-IT-0006	300534061806870	PS122/5_58-73 2020P166	02.09.20 05:14
2020P167	TUOH-IT-0007	300534061807880	PS122/5_58-89 2020P167	07.09.20
2020P168	TUOH-IT-0008	300534061809880	PS122/5_58-74 2020P168	02.09.20 05:30
2020P169	TUOH-IT-0009	300534061901380	PS122/5_58-79 2020P169	02.09.20 10:17
2020P170	TUOH-IT-0010	300534061902360	PS122/5_58-77 2020P170	02.09.20 09:06
2020P171	TUOH-IT-0011	300534061902370	PS122/5_58-90 2020P171	07.09.20
2020P172	TUOH-IT-0012	300534061903620	PS122/5_58-100 2020P172	12.09.20
2020P173	TUOH-IT-0013	300534061904360	PS122/5_58-98 2020P173	12.09.20
2020P174	TUOH-IT-0014	300534061904370	PS122/5_58-93 2020P174	07.09.20
2020P175	TUOH-IT-0015	300534061904630	PS122/5_58-75 2020P175	02.09.20 05:57
2020P176	TUOH-IT-0016	300534061905370	PS122/5_58-87 2020P176	07.09.20
2020P177	TUOH-IT-0017	300534061906370	PS122/5_58-92 2020P177	07.09.20
2020P178	TUOH-IT-0018	300534061907360	PS122/5_58-78 2020P178	02.09.20 09:40
2020P179	TUOH-IT-0019	300534061907380	PS122/5_58-88 2020P179	07.09.20
2020P180	TUOH-IT-0020	300534061907610	PS122/5_58-91 2020P180	07.09.20
2020P181	TUOH-IT-0021	300534061908610	PS122/5_58-83 2020P181	06.09.20 04:26
2020P232	SVP	300234068813600	PS122/5_58-99 2020P232	12.09.20
2020P235	SVP	300234068814630	PS122/5_58-97 2020P235	12.09.20

Sea ice strength measurements

Aim of the ice strength measurements is to determine local strength of different ice types and their seasonal variations. Measurements of vertical and horizontal ice strength were carried out according to a methodology developed in Ice Physics Laboratory of the AARI (patent №2348018) and described in “Methodic manual for studying physical-mechanical characteristics of ice formations as initial data for calculation of ice loading on shores, bottom and sea constructions” (SPb, AARI, 2011, p. 179).

For these measurements, a 20 meters x 30 meters area named “Strength“ was reserved. The site contains level first-year ice and it‘s located around 220 meters distance away from the *Polarstern*.

Ice strength measurements were conducted with an automatic hydro complex “ЛГК 131-01” deployed and stored on the Strength Area. There were two types of ice strength measurements: ice local strength measurements and ice uniaxial pressing strength measurements.

Ice local strength measurements were conducted with hydro complex “ЛГК 131-01” and borehole probe-indenter “ЛГЦ095.055.0050.002”. Measurements were carried out in the following way. Firstly, point of measurements was cleaned from snow and air, snow and ice surface temperatures were measured. Then at this point a hole with diameter 250 mm is drilled throughout ice cover. After that the hole was cleaned from brash ice and probe-intenter was deployed on a tripod over the hole. After testing of the system, the probe-indenter was oriented to the selected direction and lowered down into hole on 30 cm depth and first measurement was made. For the second measurement probe-indenter is lowered down to the 60 cm depth, then 90 cm and then 120 cm if the thickness of ice was larger than 135 cm.

Ice local strength measurements in-situ were carried out at 27.08.2020 and 10.09.2020. Four holes were made for the measurements.

27.08 Measurements at the levels 30 cm, 60 cm, 90 cm were made in all holes. Ice thickness in the holes was 130, 128, 125 and 140 cm.

10.09 Measurements at the levels 30 cm, 60 cm, 90 cm, 120 cm were made in all holes. Ice thickness in the holes was 142, 139, 135 and 142 cm.

For a determination of ice temperature, salinity, density and texture, ice cores were taken close to the strength measurement site. For more information and results please see Chapter 4.5 Table 4.5.1.

Ice uniaxial pressing strength measurements were carried out with hydro complex “ЛГК 131-01” and press “ЛГК131.01”. The measurements were carried in a following manner. After cleaning of the surface and temperature measurements, ice cores for vertical ice strength measurements were taken with the “Kovacs” 14 cm ice corer. For the horizontal strength measurements, first a block of ice with dimension of ~ 40 cm x 60 cm x ice cover thickness was taken out and then horizontal ice cores at 30 cm depth was drilled out from that block.

Ice uniaxial pressing strength measurements were carried out at 03.09.2020 and 10.09.2020. Ice cores were cut with the circular saw on 29-30 cm length samples before compressive strength measurements.

03.09.2020 the ice thickness in the measurement site was 134 cm. Horizontal strength measurements were made from 9 samples. For vertical strength measurements there were taken 4 cores. The measurements at upper layer of ice (1 to 30 cm) could not be done because of 20 cm destructed granular ice layer on top. One vertical strength measurement were made from level 32 to 62 cm, one from level 72 to 102 cm, one from level 101 to 127 and 3 other from bottom layer (108 to 134 cm). The rest of vertical samples were broken during the drilling.

17.09.2020 the ice thickness in the measurement site was 140 cm. Due to lack of time horizontal strength measurements were made only from 6 samples at levels 30 and 60 cm. For vertical strength measurements there were taken 3 cores. 3 measurements were made at

upper level (due to cold temperature the granular ice layer on top was refrozen), 3 measurements were made at middle level from 40 to 69 cm and 3 measurements were made at level from 90 to 125 cm.

The overview of device operation for ice strength measurements is presented in the Table 4.6.4. The device is hydro_com.

Tab. 4.6.4: An overview of device operations for ice strength measurements.

Date (DD.MM.YYYY)	Survey Type	hydro_com	Comment
27.08.2020	Strength Area	PS122/5_59-336	Local Strength Measurements
03.09.2020	Strength Area	PS122/5_60-292	UniAxial Pressing Strength Measurements
10.09.2020	Strength Area	PS122/5_61-187	Local Strength Measurements
17.09.2020	Strength Area	PS122/5_62-134	UniAxial Pressing Strength Measurements

Preliminary results

Seismic stations

Much ice events were well captured by seismic stations for example the crack on ice during the strong wind at 05.09-07.09. Figure 4.6.2 shows wind speed during the period 05.09-07.09 and ice oscillations at this period with crack event. Figure 4.6.3 shows ice crack at 06.09 captured by all 3 stations.

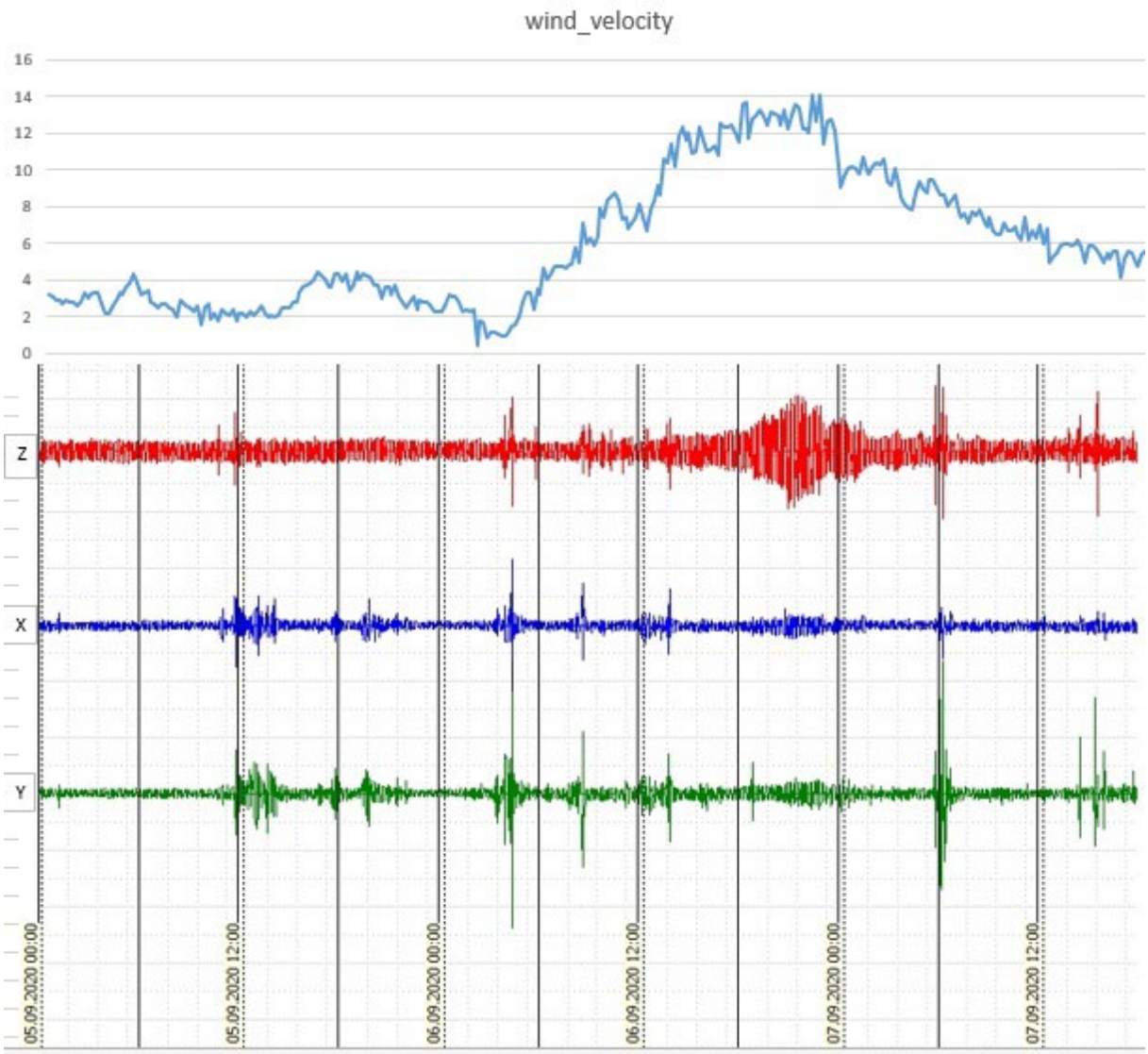

Fig.4.6.2: Appearance of ice cracks during the strong wind 05.09-07.09.

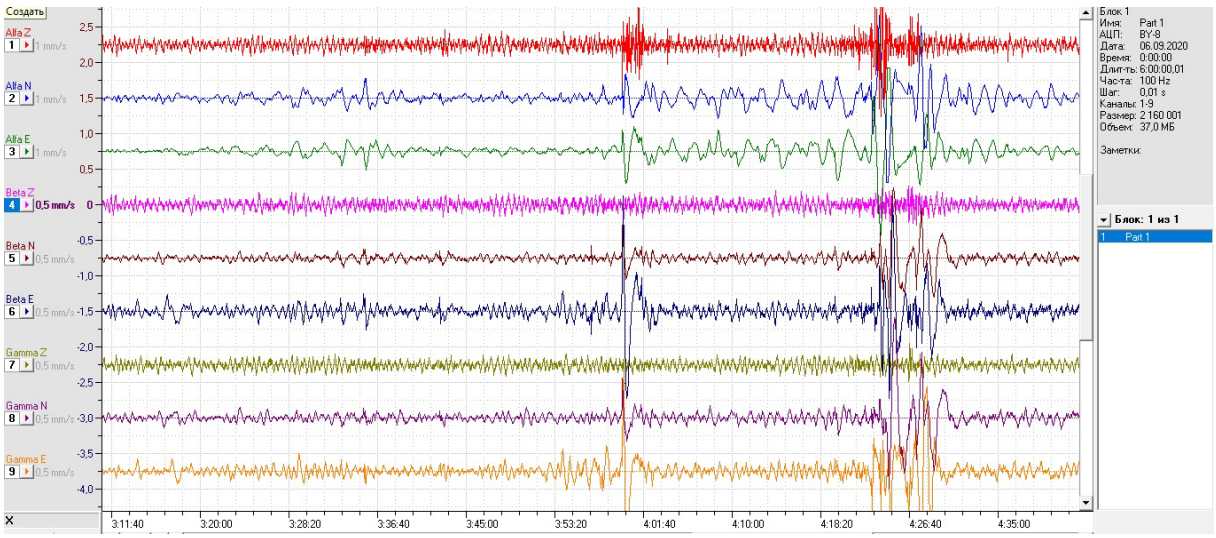

Fig.4.6.3: Appearance of ice crack at 06.09 captured by three seismic stations.

Ice radar

Images from the ship's ice radar are getting digitised by two digitising systems, one operated by FMI and one by AWI. Acquisition with the ship radar started two days after our departure from Tryoshnikov on 15th August 2020 while still sailing through the ice to our new floe.

After we got stationary at our new floe on 21st August one can observe the ice dynamics around the vessel from the radar images. For example, on 13th September the port side lead started to open up, getting about 500 m wide on 14th and closing again on 15th, however, still some open water remained (Figure 4.6.4).

Fig. 4.6.4: Example of ship radar images. Left: The port side crack starts to open on 13th Sep. Middle: Full development of lead on 14th Sep. Right: Partial closing of lead on 15th Sep. Later the lead will open again.

The following sea ice dynamic events were observed in the ship radar images:

20200815, 17:34: start of ship radar recording

20200821, ca. 7:15: at new floe, repositioning of Polarstern in the morning, final position in afternoon

20200822, 16:10 to 17:00: data missing (about 50 minutes)

20200824: opening of lead to starboard; crack through ridge; ice movement along crack starboard

20200826: lead opening on port; closing later again; some movement along the crack on starboard continue

20200828: stronger opening of the lead on port side

20200830: opening and closing of the lead on port side

20200830 evening to 20200831: movement ahead in front of floe followed by port side lead opening

20200901: convergence, lead closing, movement along shear line on starboard

20200902, 11:26 to 12:19: data missing (about 50 minutes)

20200904: lead on port side partly opening; opening of open water areas ahead beyond our floe (approx 1.5 km away)

20200905: divergence continues; crack at 8 o'clock opens and stays open; open water areas at 1 o'clock, in the crack behind ROV

20200906, 22:00: open water areas at 1 o'clock open up to a lead behind ROV.

20200907: ROV lead open up more. A lot of ice dynamics in that area. Lead closes in the afternoon again.

20200908: Ice convergence, ridge building, cracks closing

20200909: Ice movement along shear zone about 3 km away from the ship at 12 o'clock position. Floe region is stable.

20200913: Port side crack opened wide and became a lead. End not visible.

20200914: Also movement on starboard side. Port side lead even opening more in the morning and getting smaller again in the evening but never closing.

20200915: Ice movement in starboard side crack/lead behind CO. Floes moving inside port side lead.

20200917: Lead opening and movement along shear zones 2 km in front of ship

20200918: Port side lead opening up again even more. End outside radar range.

20200919 early morning: More divergence. Port side lead is now more than 500 m wide.

20200919 noon: Convergence. Port side lead closed up but not completely.

20200920, morning: a small crack (1-10 m) has formed through our floe overnight, mainly in west-east direction, originating from the larger crack on the west side of the CO (towards Hinterland). MET city is behind the crack. However, all instruments were removed the day before for our departure today. Strong ice movement along shear zone about 2 km in front of ship.

20200920, 18:00 local (13:00 UTC): departure from floe

Data management

All data are handled, documented, archived and published following the MOSAiC data policy (see APPENDIX). Original ice radar, stress panels and seismic data have been uploaded to the MOSAiC Central Data Storage. Final processed data sets will made available via the workspace section of MCS. Final data products will further be stored at the PANGAEA data repository (World Data Center PANGAEA Data Publisher for Earth & Environmental Science (www.pangaea.de)).

References

Oikkonen A, Haapala J, Lensu M, Karvonen J, Itkin P (2017), Small-scale sea ice deformation during N-ICE2015: From compact pack ice to marginal ice zone, J. Geophys. Res. Oceans, 122, 5105–5120, doi:10.1002/2016JC012387.

4.7 Sea ice and water properties based on ROV surveys

Marcel Nicolaus[1], Julia Regnery[1], Jan Rohde[1], Katrin Schmidt[2], Robert Campbell[3]

(not on board:) Christian Katlein[1], Ilkka Matero[1], Martin Schiller[1], Philipp Anhaus[1], Mats Granskog[5], Knut Vilhelm Høyland[6], Hauke Flores[1], Barbara Niehoff[1], Jutta Wollenburg[1]

[1]DE.AWI
[2]UK.UNI-Plymouth
[3]EDU.URI
[4]EDU.DARTMOUTH
[5]NO.NPOLAR
[6]NO.NTNU

Objectives

The research to be supported with the Remotely Operated Vehicle (ROV) continued the work of Legs 1 to 4 with the same objectives. The focus of Leg 5 was on processes related to autumn re-freezing and new ice formation. As such, we focussed our dives on three ice types: 1) level ice that survived summer melt and was initially covered with melt ponds, 2) the main pressure ridge and other parts of deformed ice, and 3) the newly forming ice, starting from open water in a lead close to the ROV site. Net tows were performed under the level and new ice only (see Section 6ECO.rovnet).

Work at sea

The ROV site (called ROV Oasis, Figure 4.7.1a) was set up approximately 300 meters in front of bow of *Polarstern*. The ROV control hut and the ROV hole (Figure 4.7.1b) were located within 30m from the ice edge (Figure 4.7.1c). The ice hole was used to launch the vehicle (called 'Beast', Figure 4.7.1d) and had a size of 1.5x1.5 m. Initial ice thickness was approx. 1.4m. During the initial set up, a small grid of 9 marker poles was installed. This grid drifted away by 200 to 500 m, hence it was not reachable for re-visits on all dive days and only few markers could be reached towards the end of the observation period. In that case, only individual measurements could be performed. Positioning of the ROV was done through 3 Long Base Line (LBL) transponders installed in depth of approx. 6m (Figure 4.7.1c). The ROV site was connected with a power line to *Polarstern*.

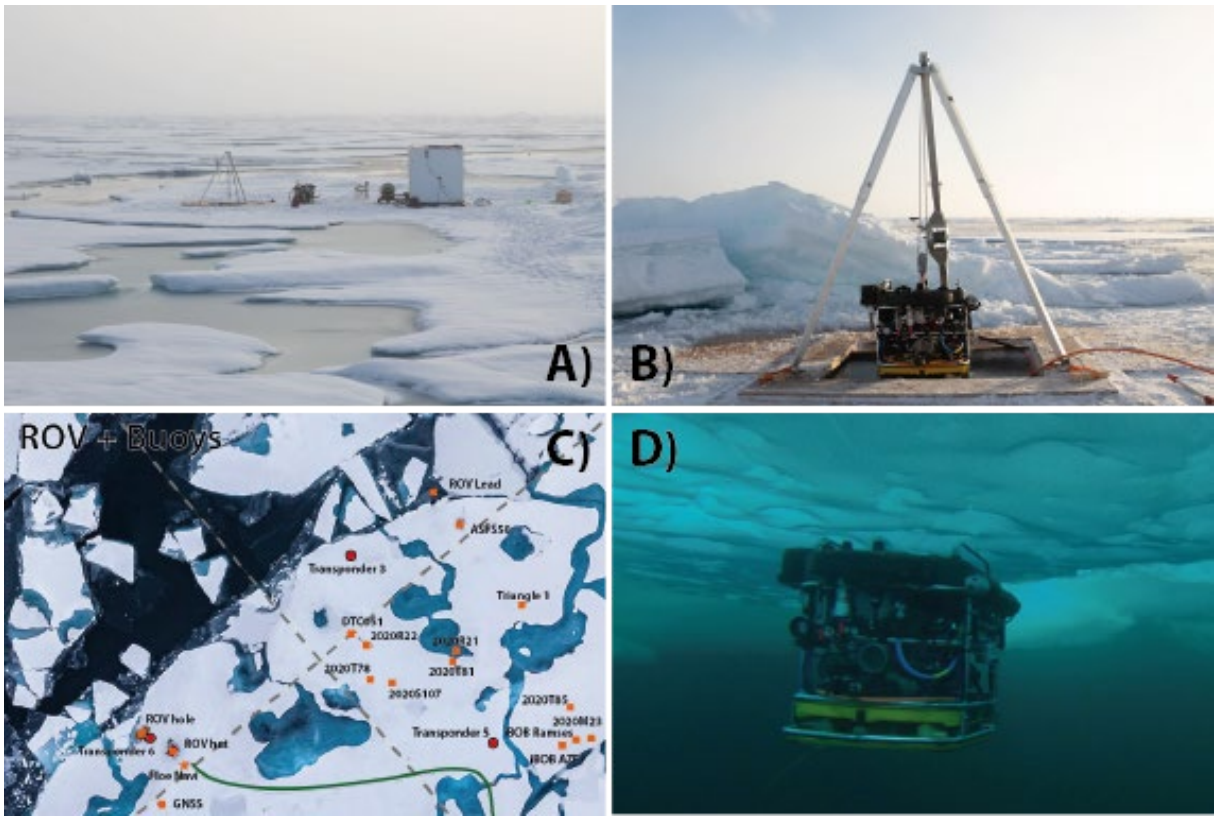

Fig.4.7.1: A) ROV site setup, B) ROV Beast on tripod over launch hole, C) Site map of the ROV site (extract of Figure 4.1.1), D) ROV Beast diving under the sea ice close to the ROV hole.

The ROV (Figure 4.7.1b and 4.7.1d) is a purpose-built measurement platform based on the M500 model (Ocean Modules). Main devices, as described in this report are: A set of two RAMSES-ACC-VIS (TriOs GmbH) spectroradiometers are used for the optics measurements, with one of the sensors mounted on the ROV, and the other one set up for synchronous measurement of apparent light above the surface. A DT101 multibeam sonar (Imagenex) and a PA500 altimeter (Tritech) are used for studying the evolution of the under-ice topography. The ROV platform also includes 3 video cameras, a still camera and a suite of sensors measuring the following parameters: radiance, conductivity, temperature, dissolved Oxygen concentration, pH, Nitrate, Chlorophyll-a, CDOM and backscatter. A full description of the measurement setup is available in Katlein *et al.*, 2017.

We performed 11 ROV dive days during PS122.5 (Table 4.7.1), with an intensified observation period for optical properties on 4 /5 Sep, when 3 dives were performed with approx. 12 hours

time difference. The dive missions continued the missions from all previous legs with the following specifications:

- Optical surveys along markers in 2.5m depth with 25% thruster force
- Optical grids in 2.5m depth with approx. 5m line spacings with 25% thruster force
- Optical depth profiles down to 100m and later 80m when noise levels were reached on both on-board sensors
- Multibeam grids in 20m depth with approx. 25m line spacings with 50% thruster force (one additional high-resolution grid was performed under the ridge with 10m line spacing in 15m depth on 10 September)
- Net tows right at the ice under side (scratching the ice) and in 10m depth for 15 to 30min dive time (see Section 6ECO.rovnet)
- New ice surveys with video inspection dives and additional CTD casts (to 10m depth)
- Video inspection of under-ice installations

Timing and GPS positions of all ROV dives can be found in the device operations under vehicle id “BEAST”.

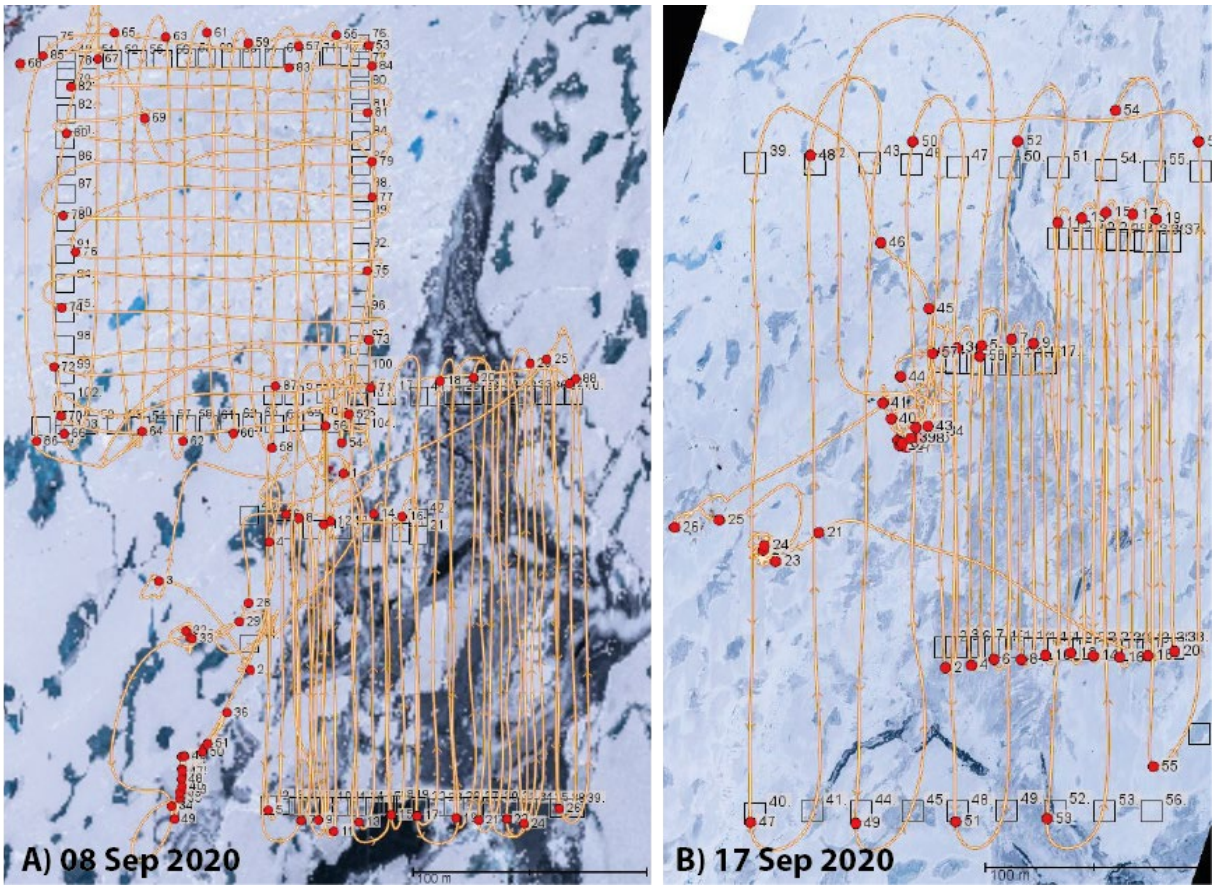

Fig.4.7.2: Exemplary dive maps as overlay on the visual floe maps (see Section 4.1) for 2 dive days: A) 8 September, B) 17 September. Yellow lines are the dive tracks. Red points are attention points for documenting the dive.

Tab.4.7.1: ROV surveys, indicating the dive missions for each day. The intensive observation period on 4/5 Sep stretched over 2 days.

	25 Aug	29 Aug	31 Aug	1 Sep	4/5 Sep	8 Sep	10 Sep	12 Sep	15 Sep	17 Sep

Optics Marker	x	x		x	x	x				
Optics Grid	x	x		x	x	x	x	x	x	x
Optics Depth					x	x	x		x	x
Multibeam Grid	x	x		x		x	x		x	x
Net / SUIT		x				x		x		
New ice					x	x	x			x
Inspection			x						x	x

The ROV site was chosen close to the ice edge in order to enable measurements of both, the re-freezing existing sea ice and the new ice forming from open water in the lead. Hence, ice conditions were only partially stable, because the active lead was changing between 29 and 12 September, while the refreezing afterwards stabilized the ice conditions again. As a consequence, the exact dive pattern for the optical measurements depended on the (variable) ice conditions. The first two dives (25 and 29 August) were performed on the original marker grid, before it moved away relative to the ROV hole. On 1 September, we performed 3 optical grids (see denser grids in Figure 4.7.4a) to connect the former on same grid. After 4 September the optical surveys mostly represent the formation of new ice. Depth profiles were performed under the buoy site, where two spectral radiation stations were installed (see Section 6ECO.rovnet). The multibeam grids made use of the full tether range and the entire area was mapped.

Preliminary results

We observed the changes in light transmittance of the re-freezing existing ice and the new ice growing from 0 to approx. 25 cm in the lead off the floe. Data processing will require to sub-sample the optical grid data for different ice types based on sea ice thickness. This can be well supported by the visual floe maps, as they were taken frequently during the observation period. Light transmittance of the new ice decreased drastically with ice growth and snow accumulation. While major fractions of the thin new ice had transmittance values of 0.3 and above (5 September and before), all ice had transmittance lower than 0.15 during our last dive on 17 September (Figure 4.7.3).

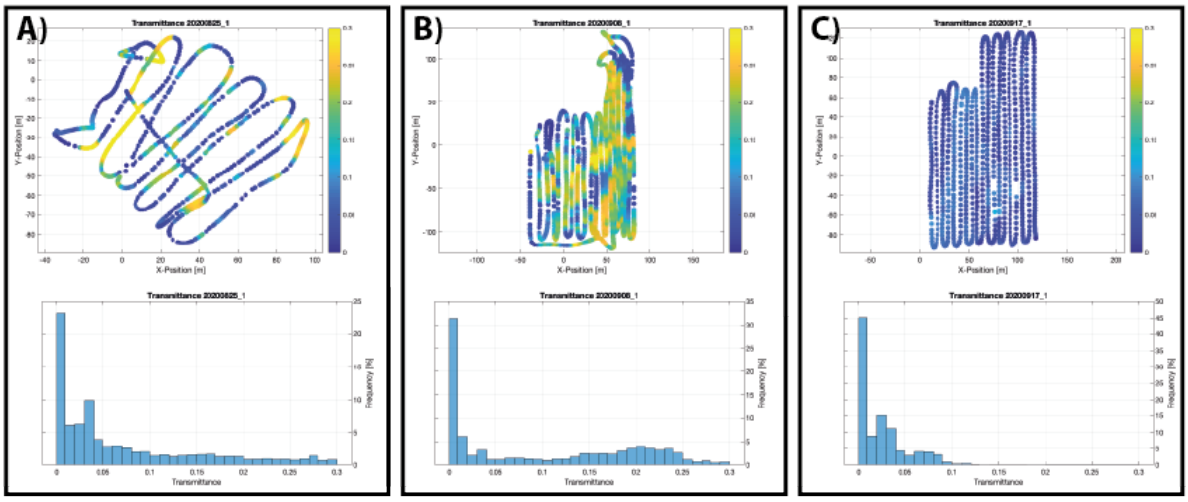

Fig.4.7.3: Light transmittance through sea ice on the optics grids on 3 dive days: A) 25 August, B) 08 September, C) 17 September. Each figure shows the spatial distribution in the top panel and the histogram in the bottom panel.

The multibeam data could only be processed qualitatively so far. Largest changes are visible in the thin/new ice area. Here, the data show the clear contrasts of new ice and remaining pieces of old ice in the lead. Figure 4.7.4 shows exemplary maps of sea ice draft as derived from our multibeam surveys. While the regular dives in 25m depth give a rather coarse image of some parts of the ridged area, the data in Figure 4.7.4b show the high detail of the ice-ocean interface in the ridged part of the floe.

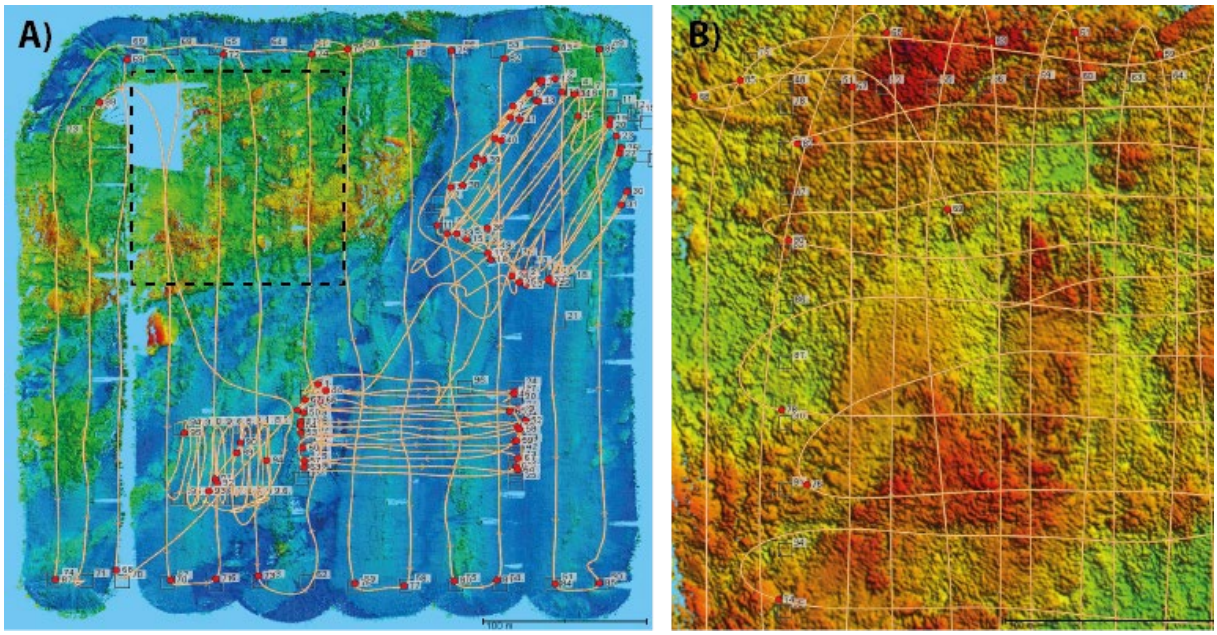

Fig.4.7.4: Sea ice draft maps from of the multibeam sensor. A) Entire survey with 25m line spacing on 01 September, B) Close-up of the ridge area with 10m line spacing on 10 September. The dashed rectangle in A) shows the approx. location of the area from B). Both plots have different colour maps without scaling. Thickest ice (highest draft) is in red and thinnest ice is in blue. Light blue shaded areas are missing data. Yellow lines show dive tracks and red points are attention points to document the ROV dives.

The visual inspections (and recordings) of the ice-ocean interface revealed the transition from summer to autumn freeze-up. We did not observe new sea ice growth at the bottom of the existing ice yet. The under-side remained in a melt stage throughout the observation period. Figures 4.7.5a and b give impressions of the existing old ice at the beginning of the observations. The underside is strongly melted and only little new ice exists along the edges of the old floes. In the beginning, a distinct layer of fresh water was found under the old ice and in the leads. Figures 4.7.5c and d show the accumulation of new ice platelets grown in the freshwater layer attached to the existing ice along their edges as well as thin ice layers in the open leads. The interface between the fresh water on top of the salty layer is visible in the ROV video footage, e.g. in Figure 4.7.5c. CTD data on the fresh water, as well as all other water properties from the sensors on the ROV are not yet calibrated and processed. Towards the end of the observation period, the new ice grew to thicknesses of a few decimetres, depending on the timing of lead formation / dynamics (Figures 4.7.5e and f). In addition, we used the ROV beast for under-ice inspection of autonomous devices (buoys, see Section 4.3) and ocean installations (see Section 5OCEAN.X). We also recorded videos of the under-ice eco-system ranging from algae over zooplankton to a seal (on 25 August). Preliminary results from the net hauls may be found in Section 6ECO.rovnet.

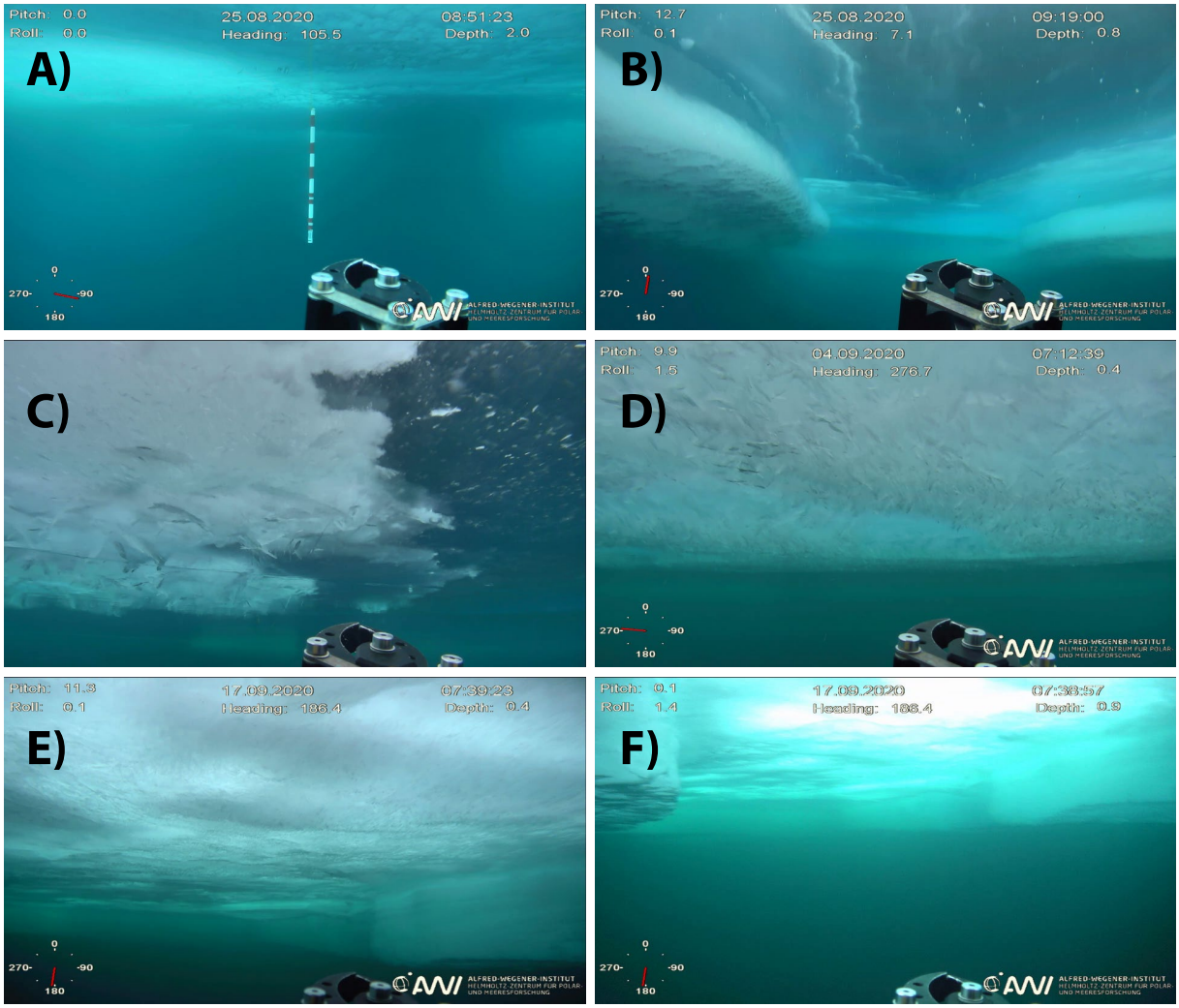

Fig.4.7.5: Still images extracted from the ROV videos. A) Marker pole (1m long) under the old ice on 25 August, B) Edge of the old ice to the new lead on 25 August, C) New ice, platelets at the transition to open water on 5 September, D) Platelet ice accumulation along the edge of an old floe on 4 September, E) New ice on 17 September, F) New ice on 17 September.

Data management

All data are handled, documented, archived and published following the MOSAiC data policy (see APPENDIX). Data recorded on the dives on PS122.5 is stored in the Mosaic Central Storage in the “exdata” folder under the vehicle id “BEAST”. The dive data is stored in separate folders for each device operation. Final data products will be stored at the PANGAEA data repository (World Data Center PANGAEA Data Publisher for Earth & Environmental Science (www.pangaea.de)).

References

Katlein C, Schiller M, Belter HJ, Coppolaro V, Wenslandt D and Nicolaus M (2017) A New Remotely Operated Sensor Platform for Interdisciplinary Observations under Sea Ice, Frontiers in Marine Science, 4(281), doi:10.3389/fmars.2017.002

4.8 Optics

Melinda Webster[1], Felix Linhardt[2], Roberta Pirazzini[3], Henna-Reetta Hannula[3], Marcel Nicolaus[4], Julia Regnery[4], Jan Rohde[4], Michael Gallagher[5], Ulrike Dietrich[4], Mario Hoppman[4], Zoe Brasseur[6], Don Perovich[7]

(not onboard:) Bonnie Light[8], Chris Polashenski[7,9], Christian Katlein[4], Lovro Valcic[X], Mats Granskog[7], Dirk Notz[10], David Brus[3]

[1]EDU.UAF
[2]DE.CAU
[3]FI.FMI
[4]DE.AWI
[5]EDU.CU
[6]FI.UNI-Helsinki
[7]EDU.DARTMOUTH
[8]EDU.UW
[9]USACE/CRREL
[10]DE.UNI-Hamburg

Objectives

A core science question of the MOSAiC observational plan for optics is: how is sunlight partitioned by the sea-ice and snow covers? The specific science questions addressed by Leg 5 measurements are:

- What is the seasonal evolution of apparent optical properties (albedo, transmittance) for representative snow and sea-ice covers during freeze-up?
- How do the high-frequency changes in atmospheric conditions affect the surface and its corresponding albedo (Figure 4.8.1)?
- What are the time-dependent inherent optical properties (e.g., scattering properties) for a variety of observed ice conditions?
- Over what spatial scales are ground measurements representative of the broader area (model grid cell and satellite footprint scales)?

The optics tasks presented in here have strong linkages to many interdisciplinary science questions within the MOSAiC framework:

- Sea ice mass balance: Surface and bottom ablation or lack thereof are strongly driven by the absorption of sunlight.
- Snow metamorphism and surface scattering layer evolution: the changing physical and optical properties of the snow and ice surfaces due to incoming radiation.
- Ocean: mixed layer dynamics are impacted by the partitioning of sunlight by the ice cover.
- BGC: photosynthetic and photolysis processes.
- ECO: primary productivity, photophysiology.
- Airborne and Remote Sensing: hyperspectral, laser and radar altimetry, and scatterometer measurements are strongly tied to surface optical/physical conditions.

The specific questions above are investigated with the following tools:

- Surface albedo surveys
- Surface characterization
- Fixed radiation stations
- ROV transmittance surveys
- Drones and helicopter measurements
- Sea ice cores for optical and texture characterization
- Profiles of optical properties
- Goniometer

This chapter describes measurements made using these tools and presents preliminary results from the albedo surveys and study sites.

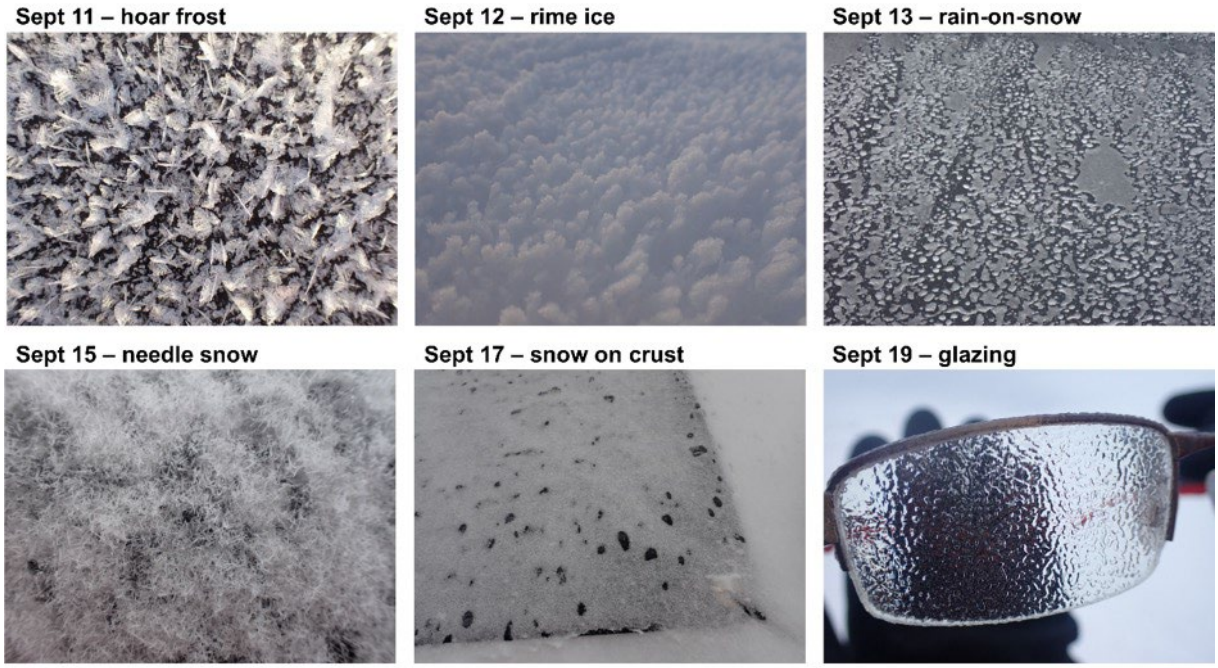

Fig. 4.8.1: Leg 5 experienced a variety of surface conditions, which motivated high-frequency measurements of spectral and broadband albedo. Photos: M. Webster

Work at sea

Ground-based albedo surveys

Spectral and broadband albedo measurements were collected on a near-daily basis from August 21 to September 15. From September 15 to September 19, only spectral albedo measurements were made due to low-light conditions.

Spectral albedo measurements were primarily made with an ASD FieldSpec3 spectroradiometer. The ASD measures radiant energy with a spectral range of 350-2500 nm. Albedos were calculated using the ratio of incident (incoming) to reflected energy at each wavelength. The unit was housed in a backpack with a fiber optic cable extending to the sensor. The sensor was mounted on the end of a 1-m long arm in a gooseneck aimed at a spectralon cosine collector. The device names and URN numbers are listed in Table 4.8.1. Broadband albedo measurements were performed with a Kipp and Zonen albedometer. It consisted of two pyranometers recording the incoming and reflected radiation in the form of an electrical signal measured with a multimeter. This setup was used during Legs 3 and 4. As with Leg 4, the setup was used with a harness and arm to increase mobility and measurement speed (Figure 4.8.2).

During every albedo survey, coincident photographs and snow, surface scattering layer, or melt pond depth were recorded every 5 m using a graduated ski pole and ruler. Melt pond lid thicknesses were measured in circumstances when the measurement process did not disturb the surface.

Tab. 4.8.1: Device names, URN numbers, and number of device operations for optical instruments used during PS122 Leg 5.

Instrument	Device shortname	URN	# device operations
Spectral surface albedo (ASD)	Dart_ASD	pack_ice:ice_ps:dart_asd	39
Broadband surface albedo (Kipps)	Dart_Kipps	pack_ice:ice_ps:dart_kipps	33
Transmittance L-Arm	Larm	pack_ice:ice_ps:larm	8
IOP Probe	IOP_Probe	light_optics:iop_probe	3
Goniometer	Cau_goniometer_1	Pack_ice:ice_ps:cau_goniometer_1	2

Fig 4.8.2: Albedo aristocrats along the Bounty Albedo Line on September 12 with the ASD and Kipps and Zonen albedometer. The ASD was used to measure spectral albedo, while the Kipps and Zonen was used for broadband albedo. Photo: U. Dietrich

A total of three albedo survey lines were established on Leg 5 (Figure 4.8.3): (1) Kinder Albedo Line, (2) Bounty Albedo Line, and (3) Toblerone Albedo Line. The Kinder Albedo Line was most frequently visited with a total of 25 site visits. It was originally 200 m in length, but sheared at the 140-m mark on August 22 and drifted away thereafter. Thus, the time-series was constrained to a 140-m survey line with measurements being collected every 5 m. The Bounty Albedo Line was established for complementary optics measurements with the ROV program (Chapter 4.7). Bounty was 60 m in length and also subjected to the same shearing event as the Kinder Line, leading to a separation from the main floe. As a consequence, the Bounty Line was limited to 6 total visits.

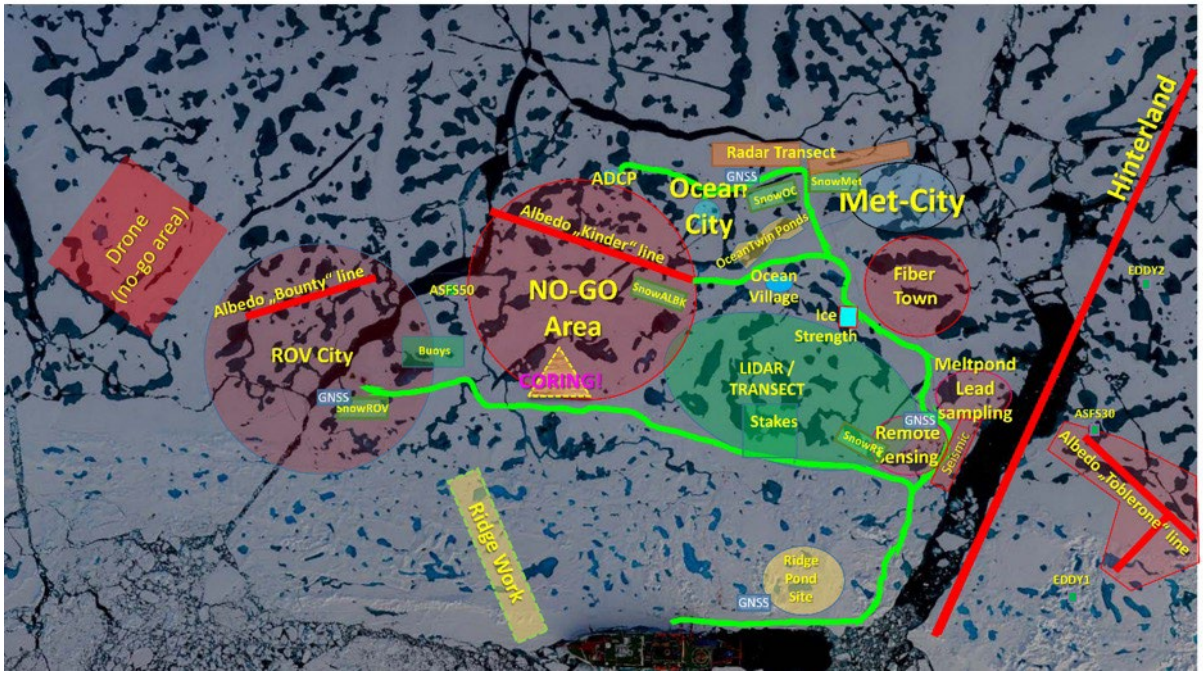

Fig 4.8.3: The Leg 5 floe with the albedo lines shown by the red bold lines, with Bounty on the far left (off-site), Kinder in the middle, and Toblerone on the far right (off-site). Drone images: S. Graupner/C. Finkbeiner.

Midway through Leg 5, a radiation flux sled (Chapter 3.ATMO section) was positioned off-site at 5 o'clock from the RV Polarstern. In coordination with the ATMO Team, the Toblerone Albedo Line was established on September 6 and visited a total of 6 times as a complementary time-series. Unique to the albedo lines, the Toblerone Line was positioned as a "T-shape" with the first 80 m being aligned east-west and the remaining 60 m being positioned north-south into ridged terrain. All albedo lines were established on FYI ranging 1-2 m in thickness (Figure 4.8.4) with the exception of the ridged terrain, which in some sections was greater than 8 m in thickness (Chapter 4.10).

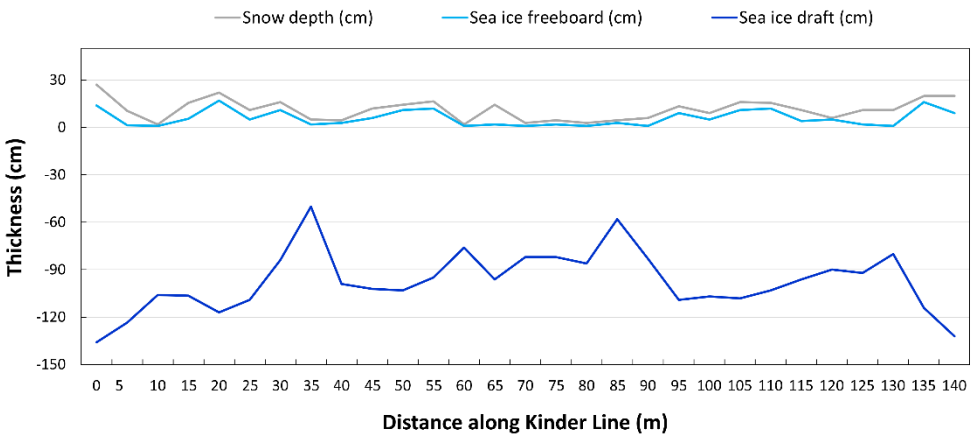

Fig. 4.8.4: Snow depth, ice freeboard, and sea ice draft (derived from freeboard minus thickness) along the Kinder Albedo Line on September 19 from drill-hole thickness measurements. Zero depth represents sea level.

On September 10, a snow target experiment was set up near the Kinder Albedo Line. This entailed establishing a black, 2-m fabric for measuring the effects of variable snowfall and

rainfall on surface albedo. On September 14, a secondary target was placed in close proximity to the first target. These results overlapped with the intensive observation period of September 14-15 (reference intensive observation period sub-chapter) and are particularly insightful for evaluating the rain-on-snow event.

Radiation stations

Two spectral radiation stations were installed at the buoy site (Figure 4.1.4 and close-up in 4.7.1). They consisted of 3 spectral radiometers (Ramses, TriOS GmbH, Germany), 2 of them installed above the surface to measure incident and reflected irradiance and 1 of them hanging under the sea ice to measure transmitted irradiance.

Station 2020R22 was installed on 1.34 m thick white ice and used the same set up as the former station 2020R15 (PS122.4). The under-ice sensor was hanging in approx. 2.4m depth, about 1m under the sea ice. The system recorded spectra on a memory card in 10min intervals and was recovered on 19 September, shortly before departure. The station is shown in Figure 4.8.4a with the under-ice sensor hanging under the ice in the middle between the tripod and the wooden pole to the left.

Station 2020R21 was installed in/under a melt pond close by on 27 August (Figure 4.8.4b). Beyond the Ramses sensors, the station also consists of a light chain, a snow height pinger, a camera and a tiltmeter for the surface sensors. Also, a SIMBA type thermistor buoy (2020T81, see Section 4.3) was co-located with the thermistor string hanging next to the light chain (Figure 4.8.4c, yellow Peli Case). Figures 4.8.4c and d show the surface evolution at the station during the drift, more details of the surface conditions and the freeze-up history are available from Section 4.1. Station 2020R21 remained at the floe after departure and reports all data by Iridium.

The FMI broadband radiation station was installed on 28 August in the Met City area, with the downward facing instruments located over a melt pond. The station includes upward and downward facing pyranometers and pyrgeometers to measure the surface shortwave and longwave radiative budgets, as well as an upward facing SPN1 sunshine pyranometer to measure the diffuse global radiation. The station operated until 18 September. More details on these measurements are provided in the Section 3.4 of the ATMOS Chapter.

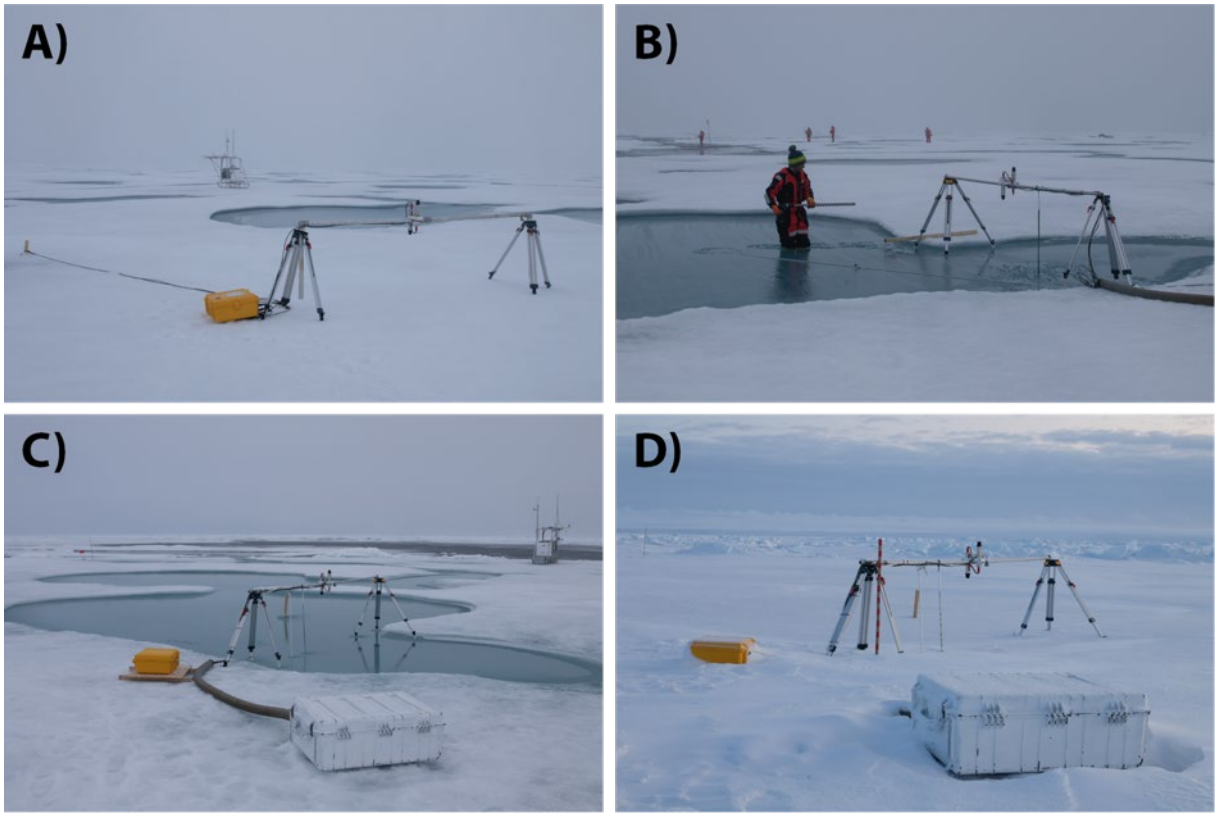

Fig. 4.8.5: Radiation stations on the main buoy site: A) 2020R22 after installation on 21 August, B) 2020R21 after installation on 27 August, C) 2020R21 on 31 August when the melt pond was completely open, D) 2020R21 on 19 September after freeze-up and new snow.

Aerial albedo measurements

Aerial albedo measurements and maps of surface topography are needed to characterize the distribution of the various surface types and to determine how they contribute to the areal-averaged albedo over different horizontal scales (Podgorny et al., 2018). These measurements will also enable the derivation of relationships between the albedo measured from ground-based platforms, which typically have metre-to-tens-of-meters footprint, and satellite observations or large-grid model outputs.

Two drones were operated during Leg 5 (Figure 4.8.6): the drone SPECTRA, equipped with paired Kipp and Zonen CM4 pyranometers measuring broadband albedo and paired Ocean Optics STS VIS (350 – 800 nm) and NIR (650-1100 nm) micro-radiometers measuring visible and near-infrared spectral albedo, and the drone Mavic 2 Pro equipped with camera to perform photography mapping of the area measured by the SPECTRA drone. The two drones were mostly operated in synergy: first, a photography mapping of the target area from an altitude of 40/50 m was performed with Mavic 2 Pro while the instruments of the SPECTRA drone were running to reach the thermal equilibrium with the ambient temperature. Then, if the Mavic drone did not experience icing on the propellers and thus did not activate a forced landing, the SPECTRA drone was operated for up to three consecutive flights, each of them lasting approximately 20 minutes. In addition, extra mapping with Mavic 2 Pro was performed over the ROV, Met City and Hinterland regions (see Figure 4.8.3) where fixed broadband or spectral radiation stations were installed, and low altitude (3 m) mapping flights to derive surface roughness at higher spatial resolution were carried out over the snow sites located at ROV, Met City, and Remote Sensing.

Figure 4.8.7 illustrates the approximate flight areas and flight paths of the two drones: the Mavic 2 Pro drone was guided along a serpentine pattern (yellow lines) to reach a high overlap

(ideally about 80%) between the photos and, thus, enable the derivation of the 3D surface topography through image processing. The SPECTRA drone was mostly guided along repeated transects at 5 m, 10 m, and 30 m elevations (red dashed lines on the left side of Figure 4.8.7) over an area that was originally in front of the ROV hut and included ROV markers (red flags) and a buoy, but on 30 August, it detached from the main floe and drifted few hundred meters away (Figure 4.8.7). Vertical profiles of albedo with SPECTRA hovering for 1-2 minutes at 5 m, 10 m, and 30 m were repeatedly carried out at the locations marked with red dots (Buoy, Red flag, Lead, Flat First-year Ice in Figure 4.8.7). This area also included the Bounty Albedo Line (see subsection above) established along the ROV markers, where ground-based spectral and broadband albedo were repeatedly measured. One SPECTRA flight was also carried out over Hinterland (red dashed line on the right side of Figure 4.8.7) with a vertical profile approximately in the middle of the Toblerone Albedo Line.

Fig. 4.8.6: Photos of the two drones with their respective pilots: R. Pirazzini with SPECTRA on the left (photo from J. Rohde), and H.-R. Hannula with Mavic 2 Pro on the right. Photo: L. Nixon

Two mapping flights with Mavic 2 Pro were carried out also during the transit toward the ice floe, before reaching the North Pole, and one flight on the ice station #2 along the “short transect” (Chapter 4.4). Altogether, 17 flights were carried out with SPECTRA during 8 days, corresponding to ~5 flight hours, and 35 flights with Mavic 2 Pro during 18 days, corresponding to ~11.5 flight hours. Table 4.8.2 summarizes date and location of the flights performed with SPECTRA (red crosses) and Mavic 2 Pro (orange crosses).

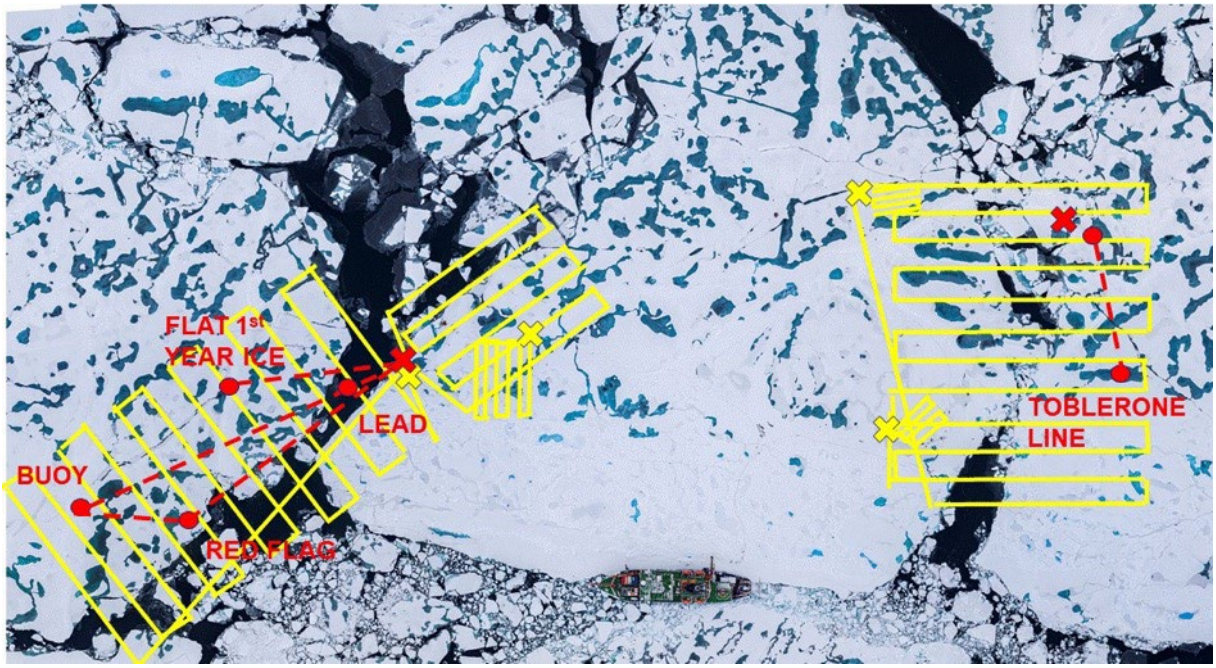

Fig. 4.8.7: Photo of the measurement area on 6 September 2020 (photo from S. Graupner & C. Finkbeiner): the flight patterns of the Mavic 2 Pro drone and of the SPECTRA drone are marked in yellow and dashed red lines, respectively. Yellow and red crosses mark the taking off and landing points of the two drones, while red dots mark the locations of hovering and vertical profiles measured with SPECTRA.

Tab. 4.7.2: Date and location of the flights performed with the drones SPECRA (red crosses) and Mavid 2 Pro (orange crosses).

	Transit	ROV Markers area	ROV Rad Stations	ROV snow site	Met City	Met City snow site	RS snow site	Hinterland	Ice Station 2
18-Aug	x								
21-Aug					x	x	x		
25-Aug		x							
29-Aug		x, x			x				
31-Aug		x, x							
01-Sept		x, x							
02-Sept		x							
04-Sept		x, x	x						
05-Sept		x	x	x					
07-Sept					x	x	x		
08-Sept		x, x		x					
10-Sept		x							
11-Sept		x, x		x					
12-Sept		x						x, x	
15-Sept					x	x	x	x	
17-Sept		x							
26-Sept									x

Many challenges were faced when operating the drones: the moist and freezing air conditions often prevented the flights, as ice quickly formed on the propellers. Moreover, the proximity with the geographical North Pole made the navigation systems very unreliable and unstable, especially in the case of the big SPECTRA drone that has a relatively big inertia and it requires more time to correct unexpected drifts. Therefore, take-off, landing, and part of the flights with SPECTRA were carried out in manual mode, without GPS positioning, and compass-driven mode was switched on/off several times until SPECTRA was stable enough also in the compass-driven mode. The detachment of the target area from the main floe made it difficult to repeat the flights over the same targets (distances from the starting point were changing, and sometimes the targets were hardly visible), and the drift of the ice floe during the flights required continuous adjustments of the loitering positions (in the case of SPECTRA) and of the lateral shifts in the serpentine pattern (in the case of Mavic 2 Pro). When temperatures dropped below -5°C, it became difficult to keep fingers warm and thus able to operate the sticks of the radio-controller for 20 consecutive minutes. Finally, the solar elevation decreased throughout the observing period, with a consequent decrease in the signal to noise ratio in the broadband radiation measurements and an increase of the integration time in spectral irradiance measurements. The SPECTRA drone was therefore not operated after 12 September, when solar elevation did not exceed 5 degrees.

Complementary data

See Table 4.8.3 for device operation codes of selected complementary data sets.

- Surface characterization

The surface scattering layer or snow was characterized along the albedo lines, which is described in more detail in Chapter 4.2.

- Mass Balance

Mass balance surveys were conducted on the Kinder Grid Transect as part of the MOSAiC Leg 5 Transect Program (Chapter 4.4). Snow depth and melt pond depths were measured using a magnaprobe, while sea ice thickness was derived from GEM-2 measurements. Kinder Grid was visited once a week between August 24 and September 19.

- ROV Optics

The ROV completed under-ice transmittance grids as part of its regular dive plan. The optical measurements of the ROV are described in detail in Section 4.7.

- L-arm measurements

Transmittance of light through sea ice was measured a number of times during the exit transit using an articulated L-Arm setup. The setup utilizes TriOS RAMSES spectro-radiometers to measure incoming and reflected irradiance above the ice surface, as well as transmitted irradiance below the ice. The under-ice sensor is lowered through a 9-cm coring hole, and then horizontally extended one meter via the L-arm. The ice core is bagged and stored for further analysis (HPLC and chl-a, see Chapter 6.ECO X.X). To capture the local variability of light transmittance through the ice, the L-Arm is rotated ~45° for four to five times per core hole. Eight of these measurements were collected during the first two ice stations on the Leg 5 return transit.

- IOP probe

An inherent optical properties (IOP) probe was used to measure the scattering profiles of ice at coring locations. Three full profiles were made in conjunction with FYI optical cores. The first series was collected at the main coring site on the Leg 5 floe. The remaining two series were collected at ice stations during the exit transit.

- Optics and texture sea-ice cores

Optics cores were collected at the FYI coring site and opportunistically at targeted sites. Opportunistic optics cores include: 3 from the Kinder Albedo Line, 8 coincident with L-arm measurements, and 2 from melt ponds during destructive sampling BGC ponds (refer to BGC/ECO melt pond chapter). Laboratory analysis of these cores for scattering and transmittance properties will be conducted after the completion of the MOSAiC field program. The work related to sea ice cores extracted for optical and texture studies are described in (Chapter 4.5).

- Melt pond program

Melt ponds were surveyed for spectral albedo and remote sensing reflectance with the Stickle setup (device cau_stickle_1, see Chapter 4.9), which provides similar output to the ASD: incoming and reflected irradiance, therefore yielding albedo. Additionally on board is a third spectrometer with a narrow viewing angle, to allow for retrieval of remote sensing reflectance (hemispherical-directional reflectance in nadir direction).

- Goniometer

The spectro-goniometer was deployed twice. During the first deployment one full run was completed. The second run, as well as the second deployment had to be aborted due to mechanical problems with the goniometer device. The goniometer was attached via USB to and controlled by the Raspberry Pi based cau_notecam_1 device. Therefore, the data on MCS is logged under this device name.

- Hyperspectral camera

The hyperspectral camera suffered from technical issues and thus was not operational during Leg 5.

- Destructive Sampling

On September 19, drill-hole thickness measurements, optics cores, NIR images, and snow micropen data were collected along the Kinder Albedo Line. The corresponding thickness results are shown in Figure 4.8.4.

- BGC melt ponds

Spectral albedo was measured at the BGC ponds on 2 September in coordination with the BGC and ECO teams (reference BGC/ECO melt pond chapter). Measurements were made with the ASD and the Stickle setup (logged under the device operation PS122/5_60-293; see also Chapter 4.9 Ponds).

Preliminary results

Ground-based albedo surveys

The optics data characterize the evolution of the surface albedo of the MOSAiC Leg 5 Central Observatory during sea-ice freeze-up, as well as during synoptic events. Figure 4.8.8

demonstrates the trajectory of the broadband albedo over a melt pond during freeze-up. Figure 4.8.9 shows two time-points during the spectral albedo time-series, going from open melt ponds and a prevalent surface scattering layer to refrozen melt ponds and a comparatively thicker snow cover.

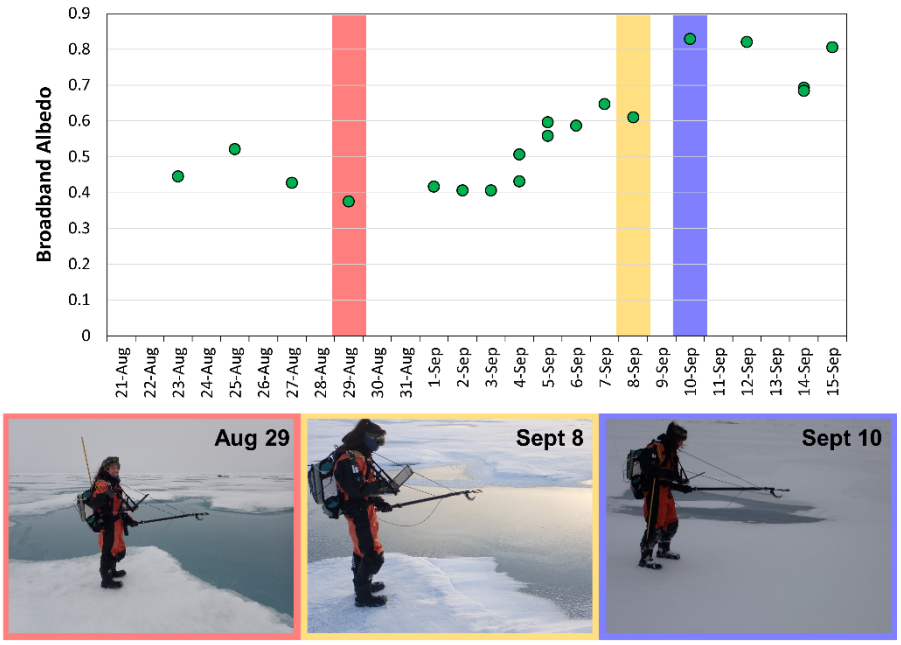

Fig. 4.8.8: Time-series of the broadband albedo from a melt pond on the Kinder albedo line during freeze-up. The surface transitioned from open ponds (August 29), to refrozen ponds (September 8), and lastly to snow-covered ponds (September 10). Photos: F. Linhardt

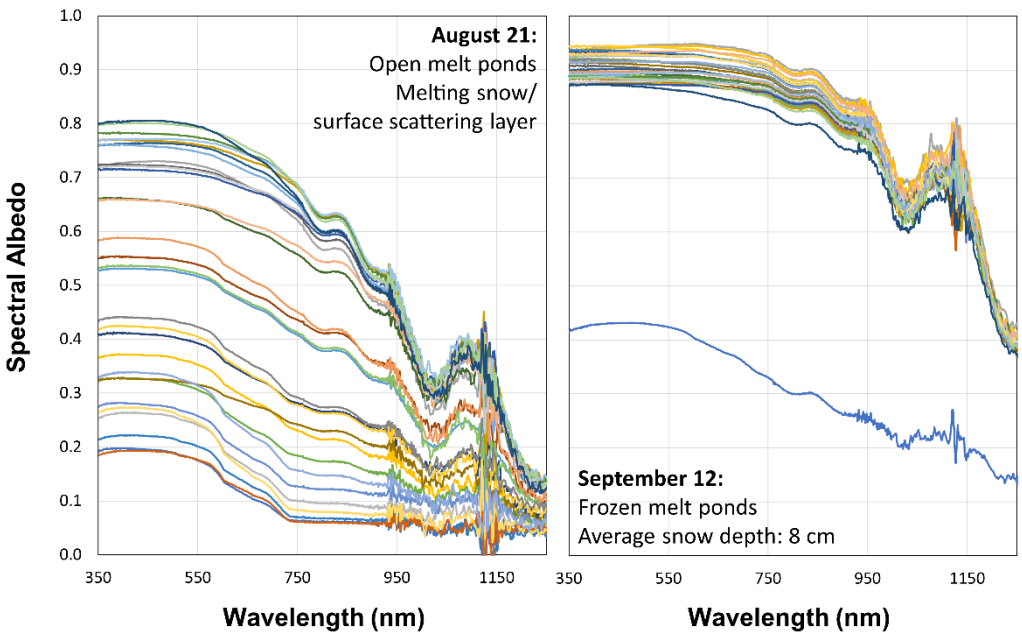

Fig. 4.8.9: The spectral albedos from every 5-m mark along the Kinder albedo line on August 21 (melting state) and September 12 (frozen state). Approximately 48% of the Kinder albedo line was ponded. By September 12, all melt ponds were frozen over and snow-covered.

The progression of the freeze-up season during Leg 5 was non-linear. Synoptic events brought melting conditions and rain-on-snow in the midst of freeze-up, which subsequently affected the physical and optical properties of the surface (Figures 4.8.10 and 4.8.11). These high-frequency changes were well-captured during the intensive observational period (refer to intensive obs chapter) during which the Kinder Albedo Line and Snow Target Experiment were sampled twice daily (Figure 4.8.12).

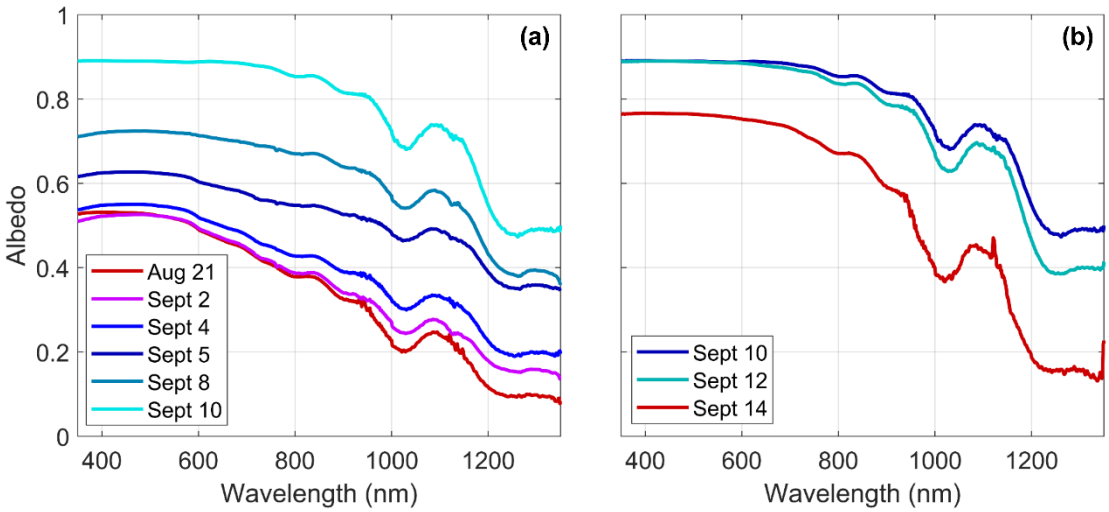

Fig. 4.8.10: Time-series of the average spectral albedo from the Kinder Albedo Line: (a) The albedo time-series corresponds to the transition from melt to freeze-up, from mostly open melt ponds to a snow-covered, frozen state; (b) the effects of rain on snow on spectral albedo over the course of four days. Freezing conditions and snowfall resumed after September 14.

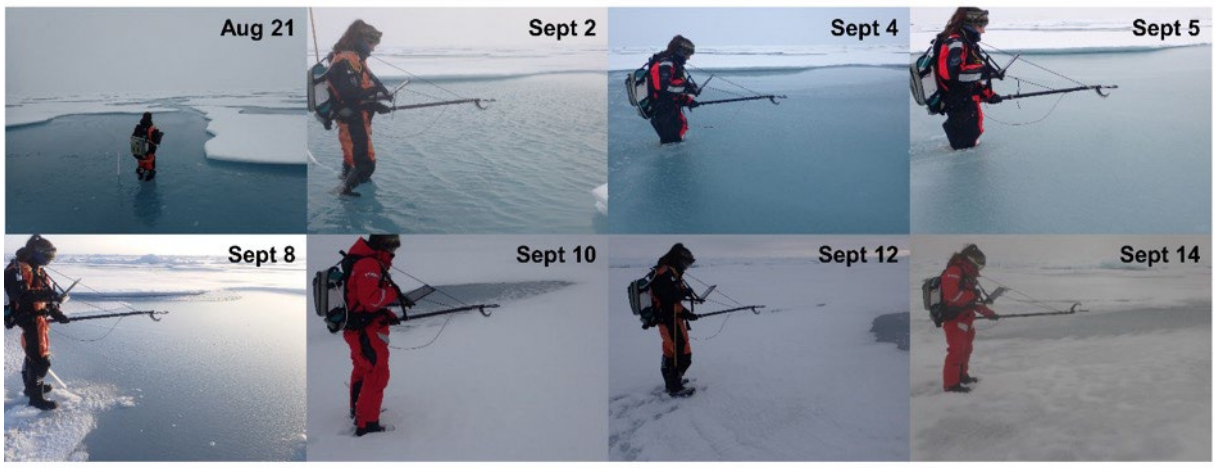

Fig. 4.8.11: Time-series of the surface conditions corresponding to the albedo measurements in Figure 4.8.8. Photos: F. Linhardt

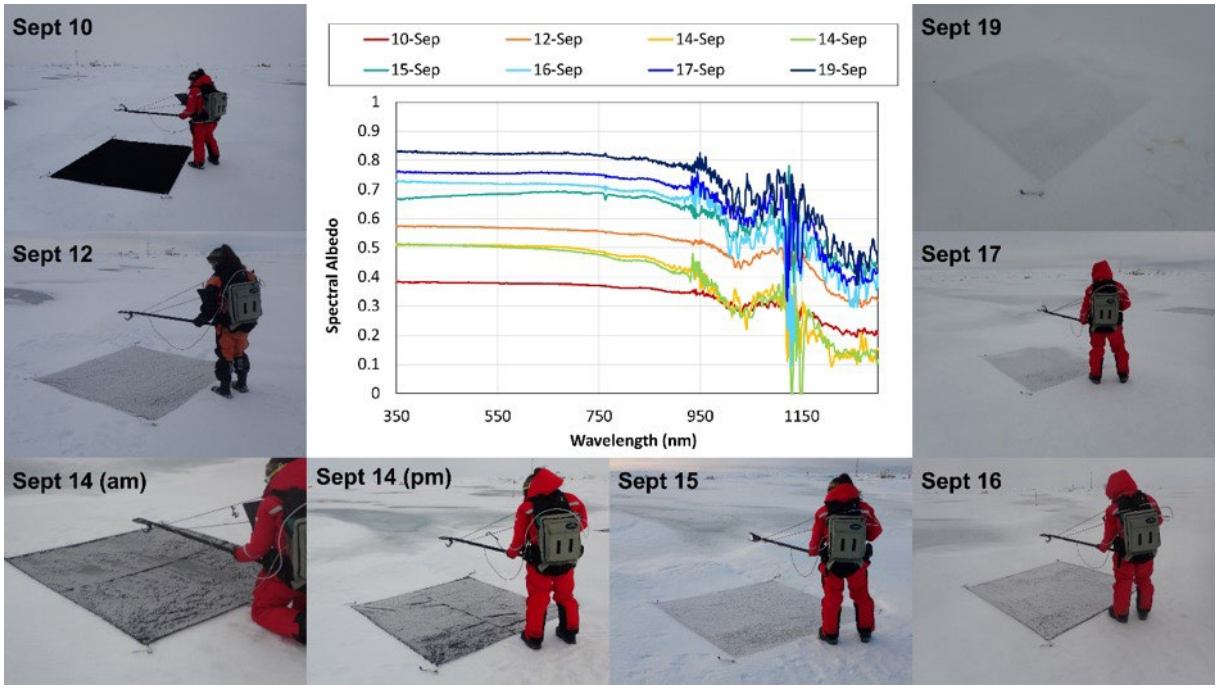

Fig. 4.8.12: Spectral albedo from the snow target experiment on September 10-19. During this period, precipitation changed from scant snowfall to above-freezing temperatures and rainfall, then transitioned back to below-freezing and light snowfall conditions. Photos: F. Linhardt

Aerial albedo measurements

The data collected with SPECTRA still need to be thoroughly checked and uncertainties properly assessed and accounted for, so no conclusion can be based on these unprocessed data. However, from a very preliminary look into some of the collected data (Figure 4.8.13), it appears that areal-averaged albedos measured at the elevation of 5 m and 10 m above sea level have a larger variability than the areal-averaged albedo measured at the elevation of 30 m (red lines in Figure 4.8.13). A certain degree of albedo variability is unavoidable even during hovering at 30 m because it is not possible to keep the drone over the same surface while the ice is drifting. However, the fact that on 1 September and 4 September, the 30-m albedo was similar even over different targets may suggest that the 30-m albedo is not significantly affected by the individual surface features and, therefore, it is potentially representative for satellite footprint and model grid area. It is also worth noticing that the 30-m albedo measured on 1 September and 4 of September was around 0.4, consistent with the average albedo value measured along the Kinder Albedo Line in the same period, although on 11 September, the 30-m albedo was clearly lower than the mean albedo along the Kinder Albedo Line. The study of the topography maps that will be derived from the Mavic 2 Pro photos and the analysis of the whole dataset will provide a better ground to interpret these results.

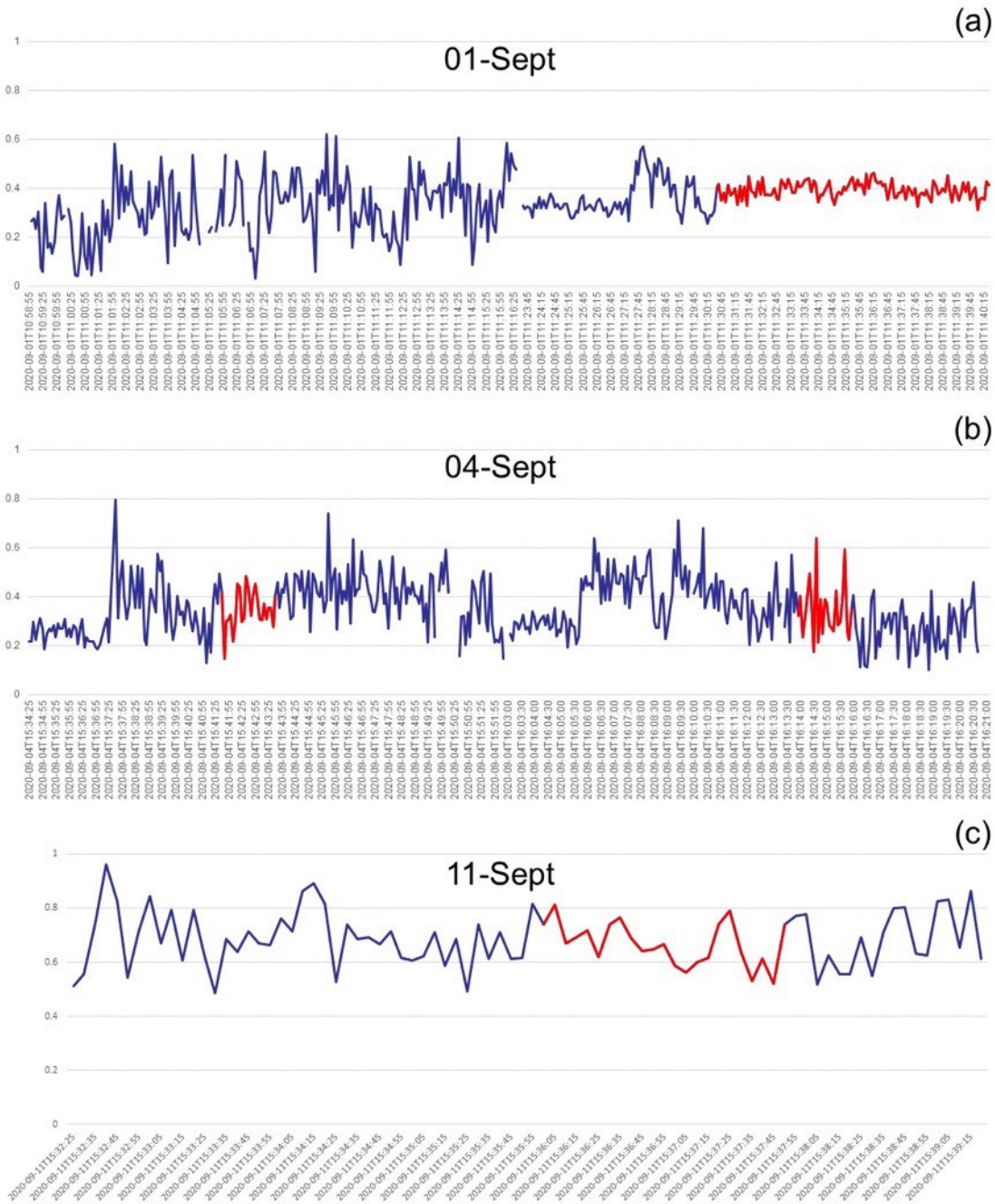

Fig. 4.8.13: Time series of broadband albedo measured with SPECTRA during selected flights on 1 September (a), 4 September (b) and 11 September (c). Red lines correspond to albedo measured at 30 m above sea level.

Data management

All data are handled, documented, archived and published following the MOSAiC data policy (see APPENDIX). Albedo data (ASD and Kipps) is stored in the Mosaic Central Storage under mcs\platforms\pack_ice\ice_ps\dart_asd\exdata\PSS122-5_xx_xxx and mcs\platforms\pack_ice\ice_ps\dart_kipps\exdata\PSS122-5_xx_xxx. Table 4.8.4 lists the DSHIP event identification numbers. Corresponding pictures are stored in separate folders for each device operation. Each folder also includes an excel spreadsheet with recorded metadata for a given set of observations, including who made the measurements, sky conditions, photo

numbers, surface characterization measurements, and other notes. Please refer to the excel spreadsheet for the appropriate photo credit information. If a photographer is not listed, refer to the cruise report and this chapter or the data set following the MOSAiC data policy (DSHIP and MSC).

The SPECTRA drone metadata spreadsheet is stored in the MCS folder mcs\platforms\fmi_spectra_copter\exdata, while the irradiances and all other measured ancillary data are stored in the folders listed in Table 4.7.5. In each folder, data are distributed in separate folders according to their DSHIP number. The explanation on the DSHIP events is provided in the metadata spreadsheet. The metadata spreadsheet for the Mavic 2 Pro drone is stored in the MCS folder mcs\platforms\uav\fmi_mavic2pro_drone\exdata. All photos taken with the Mavic 2 Pro drone are also in the same folder, distributed in separate folders according to their DSHIP number.

Albedo and core optics data will be stored at the Arctic Data Centre following the agreement between ADC and the MOSAiC Project lead. DOIs will be communicated to PANGAEA for later access via the future MOSAiC Data Portal. The rest of the data will be stored at the PANGAEA data repository (World Data Center PANGAEA Data Publisher for Earth & Environmental Science www.pangaea.de.

Tab. 4.8.3: Table of DSHIP numbers for complementary measurements during PS122 Leg 5.

Instrument	DSHIP ID	Date	Location	Comment
L-Arm	63-265	24-Sep	Ice station 1	Measurements in 5 core holes near coring site
L-Arm	63-266	26-Sep	Ice station 2	Measurements in 3 core holes along the remote sensing transect
IOP-Probe	62-18	14-Sep	Leg5 coring site	Coring site, Leg5 floe
IOP-Probe	63-45	24-Sep	Ice station 1	Coring site, ice station 1
IOP-Probe	63-112	26-Sep	Ice station 2	Coring site, ice station 2
Goniometer	60-274	03-Sep	Leg5 floe	1 full run, 1 run aborted
Goniometer	61-310	08-Sep	Leg5 floe	Aborted
Stickle	60-293	02-Sep	BGC-Ponds	Collocated with ASD data 122/5_60-54

Tab. 4.8.4: Table of DSHIP numbers for spectral and broadband albedo measurements during PS122 Leg 5. Please note that AM1 (09:00-11:30), PM1 (13:00-15:30), PM2 (15:30-17:30), and PM3 (17:30+) represent the working hours at local ship time.

Instrument	DSHIP ID	Date	Location, Local Time	Instrument	DSHIP ID
ASD	59-191	21-Aug	Kinder PM3	**Kipps**	59-192
ASD	59-236	23-Aug	Kinder PM1	**Kipps**	59-237
ASD	59-394	24-Aug	Kinder PM3	**Kipps**	59-395
ASD	59-401	25-Aug	Kinder AM	**Kipps**	59-402
ASD	59-403	25-Aug	Bounty PM1	**Kipps**	59-404
ASD	59-405	27-Aug	Kinder PM1	**Kipps**	59-406
ASD	59-407	29-Aug	Kinder PM1	**Kipps**	59-408
ASD	59-409	29-Aug	Bounty PM2	**Kipps**	59-410
ASD	60-14	31-Aug	Bounty AM	**Kipps**	60-15
ASD	60-20	1-Sep	Kinder AM	**Kipps**	60-21

ASD	60-53	2-Sep	Kinder AM	**Kipps**	60-56
ASD	60-54	2-Sep	BGC ponds AM	**Kipps**	N/A
ASD	60-55	2-Sep	Bounty PM1	**Kipps**	60-57
ASD	60-152	3-Sep	Kinder AM	**Kipps**	60-153
ASD	60-154	4-Sep	Kinder AM	**Kipps**	60-155
ASD	60-156	4-Sep	Kinder PM3	**Kipps**	60-157
ASD	60-158	5-Sep	Kinder AM	**Kipps**	60-159
ASD	60-160	5-Sep	Kinder PM3	**Kipps**	60-161
ASD	61-46	6-Sep	Toblerone PM2	**Kipps**	61-47
ASD	61-48	6-Sep	Kinder PM3	**Kipps**	61-49
ASD	61-50	7-Sep	Kinder AM	**Kipps**	61-51
ASD	61-52	8-Sep	Kinder AM	**Kipps**	61-53
ASD	61-54	8-Sep	Toblerone PM1	**Kipps**	61-55
ASD	61-108	9-Sep	Kinder PM2	**Kipps**	61-109
ASD	61-218	10-Sep	Kinder AM	**Kipps**	61-219
ASD	61-220	11-Sep	Toblerone AM	**Kipps**	61-221
ASD	61-222	12-Sep	Bounty AM	**Kipps**	61-223
ASD	61-224	12-Sep	Kinder AM	**Kipps**	61-225
ASD	61-226	12-Sep	Toblerone PM1	**Kipps**	61-227
ASD	61-228	13-Sep	Snow target PM1	**Kipps**	61-229
ASD	62-49	14-Sep	Kinder AM	**Kipps**	62-50
ASD	62-51	14-Sep	Kinder PM3	**Kipps**	62-53
ASD	62-58	15-Sep	Kinder AM	**Kipps**	62-59
ASD	62-60	15-Sep	Toblerone PM1	**Kipps**	62-61
ASD	62-172	16-Sep	Kinder AM	**Kipps**	N/A
ASD	62-174	17-Sep	Kinder AM	**Kipps**	N/A
ASD	62-176	17-Sep	Toblerone PM1	**Kipps**	N/A
ASD	62-178	19-Sep	Kinder AM	**Kipps**	N/A
ASD	62-180	19-Sep	Bounty PM1	**Kipps**	N/A

Tab. 4.7.5: Table listing the SPECTRA data and the Mosaic Central Storage folders in which they are stored.

DATA	FOLDER
Incoming broadband shortwave flux	mcs\platforms\uav\fmi_spectra_copter\cm4_up
Reflected broadband shortwave flux	mcs\platforms\uav\fmi_spectra_copter\cm4_dn
Upper gimbal accelerometer and gyroscope output	mcs\platforms\uav\fmi_spectra_copter\mpu_up
Lower gimbal accelerometer and gyroscope output	mcs\platforms\uav\fmi_spectra_copter\mpu_dn
Gps output	mcs\platforms\uav\fmi_spectra_copter\spectra_gps_bn_180_1
Downward spectral VIS irradiance	mcs\platformsuav\fmi_spectra_copter\sts-vis-up

Upward spectral VIS irradiance	mcs\platforms\uav\fmi_spectra_copter\sts-vis-dn
Downward spectral NIR irradiance	mcs\platforms\uav\fmi_spectra_copter\sts-nir-up
Upward spectral NIR irradiance:	mcs\platforms\uav\fmi_spectra_copter\sts-nir-dn

References

Podgorny I, Lubin D, Perovich DK (2018) Monte Carlo Study of UAV-Measurable Albedo over Arctic Sea Ice. Journal of Atmospheric and Oceanic Technology, 35(1): 57-66.

4.9 Ponds

Felix Linhardt[1], Gerit Birnbaum[2] [1]DE.CAU
(not on board:) Natascha Oppelt[1] [2]DE.AWI

Objectives

The overarching goal of the melt pond measurements campaign is to optically characterize melt ponds at in-situ scale and to facilitate upscaling of the gathered metrics to airborne and spaceborne observations.

Parameters of interest are inherent optical properties (IOPs) of the ponds as well as physical properties such as pond depth, sea-ice thickness and pond bottom structure.

In the data evaluation phase, the field observations will be coupled with the helicopter measurements, which yielded RGB and hyperspectral images, as well as ice thickness and surface topography data. Moreover, the field measurements will be used to validate satellite derived products such as pond depth as well as spectral radiance [W/m² µm sr] and reflectance [%] of the snow and ice surfaces neighbouring the ponds in the wavelengths region 400 to 2500 nm.

Work at sea

Instrumentation

Melt pond spectra were obtained with two different setups. The *Böötle* setup consists of a self-propelled, remotely-controlled measurement platform, primarily carrying three spectroradiometers to obtain downwelling irradiance above and below the waterline, as well as upwelling radiance below the waterline. The *Böötle* further carries an acoustic depth sensor for assessing two-dimensional pond depth data in the field.

The Stick (or *Stickle*) setup is comparable with an ASD setup (see chapter 4.7 Optics), i.e. person-mounted, measuring down- and upwelling irradiance. An additional spectrometer for measuring upwelling radiance is also attached to the stick. The *Stickle* setup can be used on snow and ice surfaces to measure spectral albedo and reflectance, but can also be used to measure reflectance of ponds. When used at pond sites, the setup is usually used together with a ruler for measuring pond depth and sometimes a drill set and thickness gauge to measure sea ice thickness. Accompanying measurements include in situ water temperature, conductivity and chlorophyll concentration. Water samples were taken and analysed in the lab to assess chlorophyll concentration and CDOM (coloured dissolved organic matter).

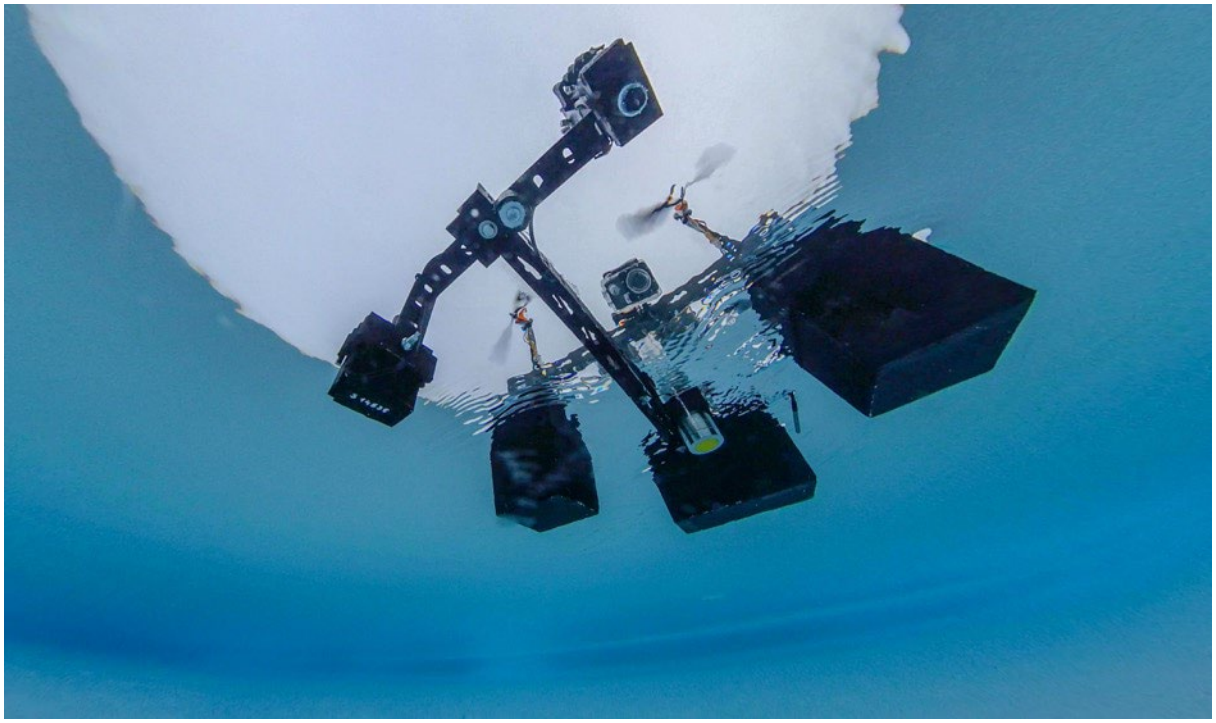

Fig. 4.9.1: Böötle seen from below (Photo: Lianna Nixon).

Locations

Pond work was conducted at several sites throughout the Leg 5 MOSAiC floe, (see figure 4.9.2):

- *Bubbly Lagoon* was the first pond to be measured. Within the first days at the floe a lead opened and separated the pond from the main floe, preventing further access.
- *Pondifex* melt pond was located next to Fiber Town. It remained the only pond to be surveyed by *Böötle*. At its shore a radative flux station by Team ATMO was deployed, monitoring long and shortwave radiation in incoming and outgoing directions.
- *Ocean Twin Ponds* was the main site for the two ice lid removal experiments, as well as a bottom ice thickness drilling transect.
- *Bali Pond* was located in the ridged area, close to the vessel.
- *BGC Ponds* were visited once to complement measurements by Teams BGC and ECO with optical data.

Sampling

In total, *Böötle* had one deployment, while *Stickle* had eleven deployments.

Tab. 4.9.1: Overview of pond work device operations.

Device Operation	Date	Main device	Location / Comment
PS122/5_59-480	2020-08-23	cau_stickle_1	Bubblylagoon
PS122/5_59-482	2020-08-28	cau_stickle_1	Pondifex and Ocean Twins
PS122/5_59-483	2020-08-29	cau_stickle_1	Balipond
PS122/5_60-273	2020-08-31	cau_boeoetle_1	Pondifex
PS122/5_60-293	2020-09-02	cau_stickle_1	BGC-Ponds

PS122/5_60-275	2020-09-03	cau_stickle_1	Ocean Twins
PS122/5_60-276	2020-09-04	cau_stickle_1	Ocean Twins and Balipond
PS122/5_61-311	2020-09-08	cau_stickle_1	Pondifex
PS122/5_61-312	2020-09-12	cau_stickle_1	OceanTwins
PS122/5_62-256	2020-09-17	cau_stickle_1	Albedo Toblerone Line
PS122/5_62-257	2020-09-19	cau_stickle_1	Albedo Kinder Line
PS122/5_62-258	2020-09-19	cau_stickle_1	Albedo Bounty Line

Water samples were collected on several occasions. Lab analysis is done with an Avantes spectrometer, with either an integrating cavity or a liquid waveguide capillary setup. The table below shows the samples taken – at the time of this writing, lab analysis is ongoing, but will be logged with reference to the original sampling device operation.

Tab. 4.9.2: Overview of pond work related water samples.

Device Operation	Date	Location / Comment
PS122/5_59-355	2020-08-28	Pondifex
PS122/5_59-356	2020-08-28	Ocean Twins
PS122/5_59-481	2020-08-23	Bubbly Lagoon
PS122/5_61-313	2020-09-12	Ocean Twins

Experiments

On August 28th a short drilling transect through *Ocean Twin Ponds* was done to retrieve water depth and bottom ice thickness.

Two ice removal experiments were conducted at *Ocean Twin Ponds* to investigate the optical effect of the ice lid's presence.

On September 4th the ice lid had a thickness of approximately 2cm, and the pond had not yet frozen over completely. The measurements on September 12th were done on 15cm thick ice. On that date, also a MicroCT sample of the pond lid and water samples were taken.

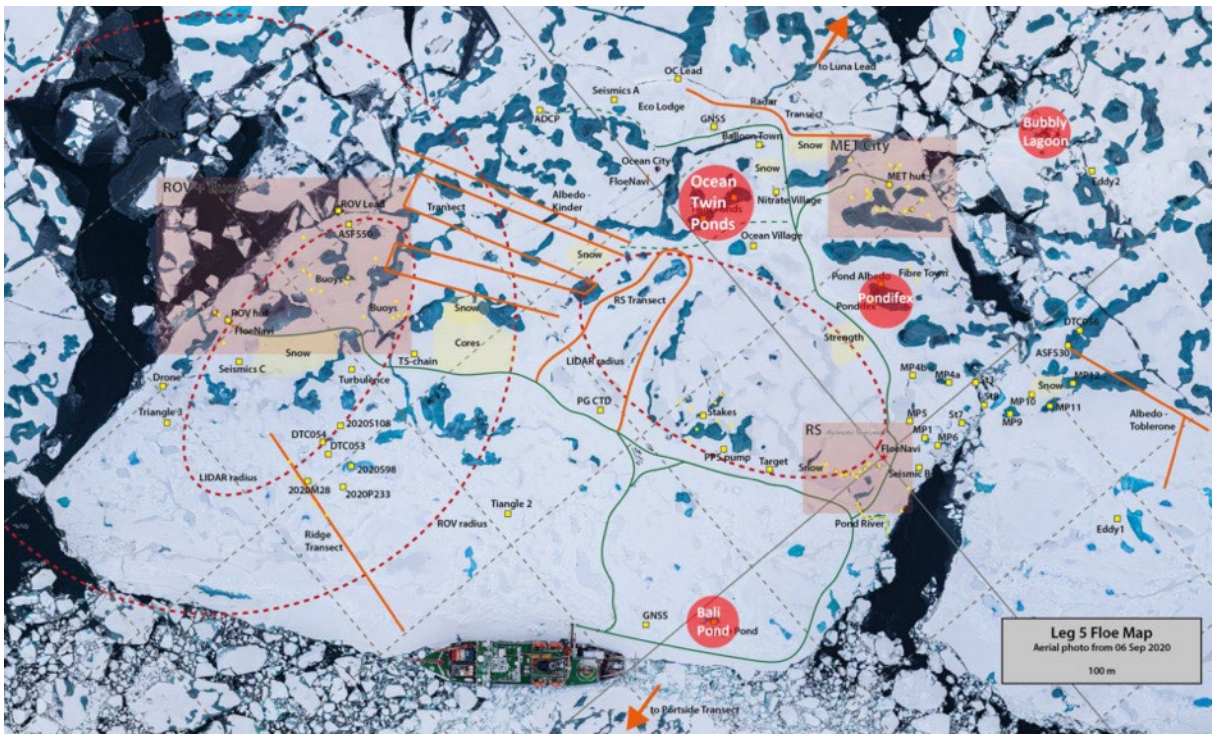

Fig. 4.9.2: General floe map with marked out pond areas. (Map: Marcel Nicolaus)

Preliminary results

To quantify the spectral signature of melt pond water and melt pond bottom, spectrometric lab analysis was conducted. One example spectrum can be seen in figure 4.9.3. The displayed values are referenced to pure water, therefore resulting in the absorption spectrum of all non-water constituents of that sample.

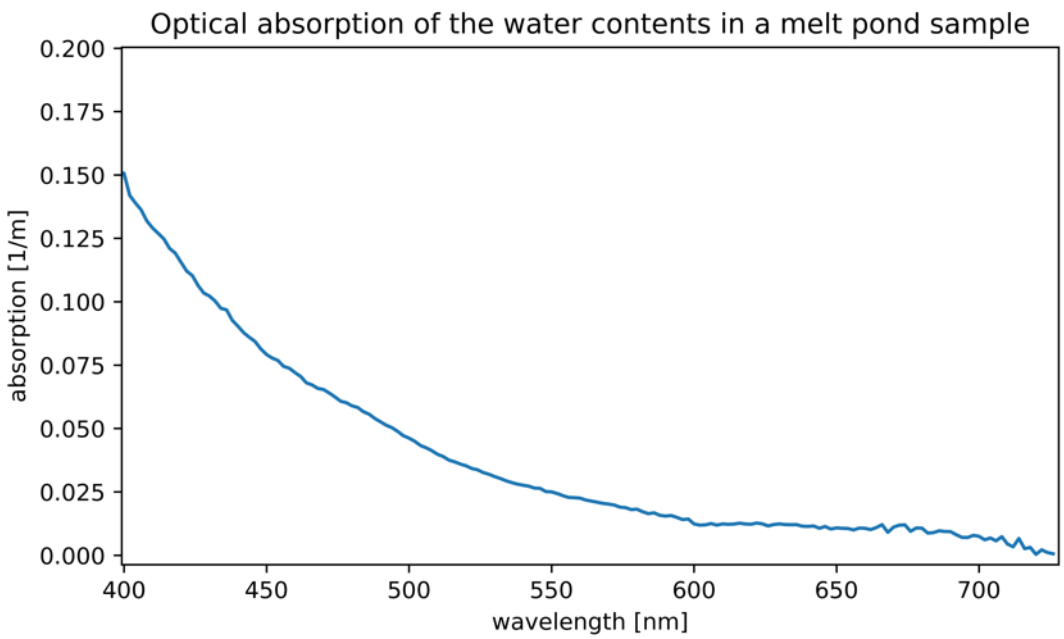

Fig. 4.9.3: Absorption spectrum of a pond water sample, referenced to pure water.

Data management

All data are handled, documented, archived and published following the MOSAiC data policy (see APPENDIX). All instrument deployments were logged in DShip, and all data, including notes and documentation photographs were uploaded onto MCS.

The data of each half day (AM/PM) was zipped, and uploaded under the respective device operation folder of the main instrument (cau_boeoetle_1, cau_stickle_1). All other instruments are either SensorWeb-child-devices of the main instrument (e.g. spectrometers), or co-deployed (e.g. cameras). Co-deployments have a readme-file in their respective device operation folders, pointing the user to the collective *.zip.

Data will be stored at the PANGAEA data repository (World Data Center PANGAEA

Data Publisher for Earth & Environmental Science www.pangaea.de.

4.10 Ridge studies

Nikolai Kolabutin[1], Egor Shimanchuk[1], Melinda Webster[2], Linda Thielke[3], Julia Regnery[4]

(not on-board:) Mats Granskog[5], Ilkka Matero[4], Martin Schneebeli[6], Benjamin A. Lange[5], Evgenii Salganik[7], Igor Sheykin[1], Knut Vilhelm Høyland[7], Ian A. Raphael[8]

[1]RU.AARI
[2]EDU.UAF
[3]DE.UNI-Bremen
[4]DE.AWI
[5]NO.NPOLAR
[6]CH.WSL
[7]NO.NTNU
[8] EDU.DARTMOUTH

Objectives

Pressure ridges are formed by the piling up of crushed ice blocks during sea ice convergence. Often the features shear during these events. While the ridge sail is the obvious surface part of the ridge, the submerged part – the ridge keel, is typically much larger and voluminous, and can make up 90% of the ridge volume. Both sails and keels are important surface roughness features that cause turbulence in the atmosphere and ocean.

Work at sea

The ridge works were carried out on the main ridge located on the edge of Leg 5 ice floe. There were snow and ice thickness measurements by drilling along the selected line crossing ridge area (Ridge transect). Also there were snow and ice thickness measurements by GEM-2. 11.09 there was taking cores at point of ridge for ice physical properties analyzing.

Ice thickness measurements by drilling

The length of Ridge transect line is 120 meters. Every 10 meters there were points for measurements, totally 13 points. The thickness measurements were carried out by using the drill with 5cm augers, ice gauge and pocket ruler. Before ice drilling snow height measurements by pocket ruler were done. After that a hole was being drilled in the ice and then in the hole the ice thickness by the ice gauge and freeboard by the pocket ruler were measured.

These measurements were carried out every Friday (28.08, 04.09, 11.09 and 18.09). At 18.09 there were measurements only in 8 points due to time constraints.

The overview of device operation for ridge thickness measurements is presented in Table 4.10.1. The device is Ice_gauge.

Tab. 4.10.1: An overview of device operations of the ridge thickness measurements using the drill and ice gauge.

Date (DD.MM.YYYY)	Survey Type	Ice_gauge
28.08.2020	Ridge survey	PS122/5_59-496
05.09.2020	Ridge survey	PS122/5_60-296
11.09.2020	Ridge survey	PS122/5_61-330
18.09.2020	Ridge survey	PS122/5_62-284

Ridge transect and magnaprobe surveys

As part of the ridge program on Leg 5, GEM-2 and Magnaprobe surveys were carried out along the 100-m ridge survey. Measurements were made every ~1 m along the drill hole thickness survey line. On two occasions (August 28 and September 3), two survey lines in parallel were conducted, while on September 18, only one survey was completed due to time constraints. For a list of GEM-2 and Magnaprobe DSHIP identification numbers, please see table 4.10.2. Snow depth on September 4 was measured using a ruler rather than the Magnaprobe due to the snow cover being less than 1 cm in depth for the majority of the survey line. The accompanying snow depth notes are listed in MCS under: RidgeSurvey_SnowDepth_Sept04_2020.txt. For more information regarding GEM-2 calibration data and transect data, please see Chapter 4.4.

Tab. 4.10.2: An overview of device operations of the ridge survey using the GEM-2 and Magnaprobe. A total of three GEM2/Magnaprobe surveys were conducted.

Date (MM/DD/YYYY)	Survey Type	GEM-2	Magnaprobe
8/28/2020	Ridge survey	PS122/5_59-428	PS122/5_59-412
9/4/2020	Ridge survey	PS122/5_60-162	N/A - see spreadsheet titled: "RidgeSurvey_SnowDepth_Sept04_2020"
9/18/2020	Ridge survey	PS122/5_62-198	PS122/5_62-242

Ridge coring

11.09 ice cores for ice physical properties analyzing (temperature, salinity, density, texture) at point of ridge were taken. For more information and results please see Chapter 4.5 Table 4.5.1.

Preliminary Results

The ice thickness at ridge along the Ridge transect line is variated between 2 and 9 meter. The Figure 4.10.1 shows some ice thickness profile with max ice thickness (11.09). The max ice thickness was 8,84 meters. The Figure 4.10.2 shows some sea ice thickness derived from the GEM-2 survey at 28.08.2020.

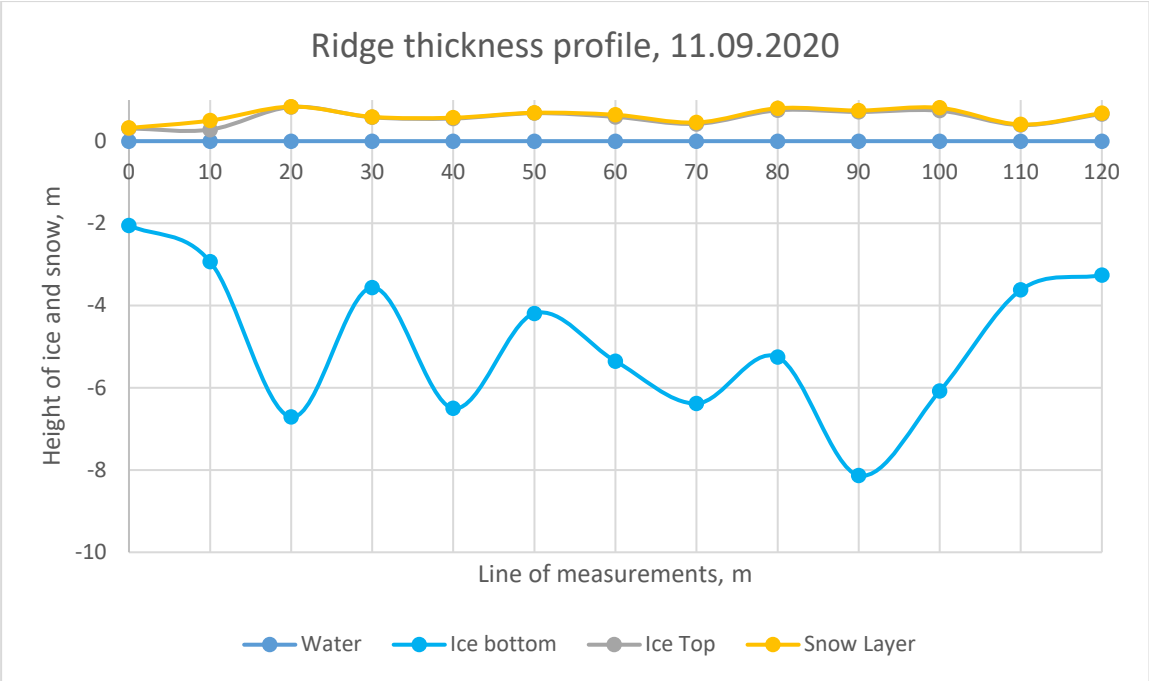

Fig. 4.10.1: The ice thickness profile along the Ridge transect line 11.09.2020

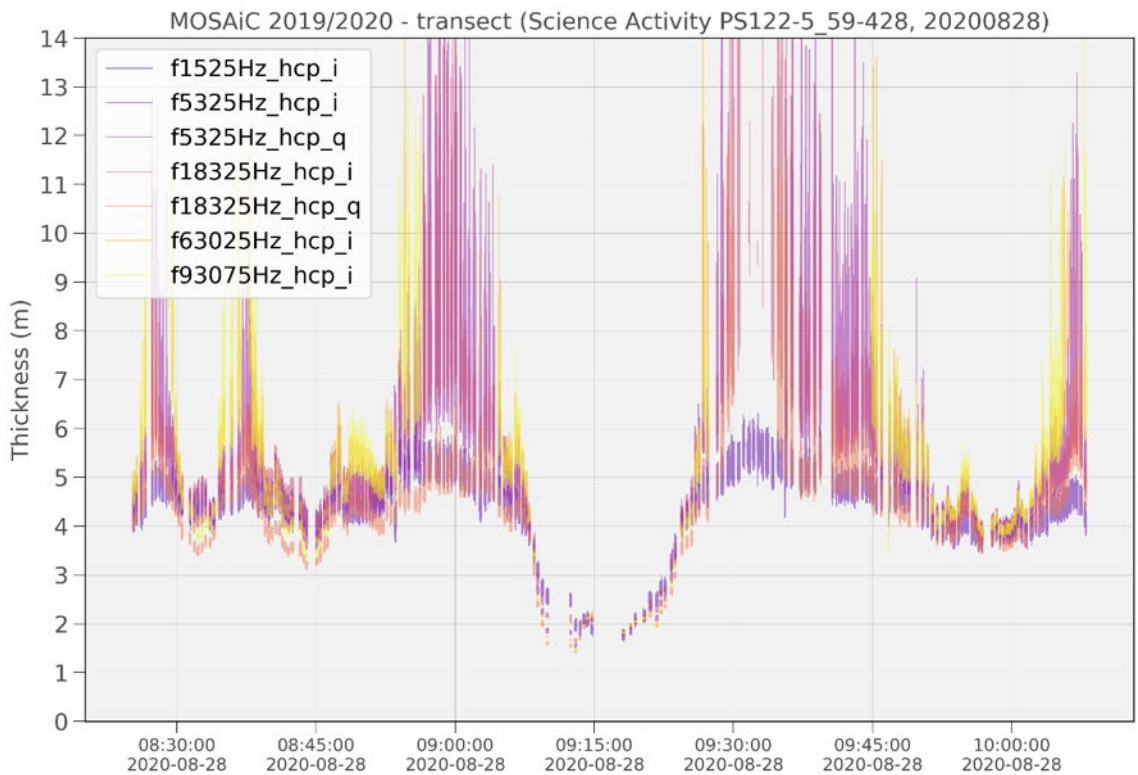

Fig. 4.10.2: Quicklook of sea ice thickness derived from the GEM-2 survey on 28 August 2020.

Data Management

All data are handled, documented, archived and published following the MOSAiC data policy (see APPENDIX). All of the instruments have been added into the system of SENSOR.awi.de

and all the data has been added to the MCS. The data will be submitted according the data policy of MOSAiC. Data will be stored at the PANGAEA data repository: World Data Center PANGAEA Data Publisher for Earth & Environmental Science www.pangaea.de. DOIs will be communicated to PANGAEA for later access via the future MOSAiC Data Portal.

4.11 Airborne Sea Ice Survey (HELI)

G. Birnbaum[1], J. Rohde[1], L. Thielke[2], G. Spreen[2]

(not on board:) S. Hendricks[1], N. Fuchs[1], R. Ricker[1], A. Jutila[1], B. Hwang[3]

[1]DE.AWI

[2]DE.UNI-Bremen

[3]UK.AC.HUD

Objectives

The objectives of the helicopter-borne sea-ice surveys during MOSAiC have been described in the Helicopter Observational Plan, the Expedition Programme and the cruise reports for PS122.1, PS122.2, PS122.3 and PS122.4. Here we provide a short summary for PS122.5, which took place during the end of the melt season and during start of freeze-up:

1. With respect to the overarching MOSAiC Science Plan questions, we mainly contribute to: How does sea ice formation, drift, deformation and melting couple to atmospheric, oceanic and ecosystem processes?
2. With respect to the overarching MOSAiC Science Plan goals, we especially contribute to: What are the spatial variability and temporal evolution of the snow and sea ice cover?
3. What is the spatial distribution of sea ice freeboard and surface roughness in the region of the central observatory (CO) floe and in other sea ice regions encountered during transit from/to the marginal ice zone (MIZ)? How do these parameters evolve during melt season and freeze-up?
4. What is the surface roughness upwind of the meteorological installation at the central observatory (CO)?
5. What is the sea ice thickness distribution in the region of the CO floe and in other sea ice regions encountered during transit from/to the MIZ? How does it evolve during melt season and freeze-up?
6. What is the spatial distribution of melt pond fraction and melt pond properties (e.g., size distribution, shape, depth) in the region of the CO floe and in other sea ice regions encountered during transit from/to the MIZ? How do those parameters evolve during melt season and freeze-up?
7. What is the temporal evolution of floe size distribution in the region of the CO floe?
8. What is the thickness distribution of newly formed ice in various sea ice regions encountered during transit from/to the MIZ?

In the present report, we focus on the helicopter measurement programme performed by Team ICE during PS122.5.

Work at sea

Sensors

The following sensors/instrumentation have been operated during PS122.5 on the D-HARK helicopter (ALS&CAM configuration):

- Airborne laser scanner (ALS)
- 2 RGB cameras: 14 mm wide-angle lens and 8 mm fisheye lens (CAM)
- Hyperspectral camera AisaEagle (till 19 September 2020)
- IR Camera (from 20 September 2020)
- DMS including operation of radiation thermometer KT-19 and upward and downward looking pyranometers CMP22

The following sensors/instrumentation have been operated during PS122.5 on the D-HAPS helicopter:

- EM-Bird (Orphan till 18 August 2020, Rosie from 19 August 2020)
- 2 GoPros

Mission types

There were three different mission types during leg 5:

- CO floe grid -
  D-HARK (ALS&CAM)
- Buoy pattern (triangles, rectangle) around CO -
  D-HARK (ALS&CAM) & D-HAPS (EM-Bird)
- Transect pattern (triangles, square) during transit from/to the MIZ -
  D-HARK (ALS&CAM) & D-HAPS (EM-Bird)

Between 18 August and 28 September 2020, we performed 13 survey flights (Table 4.11.1). Two flights had to be aborted after a certain time due to deteriorating weather conditions (fog; ceiling became too low). In the following, the different mission types are explained in more detail.

For the D-HARK ALS&CAM configuration (8 flights), flight altitude (400 ft to 1500 ft) and ground speed (60 kn or 80 kn) were adjusted to ceiling and mission goals for every flight. For floe grid flights with a special focus on melt pond properties, we operated at 200 ft and 10 kn ground speed over the floe.

With the D-HAPS EM-Bird configuration (5 flights), we carried out all surveys on 40 ft operational bird altitude above ground level and 60 to 80 kn air speed.

Floe grids

In total, 4 floe grid surveys were carried out with the D-HARK ALS&CAM configuration. The floe grid surveys at 200 ft altitude on 07, 11 and 15 September 2020 were only carried out over the CO floe and surrounding floes. The last floe grid survey on 19 September 2020 flown at 1000 ft followed a mow-the-lawn pattern more or less centered over the CO floe with a target side-length of about 5 km.

Buoy Surveys

Real-time coordinates from four GPS buoys deployed during our stay at the CO floe were used to span two triangles and a rectangle. The primary objective of this type of mission during leg 5 was to map temporal changes in sea ice thickness distribution, surface roughness, floe freeboard, floe size distribution and melt pond properties in a larger area. However, only 1 buoy survey with the D-HARK ALS&CAM and 3 surveys with the D-HAPS EM-Bird configuration could be performed.

Transect pattern during transit

During the transit from the MIZ to the CO floe and during the transit from the CO floe to the MIZ, we carried out 5 transect flights (triangles, squares) up to 40 nm away from Polarstern, in order to investigate spatial variability of sea ice properties in different regions. Three transect pattern were carried out with the D-HARK ALS&CAM and 2 pattern with the D-HAPS EM-Bird configuration.

Preliminary (expected) results

Airborne laser scanner

We continued the routine workflow and quick-view processing of the airborne laser scanner data during PS122.5. On flights at altitudes between 200 ft and 500 ft, we used a high-resolution configuration of the laser scanner settings. Hence, processing the data all the way to the final level-4 gridded product took about twice as long as on legs 1-3 (up to 2 days). During processing, we increased the spatial resolution of the quicklooks to 25 cm. Fig. 4.11.1 shows the ALS map of the CO floe and surrounding floes obtained on 15 September 2020. Main changes in surface topography during PS122.5 were caused by the opening and closing of leads and narrow breaks, when ridging and rafting occurred.

RGB cameras with 14 mm wide-angle and 8 mm fisheye lens

During the ALS flights, we operated two downward looking nadir cameras (14 mm wide-angle and 8 mm fisheye lens) collecting high-resolution images of the ice surface. We use a processing chain based on the images from the 14 mm lens camera to retrieve orthomosaics and eventually a digital elevation model (DEM). During the melt season, the main goal was to derive melt pond fraction and melt pond properties like pond size distribution and shape of ponds. Figure 4.11.2 shows a comparison of three orthomosaics of the CO floe, which were obtained on 07, 11 and 15 September 2020.

Hyperspectral camera

The hyperspectral camera was primarily operated to derive melt pond depth. Processing of the AisaEagle data is complex and could not be done with the resources available onboard.

IR camera

There were two survey flights done with the IR-Camera on 21 and 28 September 2020. The IR-Camera was operated with a sampling rate of 4 Hz and a NUC of 15 seconds. The sky was overcast or partly overcast with changing cloud conditions during the two surveys.

The first flight on 21 September was performed over pack ice as a regional flight in two triangles with a total distance of 120 nm. The first triangle was flown at 1000 ft with 80 kt ground speed, the second triangle at 500 ft and 60 kt ground speed due to decreasing cloud height. During this flight some very transparent fog patches were present above the surface, which did not seem to influence the data in the IR neither in the visible range. The main aim of the flight was to investigate the thermal properties of melt ponds. Since the melt ponds were already over-frozen and covered with snow, the brightness temperature are only 1 to 2 K higher than the surrounding ice. Nevertheless melt pond pattern can be distinguished and the comparison with the visible images shows an agreement in the pattern. Therefore the melt pond fraction could be derived and compared with the other data from this helicopter flight (visible images, ALS).

The second flight on 28 September was planned as survey between the MIZ and thicker pack ice during our transit back to Svalbard. The flight pattern had to be shortened due to low clouds

and fog in the North. Thus a thin ice survey was done. The flight altitude was between 300 and 400 ft with a ground speed of 60 kt. Since the thermal infrared is most sensitive for open water and thin ice, the differences in surface brightness temperature allow a clear identification of different thin ice types. The distribution of the different surface types and its thermal properties can be used for an analysis of the heat exchange between ocean, ice and atmosphere during freeze-up. Figure 4.11.3 shows one example image of each flight taken by the IR-Camera.

Pyranometers

From the pyranometer data, area averaged albedo will be calculated for flights in overcast conditions. The necessary attitude post-processing will be done after the expedition.

EM-Bird

EM-Bird surveys were carried out in order to map the total sea ice thickness distribution around the ships position during transit and during camp phase. On leg 5 no small-scale floe surveys were done. Note that total thickness refers to here as snow+ice thickness.

During transit towards the floe search area, one EM-Bird survey has been performed around 89°N and 20°W on 18 August 2020. A triangle pattern towards the East was flown.

During the camp phase of leg 5 three surveys could be carried out around the CO. On 07 September 2020 a square around the floe was flown which was repeated the next day on 08 September 2020 after buoys have been deployed in the vicinity of the CO. The modal thicknesses measured were 0.7 m, 0.9 m, and 0.6 m for different profiles along the flight path. Due to weather conditions those buoy positions were visited only one more time on 17 September 2020. This survey was flown in a “butterfly pattern” consisting of one triangle to the north and one triangle to the south.

During the transit to Svalbard one flight from the MIZ towards the pack ice was performed in the area around 82.22°N and 25°E. Although the northernmost waypoint could not be reached due to deteriorating weather conditions, the transition from new ice to pack ice was still surveyed.

Data management

All data are handled, documented, archived and published following the MOSAiC data policy (see APPENDIX). All device operations were logged in the AWI sensorweb portal and all sensor raw data files are stored in platform section of MCS. Data will be stored at the PANGAEA data repository (World Data Center PANGAEA Data Publisher for Earth & Environmental Science www.pangaea.de). Final geophysical parameters will be made available via the workspace section of MCS and archived in the PANGAEA data repository according the MOSAiC data policy. Data from the data acquisition system of Polar Research Aircraft (DMS) can be accessed after registration at https://dship.awi.de/exportdisplay/.

Tab. 4.11.1: Overview of all helicopter sea ice surveys from Polarstern during PS122.5. TO and LDG designate take-off and landing times in UTC respectively. Grey shades indicate D-HARK surveys with the ALS&CAM configuration.

Flight ID	Device Operation	TO	LDG	Aircraft	Mission Type
20200818_01	PS122/5_59-180	11:04	12:34	D-HAPS	Transects (triangle) during transit
20200818_02	PS122/5_59-139	15:30	16:25	D-HARK	Transects (triangle) during transit*

20200907_01	PS122/5_61-62	04:21	06:20	D-HARK	CO floe grid
20200907_02	PS122/5_61-56	11:58	14:10	D-HAPS	Rectangle around CO
20200908_01	PS122/5_61-61	08:14	10:28	D-HAPS	Rectangle around CO
20200908_02	PS122/5_61-63	12:22	13:58	D-HARK	Buoy pattern (2 triangles)
20200911_01	PS122/5_61-190	05:30	07:43	D-HARK	CO floe grid
20200915_01	PS122/5_62-67	04:44	06:25	D-HARK	CO floe grid
20200917_01	PS122/5_62-151	07:04	08:59	D-HAPS	Buoy pattern (2 triangles)
20200919_01	PS122/5_62-166	10:02	12:12	D-HARK	Floe grid
20200921_01	PS122/5_63-3	07:46	09:43	D-HARK	Transects (2 triangles) during transit
20200928_01	PS122/5_63-117	06:53	09:03	D-HAPS	Transects (square) during transit
20200928_02	PS122/5_63-118	11:10	12:20	D-HARK	Transects (square) during transit*

*aborted due to deteriorating weather conditions (fog; ceiling became too low)

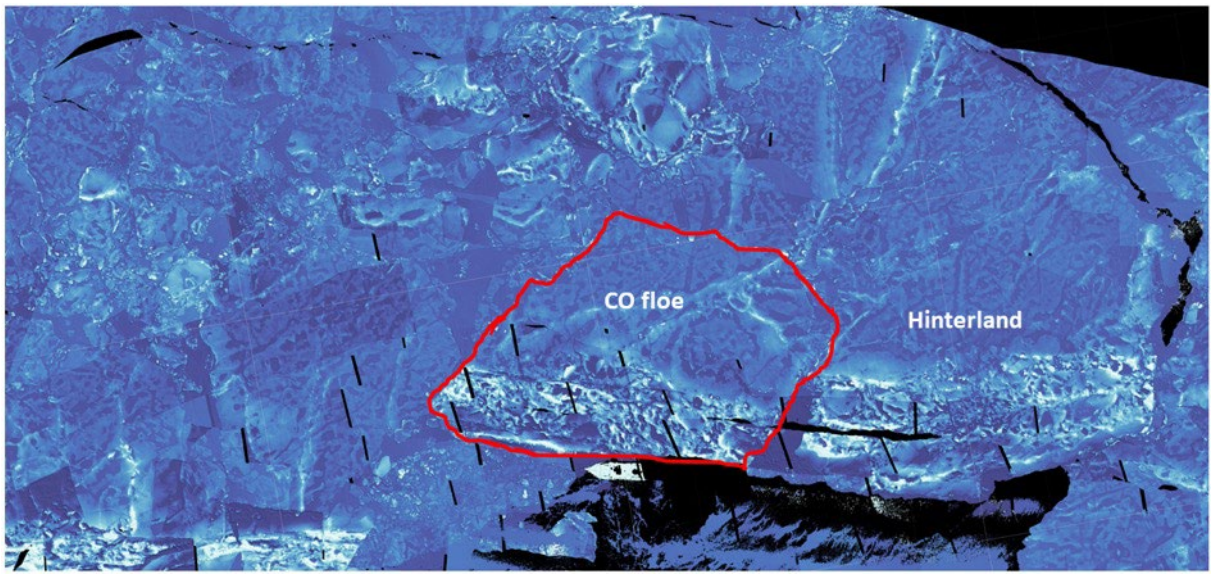

Fig. 4.11.1: ALS floe map of CO floe and surrounding floes obtained on 15 September 2020. The map gives an impression of the surface topography. White structures indicate pressure ridges

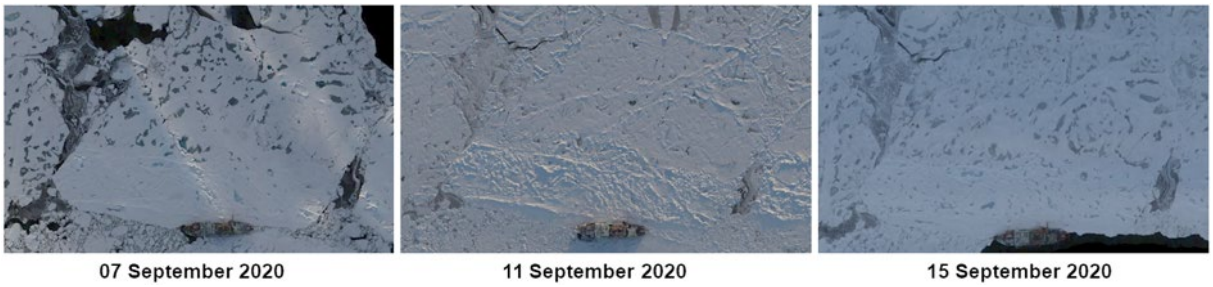

Fig. 4.11.2: Comparison of three maps of the CO floe. The orthomosaics are based on RGB images taken on 07, 11 and 15 September 2020. Due to freezing and snowfall between 07 and 11 September many melt ponds were no longer easily visible on 11 September. However, warm air advection afterwards caused melting of snow, which resulted in visible ponds again on 15 September.

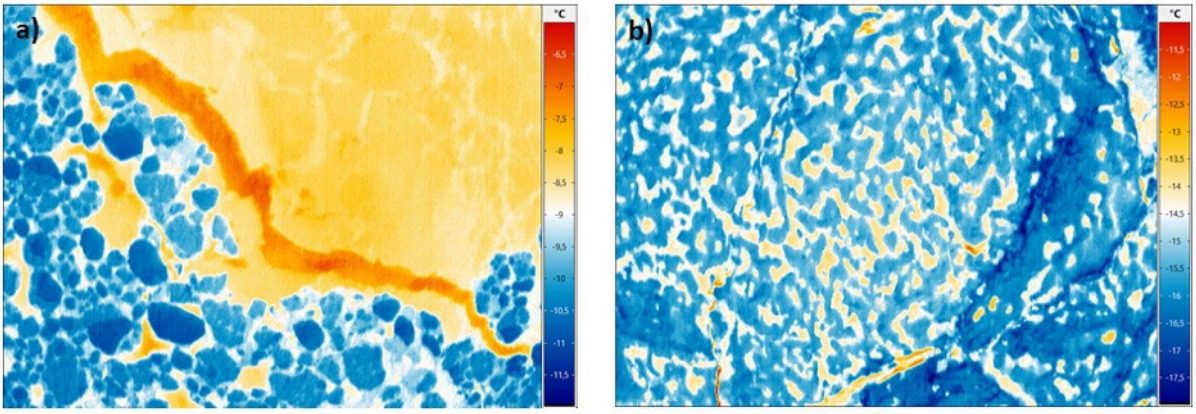

Fig. 4.11.3: Uncorrected surface brightness temperature in degree Celsius in two example images from the IR-Camera during the helicopter flight on 21 September (a) and on 28 September (b). On 21 September, the survey was performed about thicker ice and melt ponds were over-frozen and mainly covered with snow, but still visible in the temperature because of 1 to 2 K higher temperatures. On 28 September, the flight was performed mainly over thin ice at the ice edge. Different thin ice types can be clearly identified by its different surface brightness temperatures in the thermal infrared range.

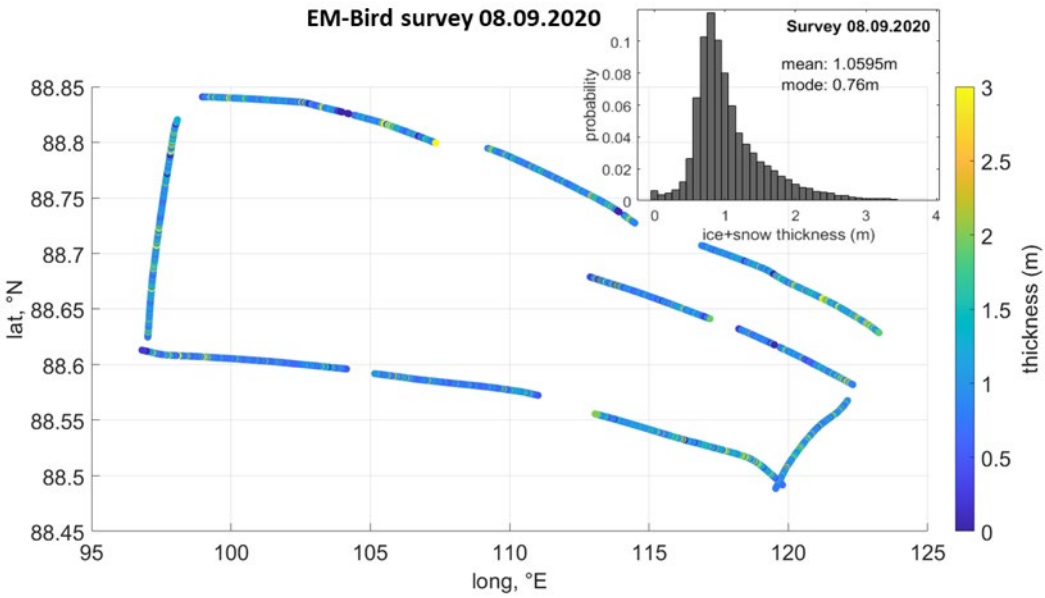

Fig. 4.11.4: Sea ice thickness retrieved from EM-Bird survey on 08 September 2020.

4.12 Remote Sensing Measurements On-ice and Onboard *Polarstern*

Gunnar Spreen[1], Linda Thielke[1]

(not on board:) Estel Cardellach[2], Tania Casal[3], Friederike Fohlmeister[4], Carolina Gabarró[2], Steen Savstrup Kristensen[5], Randy K. Scharien[6], Mike Schwank[7], Maximilian Semmling[8], Julienne Stroeve[9,10]

[1]DE.UNI-Bremen
[2]ES.ICM-CSIC
[3]INT.ESA
[4]DE.DLR
[5]DK.DTU
[6]CA.UVICTORIA
[7]CH.WSL
[8]DE.GFZ
[9]COM.UCL
[10]CA.UMANITOBA

Objectives

Satellite remote sensing is the ideal tool to obtain Arctic-wide and long-term observation of the sea ice cover, ocean, and the atmosphere above. Remote sensing datasets can be used to extend the local MOSAiC observations to a larger scale and set them in context with preceding environmental conditions, like the history of the MOSAiC ice floes. MOSAiC provides ideal conditions for evaluation of satellite remote sensing observations: It is a rare case to observe the complete seasonal cycle. During leg 5 specifically the ice freeze-up and summer to winter transition of the surface scattering layer to snow covered ice are of interest.

One scientific goal of MOSAiC for remote sensing is to develop new method to retrieve improved sea ice parameters from satellites. In the microwave domain a better understanding of the microwave emissivity and backscatter depending on snow and ice properties and environmental conditions are needed. Thus, remote sensing instruments are co-deployed with intense sampling of snow and ice. In turn radiative transfer modelling of snow and ice can be improved on the basis of these measurements.

During leg 5 the drift of the MOSAiC floe took place north of 88°N and with that in the pole hole of almost all satellite observations used for sea ice. Thus, no direct comparisons, e.g. of the helicopter data, with satellite measurements can be performed during leg 5. Also, the characterization of the larger region around the MOSAiC leg 5 ice floe by satellite observations is hindered by the reduced satellite data availability.

Research questions for leg 5 are:

- Can co-located ground-based sea ice/snow and microwave measurements help to develop improved satellite retrieval methods for ice area, thickness, type, and snow depth?
- What is the prospect to retrieve additional physical parameters with satellite remote sensing to expand the observational capability of processes at the ice/atmosphere interface like surface roughness?

Most observed changes of the Arctic climate system are based on results from satellite remote sensing, which is one of the most important and reliable tools for Arctic monitoring. However, most satellites do not directly measure the geophysical parameters that are needed for research and monitoring. Sea ice concentrations, for example, are typically derived from passive microwave brightness temperatures or high-resolution radar images. Both methods make use of the characteristic difference between surface properties of open water and sea ice, which can be complicated by a variety of seasonal and conditional factors. Sea ice thickness is derived from microwave brightness temperature (thin ice) or from altimeters. Altimeters measure the ice or snow freeboard, which is then converted to ice thickness based

on critical assumptions on snow depth and snow/ice densities. Continuous development of methods and algorithms to analyse satellite measurements is necessary to improve observational capabilities, reduce uncertainties, and ensure consistency of satellite data sets.

The comprehensive collection of remote sensing instruments looking at the ice during leg 5 during a time of freeze-up and melt-refreeze cycles with rapid changes of the surface and snow properties will help to quantify uncertainties of current satellite retrievals and develop improved, new ones.

Work at sea

Several remote sensing (RS) instruments were operated on the ice and from the ship. Table 4.12.1 gives an overview about all instruments and the responsible PI on land and during leg 5. Many more people are involved with the measurements.

All measurements are taken quasi-continuously.

On the way back from the leg 5 MOSAiC floe out of the ice three more ice stations were conducted.

Tab. 4.12.1: List of remote sensing instruments operated during leg 5. Details are given in the sections below.

Instrument	***Details***	***PI***	***Institution***	***Leg 5 responsible***
On the ice				
Ku/Ka-band radar	Fully-polarimetric wideband FMCW radar (Ku-band: 12-18 GHz; Ka-Band: 30-40 GHz)	J. Stroeve	U Manitoba	G. Spreen
L-band Scatterometer	Fully-polarimetric 1.26 GHz scanning radar	R. Scharien	U Victoria	G. Spreen
HUTRAD	6.85, 10.65, 18.70 GHz radiometers	J. Lemmetyinen/ T. Casal	FMI/ESA	L. Thielke
MW Radiometer ELBARA	1.4 GHz (L-band), only V-pol	M. Schwank/ T. Casal	WSL/ESA	G. Spreen
MW Radiometer SSMI	19, 37, 89 GHz (K, Ka, W-band), dual-pol	J. Stroeve	U Manitoba	L. Thielke
MW Radiometer Balamis ARIEL	1.4 GHz (L-band)	C. Gabarro	ICM-CSIC	L. Thielke
GNSS-R	Reflected GNSS signals from snow/ice	E. Cardellach/ T. Casal	ICE-CSIC / ESA	L. Thielke
Infrared Camera	Surface temperature	G. Spreen	U Bremen	G. Spreen
Video Camera	Visual overview of RS site	G. Spreen	U Bremen	G. Spreen
On *Polarstern*				
GNSS-R & atmosphere	Reflected GNSS signals from snow/ice and GNSS for atmospheric water vapor	M. Semmling	GFZ	G. Spreen

GNSS Ionosphere	Ionospheric scintillations for GNSS measurements	F. Fohlmeister	DLR	G. Spreen
MW Radiometer EMIRAD2	1.4 GHz (L-band)	S. Savstrup Kristensen/ T. Casal	DTU/ESA	L. Thielke

Remote Sensing Site (22.08. to 19.09.2020)

The RS site was operational from 22 August, one day after the arrival, until 19 September, the last day before leaving the floe. The site was established about 200 m away from *Polarstern* (Figure 4.12.1) at a central position in the CO. The site remained stable throughout leg 5. See the tables in the "Instruments" subsection for a list of measurement durations for each instrument. The mobile instruments ARIEL, Ku/Ka-radar and IR camera were moved along transect lines or setup at lead and melt pond locations, which is described under the respective instrument.

Figure 4.12.1 shows a map with the layout of the RS site with an aerial picture from 6 September in the background. The site has homogenous ice in the centre and is framed by melt ponds on three sides. The photos in Figure 4.12.2 give an overview of the RS site. All instruments look at a homogenous ice area with similar properties. The initial ice thickness on 22-24 August was 137±2 cm and did not change significantly until the end (19 September ice thickness: 136±2 cm). At the beginning there was a surface scattering layer of about 2 to 5 cm depth. At the end snow depth was 4±0.5 cm.

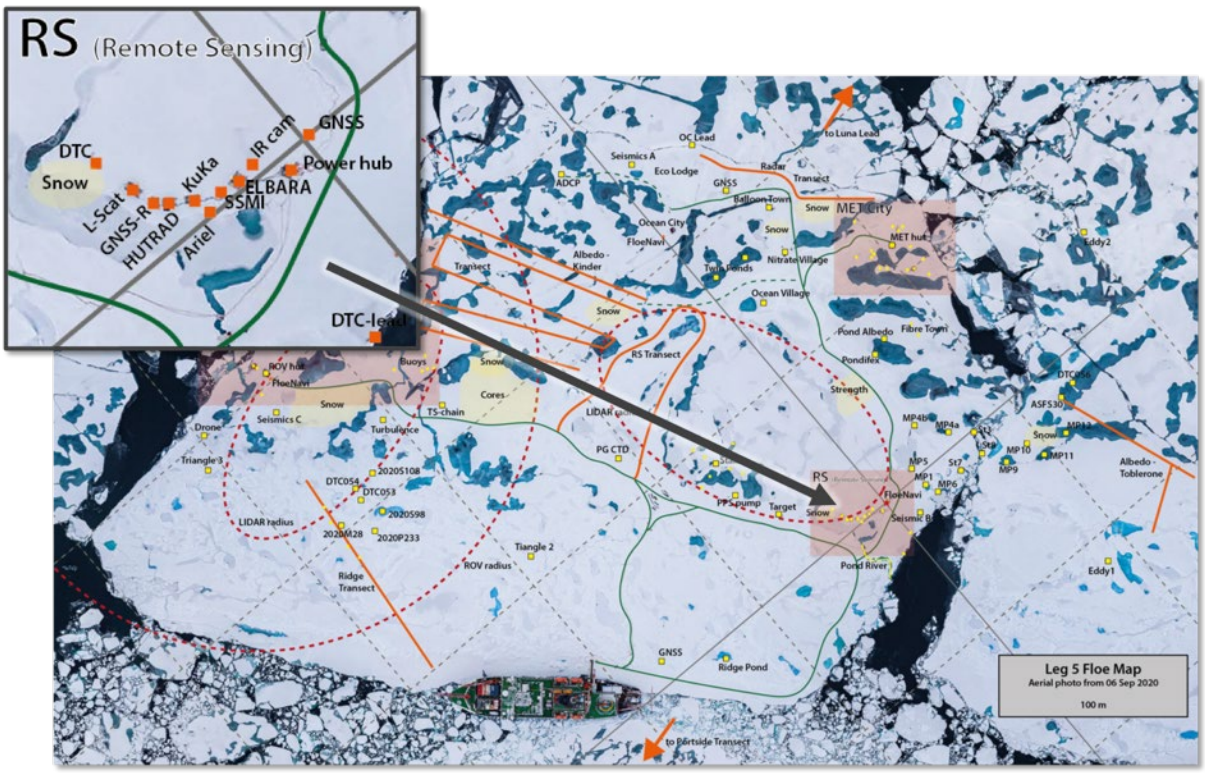

Fig. 4.12.1: Map of the leg 5 CO. The detail on the top left shows the RS site layout. Mind the overfrozen melt pond used for the melt pond experiments. The background shows an aerial photo (Steffen Graupner/Charles Finkbeiner) taken by a drone on 6 September 2020.

Fig. 4.12.2: Remote Sensing Site on 29 August (left image) and 8 September 2020, when all instruments were deployed. The mobile Balamis ARIEL radiometer is missing as it was measuring at a close by lead during that time. The melt pond seen in front on the left image was used for the melt pond experiments. On 29 August it still had a wet surface. The homogenous ice area seen in the front of the right image was the main target area for the RS measurements. (photos: Gunnar Spreen)

Onboard Polarstern

All instruments onboard *Polarstern* were installed on the port side of upper and lower Peil deck, the highest deck of *Polarstern*. Figure 4.12.5 gives an overview of the installations. Processing and data recording units were installed in the observation alley in front of the meteorologist's office.

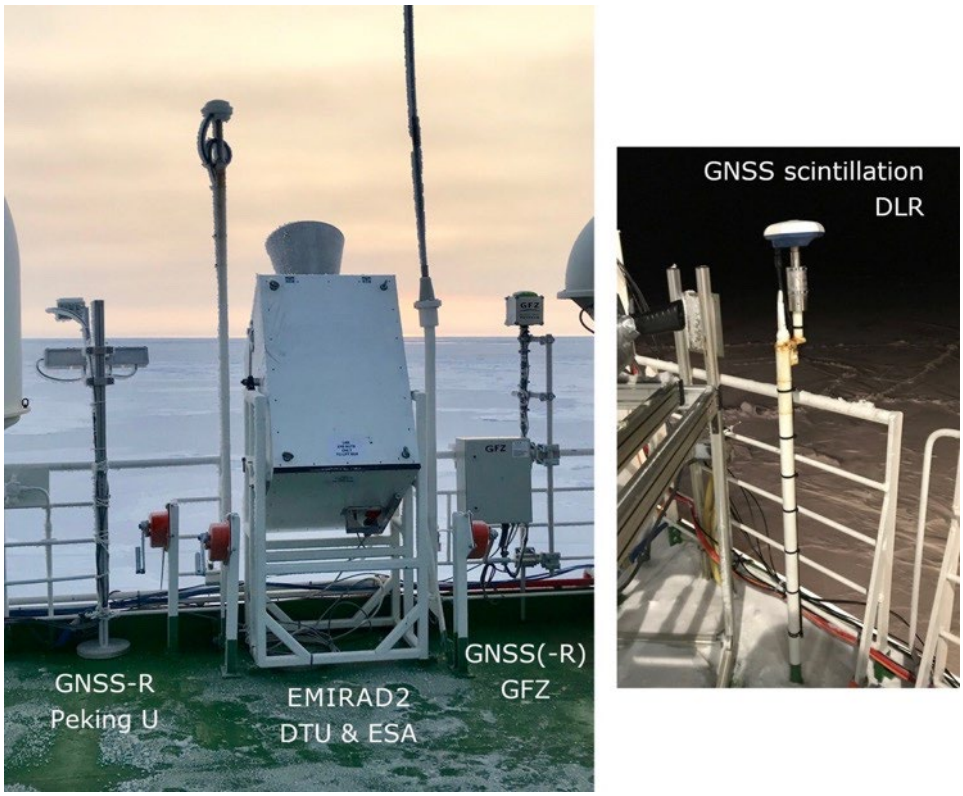

Fig. 4.12.3 Remote sensing installations on the port side of Peil deck onboard Polarstern.

Ice stations during transit (24, 26, 30 September)

On the way out of the ice after the end of the MOSAiC ice floe measurements, three ice stations were conducted: on 24.12.20 at 86°N 59.5°E, on 26.9.20 at 86.03°N 35.5°E, and on 30.9.20 at 81.7°N 1.5°E.

For remote sensing joined transect of the Balamis ARIEL MW radiometer together with the IR camera were performed (see respective instrument sections below). Transect consisted of measurement stops every 50 to 100 m and dedicated thin ice measurements. Ice and snow properties were measured at every stop. As the ice was thinner during the ice station than at the leg 5 MOSAiC floe this is especially useful for the ARIEL L-band ice thickness measurements. The transects were performed as joined activity with the ATMOS flux sledge (Section 3.ATMOS.XX).

Instruments and measurement periods

In total 12 different instruments were operated as part of the Remote Sensing task, 9 on the ice and 3 onboard. Here we give a brief overview of the instruments and their measurement periods during leg 5. A complete list of device operations can be found in Appendix A.XX.

Radar Ku/Ka-band

- List of measurement periods at RS site in Table 4.12.2 and for transects in Table 4.12.3
- Ku- (12–18 GHz) and Ka-band (30–40 GHz) radar
- Nadir view for altimetry application; elevation and azimuth scanning as scatterometer
- DSHIP/SensorWeb: Radar dual Ka- and Ku-band altimeter (KuKa_Radar)
- University of Manitoba
- Projects: U Manitoba internal, NERC MOSAiC funding, and ESA MOSAiC remote sensing
- Corresponding satellite observations: CryoSat-2, Sentinel-3, AltiKa, ERS-1/2, Envisat, and future CRYSTAL altimeters; QuikSCAT, OSCAT, CFOSAT scatterometers

The instrument was operated in a permanent scanning mode stationary at the RS sites (typical ±30° azimuth, 0–60° elevation, 3° steps) with a break of 50 minutes between the scans. The azimuth scanning was reduced to ±30° to avoid influence from neighbouring instruments as the RS site was rather small and instruments had to stand close together. Occasionally the instrument was turned around to measure the melt pond on the other side together with HUTRAD, L-SCAT and IR-camera. Table 4.12.2 lists all measurements done at the RS site including the melt pond studies.

The radar was operated along a short about 150 m long “radar transect” on a regular basis (see more details below) to account for spatial variability. As the frame for the transect sled was sent back after leg 3 by accident, we towed the radar along the transect in nadir configuration on its original sled. Table 4.12.3 lists all measurements done during the transect work.

More details can be found in the PS122/1, 2, and 4 cruise reports.

Fig. 4.12.4: Ku/Ka-band radar leg 5 (photo: Gunnar Spreen)

Tab. 4.12.2: List of measurement periods of the Ku/Ka-band radar at the RS site.

Activity - Device Operation	*Timestamp*	*Action*	*Comment*
PS122/5_58-51 KuKa_Radar	23.08.20 14:53	recording start	Nadir stare mode; Wet ice surface, light snowfall; first on battery; around 15:30 UTC change to cable power
PS122/5_58-51 KuKa_Radar	23.08.20 15:01	information	Manual scanning on a 2 m line at position at remote sensing site; 5 times; End 15:03 UTC
PS122/5_58-51 KuKa_Radar	23.08.20 15:27	recording end	end of nadir stare measurements without scanning
PS122/5_58-62 KuKa_Radar	25.08.20 06:14	recording start	First scan sequence after power was connected at RS site. Azimuth -50° to 50°, Elevation 0° to 60°, delta 3°, sleep 50 minutes"
PS122/5_58-62 KuKa_Radar	27.08.20 09:23	information	changed azimuth to -40 to 40 (to avoid sled). Pedestal height 109 cm
PS122/5_58-62 KuKa_Radar	28.08.20 04:41	recording end	After installing a new LAN cable recording stopped for unknown reason.
PS122/5_58-62 KuKa_Radar	29.08.20 10:34	recording start	Start new recording after network connection is established again. Azimuth was reduced to avoid sled and other instruments: azimuth -30° to 30°; elevation 0° to 60°, delta 3°, pedestal height 109 cm
PS122/5_58-62 KuKa_Radar	04.09.20 07:35	recording end	End of measurement at remote sensing site to make measurements at melt pond (together with L-SCAT, HUTRAD, and IR camera).
PS122/5_58-62 KuKa_Radar	04.09.20 09:00	recording start	Measuring melt pond next to RS site (together with L-SCAT, HUTRAD, and IR camera). FEEDHORNS have icing! Not clear how useful measurements will be. azimuth: -30° to 30°; elevation: 0° to 50°; delta: 3°; sleep time: 5 minutes. Freeboard of melt pond at Ku/Ka-radar: 15 cm -> pedestal height: 124 cm"
PS122/5_58-62	04.09.20	recording end	End of melt pond scan. Moving back to RS site.

KuKa_Radar	10:14		
PS122/5_58-62 KuKa_Radar	04.09.20 10:28	recording start	Back at remote sensing site after melt pond scan. FEEDHORNS have icing! Not clear how useful measurements are. Same parameters as previously: azimuth: -30° to 30°; elevation: 0° to 60°; delta 3°. By mistake measurements are done with a sleep time of only 5 minutes until 16:21:03 UTC. Thereafter changed to 50 minutes sleep time.
PS122/5_58-62 KuKa_Radar	04.09.20 23:13	recording end	End of recording due to data storage issues.
PS122/5_58-62 KuKa_Radar	09.09.20 00:20	recording start	Continuation of measurements. Icing was removed from feedhorns. Azimuth: -30° to 30°; elevation: 0° to 60°; delta 3°, sleep 50 minutes."
PS122/5_58-62 KuKa_Radar	10.09.20 08:11	recording end	Stopped scans to perform transect and melt pond measurements
PS122/5_58-62 KuKa_Radar	10.09.20 10:09	recording start	Start of scan at melt pond next to RS site. Azimuth: -30° to 30°; elevation: 0° to 60°; delta 3°. Sleep 10 minutes"
PS122/5_58-62 KuKa_Radar	10.09.20 11:19	recording end	End of melt pond measurements. Move back to regular RS site.
PS122/5_58-62 KuKa_Radar	10.09.20 11:43	recording start	Restart of regular measurement scans at RS site after transect and melt pond measurements.
PS122/5_58-62 KuKa_Radar	17.09.20 08:36	recording end	Stop of scan at RS site. Preparing for radar transect.
PS122/5_58-62 KuKa_Radar	17.09.20 10:59	recording start	Start of regular scan at RS site after radar transect. Azimuth: -30° to 30°; elevation: 0° to 60°; delta 3°, sleep 50 minutes."
PS122/5_58-62 KuKa_Radar	18.09.20 04:50	recording end	Stop of measurements at RS site. Doing melt pond measurements.
PS122/5_58-62 KuKa_Radar	18.09.20 05:00	recording start	Start of scan at melt pond next to RS site. Azimuth: -30° to 30°; elevation: 0° to 60°; delta 3°. Sleep 5 minutes
PS122/5_58-62 KuKa_Radar	18.09.20 06:16	recording end	End of measurements at RS melt pond. Back to RS site.
PS122/5_58-62 KuKa_Radar	18.09.20 06:19	recording start	Back to RS site. Continue regular scans. Azimuth: -30° to 30°; elevation: 0° to 60°; delta 3°. Sleep 50 minutes
PS122/5_58-62 KuKa_Radar	19.09.20 03:53	recording end	End of measurements at RS site and end of measurements during MOSAiC leg 5.

Tab. 4.12.3: List of transects of the Ku/Ka-band radar.

Activity - Device Operation	*Timestamp*	*Action*	*Comment*
PS122/5_60-141 KuKa_Radar	2020-09-05 09:11:35	recording start	Nadir configuration. New file every 5 minutes. Snow thickness recorded. Line 1: road at balloon city corner to end of snow. End at 9:12

PS122/5_60-141 KuKa_Radar	2020-09-05 09:18:00	information	Line 2: from end of snow to ocean city End at 09:24
PS122/5_60-141 KuKa_Radar	2020-09-05 09:23:00	information	Line 3: from Ocean City back to the road corner at balloon town. End at 09:25.
PS122/5_60-141 KuKa_Radar	2020-09-05 09:25:00	recording end	End of transect at corner of road at balloon town.
PS122/5_61-158 KuKa_Radar	2020-09-10 09:35:38	recording start	Line 1: balloon town corner to end of snow End: 09:39
PS122/5_61-158 KuKa_Radar	2020-09-10 09:41:00	information	Line 2: snow to OC End: 09:44:30
PS122/5_61-158 KuKa_Radar	2020-09-10 09:48:00	information	Line 3: OC to balloon town corner End: 09:50
PS122/5_61-158 KuKa_Radar	2020-09-10 09:50:04	recording end	End of transect at balloon town
PS122/5_62-164 KuKa_Radar	2020-09-17 10:14:19	recording start	Start of line 1: balloon town to end of snow.
PS122/5_62-164 KuKa_Radar	2020-09-17 10:16:00	information	end of line 1 at end of snow
PS122/5_62-164 KuKa_Radar	2020-09-17 10:19:00	information	start of line 2: snow to OC
PS122/5_62-164 KuKa_Radar	2020-09-17 10:23:00	information	End of line 2 at OC
PS122/5_62-164 KuKa_Radar	2020-09-17 10:25:00	information	Start of line 3: OC to balloon town corner.
PS122/5_62-164 KuKa_Radar	2020-09-17 10:28:00	recording end	End of line 3 at balloon town. End of transect, back to RS site.
PS122/5_60-141 KuKa_Radar	2020-09-05 09:11:35	recording start	Nadir configuration. New file every 5 minutes. Snow thickness recorded. Line 1: road at balloon city corner to end of snow. End at 9:12
PS122/5_60-141 KuKa_Radar	2020-09-05 09:18:00	information	Line 2: from end of snow to ocean city End at 09:24

Scatterometer L-band

- List of measurement periods in Table 4.12.4

- L-band (1.26 GHz), full-polarimetric (HH, VV, HV, VH) scatterometer
- Bandwidth: 500 MHz, range resolution 0.3 m
- Antenna beamwidth: 14°
- Transmit power: -13.5 dBm
- DSHIP/SensorWeb: Scatterometer L-band (Scat-L)
- University of Victoria
- Project: CanScat supported by Canadian Space Agency and EUMETSAT
- Corresponding satellite observations: L-band SAR: ALOS/PALSAR-1, -2, and -3; SAOCOM; NISAR; ROSE-L

The instrument was operated in a permanent scanning mode stationary at the RS sites (typical -45° to 30° azimuth scan, 15–45° elevation, 3° steps) with a break of 50 minutes between the scans. In addition, the melt pond next to the RS site was scanned on a regular basis together with the Ku/Ka-radar, HUTRAD and the IR camera. Times and durations of all measurements are listed in Table 4.12.4.

The instrument fell over during leg 3 and needed some repair during leg 4. As a consequence, the scanning mechanism was not working smoothly all the time and the scans sometimes had a wobbly or wavy motion. This effect was worth at higher elevations, which therefore were avoided during later scans.

More details can be found in the PS122/1, 2, and 4 cruise reports.

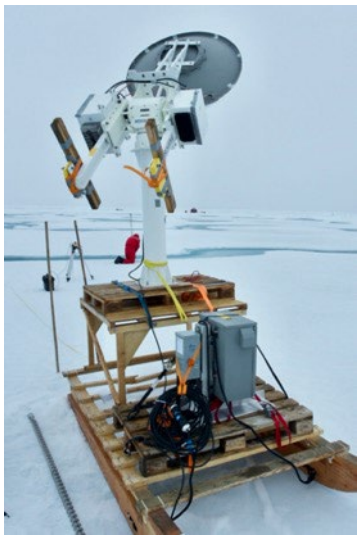

Fig. 4.12.5: L-band scatterometer (photo: Gunnar Spreen)

Tab. 4.12.4: List of measurement periods of the L-band scatterometer.

Activity - Device Operation	*Timestamp*	*Action*	*Comment*
PS122/5_58-58 Scat-L	27.08.20 11:29	recording start	Start of first L-SCAT measurement. pedestal height: 240 cm; azimuth: -45° to 30°; elevation: 15° to 55°; elevation delta: 3°
PS122/5_58-58 Scat-L	01.09.20 05:20	information	2° tilt backwards.
PS122/5_58-58 Scat-L	04.09.20 08:17	recording end	End of measurement of remote sensing site to do melt pond scan.
PS122/5_58-58	04.09.20	recording start	Scans of melt pond next to remote sensing site

Scat-L	08:43		(together with Ku/Ka-radar, HUTRAD, and IR camera). azimuth: -30° to 30°; elevation: 15° to 45°; delta: 3°; sleep time: 5 minutes. Freeboard of melt pond at L-SCAT: 12 cm -> pedestal height: 252 cm
PS122/5_58-58 Scat-L	04.09.20 10:12	recording end	end of recording at melt pond
PS122/5_58-58 Scat-L	04.09.20 10:34	recording start	Back to remote sensing site. Continue with previous settings. Azimuth: -45° to 30°; elevation: 15° to 55°; delta: 3°; sleep: 50 minutes
PS122/5_58-58 Scat-L	05.09.20 05:37	recording end	Stopped scan cycle because of wobbling motion of L-SCAT antenna in upper parking position.
PS122/5_58-58 Scat-L	05.09.20 06:18	recording start	Restart of scan measurements with reduced elevation because of wobbling motion of antenna at 55° elevation, -45° azimuth position. New settings: azimuth: -45° to 30°; elevation: 15° to 50°; delta: 3°; sleep time: 50 minutes
PS122/5_58-58 Scat-L	05.09.20 10:50	recording end	Scan stopped for unknown reason. Likely due to the swinging/wobbly motion observed before.
PS122/5_58-58 Scat-L	06.09.20 14:00	recording end	Scanning stopped. Put radar in park position. a) because of forecasted wind. b) because scan was not working anymore (wobbly motion?) and needs investigation
PS122/5_58-58 Scat-L	07.09.20 10:35	recording start	Restart of scan after wind event. Because of wobbly motion in parking position elevation was reduced to 45°. Azimuth -45° to 30°; elevation 15° to 45°; delta 3°; sleep 50 minutes
PS122/5_58-58 Scat-L	10.09.20 08:03	recording end	Stopped measurement at RS site to measure melt pond next to RS site (together with Ku/Ka-radar, HUTRAD, IR camera).
PS122/5_58-58 Scat-L	10.09.20 09:34	recording start	Measurement of melt pond next to RS site (together with Ku/Ka-radar, HUTRAD, IR camera). Same parameters as before: Azimuth -45° to 30°; elevation 15° to 45°; delta 3°; sleep 50 minutes
PS122/5_58-58 Scat-L	10.09.20 11:24	recording end	End of melt pond measurements
PS122/5_58-58 Scat-L	10.09.20 11:44	recording start	Restart of regular scans at RS site after melt pond measurements. Azimuth -45° to 30°; elevation 15° to 45°; delta 3°; sleep 50 minutes
PS122/5_58-58 Scat-L	18.09.20 04:30	recording end	End of measurement at RS site during leg 5. Switching to melt pond for a last measurement cycle there before pulling the instrument in.
PS122/5_58-58 Scat-L	18.09.20 04:42	recording start	Start of measurement at RS melt pond. Azimuth -45° to 30°; elevation 15° to 45°; delta 3°; sleep 5 minutes
PS122/5_58-58 Scat-L	18.09.20 05:44	recording end	End of measurements at RS melt pond and end of measurements during leg 5. Bringing instrument back onboard.

Microwave radiometer HUTRAD

- List of measurement periods in Table 4.12.5
- Three dual-pol frequencies: 6.85 GHz, 10.65 GHz, 18.70 GHz
- Helsinki University of Technology RADiometer (HUTRAD)
- DSHIP/SensorWeb: Microwave Radiometer HUTRAD C-, X-, K-band (HUTRAD)
- Project: ESA MOSAiC remote sensing and ESA CIMRex
- Corresponding satellite observations: upcoming Copernicus CIMR mission, AMSR-E/2/3

The microwave radiometer HUTRAD was operated at the remote sensing site. The instrument consists of three different radiometers measuring in three different frequencies. HUTRAD was mainly turned to the remote sensing site in an angle of -30° to avoid influence by the sled below. During Leg 5 we did melt pond measurements for three times in parallel to L-Scat, Ku/Ka Radar and the IR-Camera. The melt pond was over frozen from the beginning. Several calibrations were performed. Regular sky measurements at multiple elevation angles were performed for later calibration of HUTRAD data and computation of brightness temperatures. The calibration documentation can be found in the MCS folder. The actions are listed in Table 4.12.5.

Fig. 4.12.6: HUTRAD three frequency microwave radiometer. (photo: Gunnar Spreen)

Tab. 4.12.5: List of measurement periods of HUTRAD microwave radiometer.

Activity - Device Operation	*Timestamp*	*Action*	*Comment*
PS122/5_58-50 HUTRAD	2020-08-23 15:24:47	recording start	45° down-looking position to avoid snow accumulations at the radiometer; Time offset: +52 minutes 10 seconds
PS122/5_58-50	2020-08-24 07:22:39	recording end	Power outage due to crack
PS122/5_58-50	2020-08-25 06:00:00	information	No power until 25.08.2020 about 6:00 UTC due to Lead event.
PS122/5_58-50	2020-08-25 06:07:10	recording start	Restart after power outage
PS122/5_58-50	2020-08-25 12:45:00	calibration	Warm target/absorber; cold reference/angle variation

PS122/5_58-50	2020-09-01 04:24:00	information	Time correction: 52 minutes back
PS122/5_58-50	2020-09-01 04:33:00	calibration	Warm target/absorber; cold reference/angle variation
PS122/5_58-50	2020-09-04 08:47:00	information	Melt pond measurement until 10:19 UTC.
PS122/5_58-50	2020-09-05 05:17:00	calibration	Warm target/absorber; cold reference/angle variation
PS122/5_58-50	2020-09-09 11:35:00	calibration	Warm target/absorber; cold reference/angle variation
PS122/5_58-50	2020-09-10 08:50:00	information	Melt pond measurement from 09:00 to 11:30 UTC
PS122/5_58-50	2020-09-12 10:30:00	calibration	Warm target/absorber; cold reference/angle variation
PS122/5_58-50	2020-09-15 04:30:00	information	De-icing and moving from 04:30 to 4:35 UTC and from 05:05 to 05:17 UTC.
PS122/5_58-50	2020-09-15 05:18:00	information	Melt pond measurement from 05:18 to 06:08 UTC.
PS122/5_58-50	2020-09-18 04:46:00	information	Melt pond measurements from 04:48 to 06:11 UTC.
PS122/5_58-50	2020-09-19 04:35:25	recording end	End of measurement Leg 5.

Microwave radiometer ELBARA

- List of measurement periods in Table 4.12.6
- L-band (1.4 GHz)
- Swiss Federal Institute WSL
- DSHIP/SensorWeb: Microwave Radiometer ELBARA L-band (ELBARA)
- Project: ESA MOSAiC remote sensing
- Corresponding satellite observations: SMOS, SMAP, Aquarius

ELBARA was also positioned at the remote sensing and operated continuously at a constant incidence of 50°. Three calibrations were performed. The H-polarisation antenna was broken since Leg 3. There was no deployment of ELBARA during Leg 4. The broken polarisation could not be fixed during this Leg 5, because the spare part was not findable. We did one direct comparison measurement with the mobile Balamis Microwave Radiometer Ariel at the remote sensing site because both instruments measure at the same frequency. During the measurement period there was some snow accumulation in front of the sled which caused a relatively high snow cover compared to the rest of the remote sensing site.

More details can be found in the PS122/1, 2, and 3 cruise reports.

Fig. 4.12.7: ELBARA L-band microwave radiometer (photo: Gunnar Spreen)

Tab. 4.12.6: List of measurement periods of the ELBARA microwave radiometer.

Activity - Device Operation	*Timestamp*	*Action*	*Comment*
PS122/5_58-63 ELBARA	2020-08-29 09:52:00	calibration	Calibration from -50° to 80° in 10° steps. Running ./data_acquisition.sh at each step. From 09:52 UTC until 10:25 UTC. Data files have wrong time stamp by +1 hour.
PS122/5_58-63 ELBARA	2020-08-29 10:26:00	recording start	Start recording at -50° at 12:25 UTC Time correction at 12:15 UTC
PS122/5_58-63 ELBARA	2020-09-09 09:55:00	calibration	start 09:57 UTC; data_acquisition_sky_nomo.sh at +40°; MW absorber with data_acquisition_nomo.sh; angle dependent calibration from -50° to +80° with data_acquisition_nomo.sh; back to -50° at 10:22 UTC
PS122/5_58-63 ELBARA	2020-09-16 04:25:00	calibration	start with absorber target at 04:26 UTC (data_acquisition_nomo.sh); angle dependent measurement from -50° to +80° (./data_acquisition_nomo.sh); sky calibration at +40° at 04:42 UTC (./data_acquisition_sky_nomo.sh)
PS122/5_58-63 ELBARA	2020-09-16 04:43:00	recording end	End of measurements

SSMI microwave radiometer 19-37-89-GHz

- List of measurement periods in Table 4.12.7
- Dual-polarization microwave radiometers
- 19 GHz, 1 GHz bandpass, 0.04 K sensitivity for 1 second delta T, direct detection (AC1900)
- 89 GHz, 4 GHz bandpass, 0.08 K sensitivity for 1 second delta T, double-sideband downconvert (AC8900)
- The 37 GHz channel was broken
- Manufacturer: Radiometrics Corporation

- Kipp & Zonen 2AP positioner
- DSHIP/SensorWeb: Microwave Radiometer 19, 37, 89 GHz (SSMI type) (SSMI_radiometer_SN002)
- University of Manitoba
- Projects: U Manitoba internal and NERC MOSAiC funding
- Corresponding satellite observations: AMSR-E/2, SSM/I, SSMIS, CIMR, MWR

The SSMI radiometer was mainly operated in continuous scanning mode with a typical incidence angle range of 40° to 70° in 5° steps. In addition to the three radiometers a visual camera obtains pictures of the observed surface in regular time intervals. One calibration was performed during leg 5 using the two microwave absorber targets. The 37 GHz frequency channels were broken since leg 3 and measurements were only performed at 19 ang 89 GHz. More details can be found in the PS122/1, 2, and 3 cruise reports.

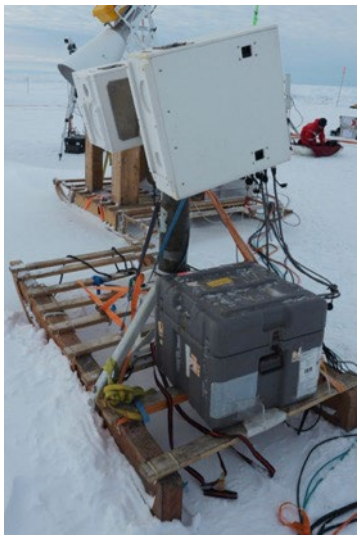

Fig. 4.12.8: SSMI microwave radiometer 19-37-89-GHz (photo: Gunnar Spreen)

Tab. 4.12.7: List of measurement periods of the SSMI microwave radiometer 19-37-89-GHz.

Activity - Device Operation	*Timestamp*	*Action*	*Comment*
PS122/5_58-86 SSMI_radiometer_SN002	08.09.20 06:08	recording start	Start continuously scanning at RS site. Elevation from 40° to 120° in 5° steps.
PS122/5_58-86 SSMI_radiometer_SN002	09.09.20 10:29	recording end	Stopped recording for calibration
PS122/5_58-86 SSMI_radiometer_SN002	09.09.20 10:41	calibration	Calibration 19 GHz with low frequency absorber; Elevation 0°; Temperature absorber: -3.6°C; 10:41:15 to 10:43:15
PS122/5_58-86 SSMI_radiometer_SN002	09.09.20 10:46	calibration	Calibration 89 GHz with MT24 high frequency absorber. Elevation 0°; Temperature absorber: -3.4°C; 10:46:35 to 10:48:35
PS122/5_58-86 SSMI_radiometer_SN002	09.09.20 10:53	calibration	Sky calibration 120° to 180° elevation; end 11:00

PS122/5_58-86 SSMI_radiometer_SN002	09.09.20 11:13	recording start	Start of scan with elevation 40° to 60° and delta=5°.
PS122/5_58-86 SSMI_radiometer_SN002	12.09.20 09:42	recording end	End of scan for data download.
PS122/5_58-86 SSMI_radiometer_SN002	12.09.20 09:53	recording start	Start of measurements with constant elevation angle of 55°. Was planned as scan measurement. Not clear why scan did not start.
PS122/5_58-86 SSMI_radiometer_SN002	15.09.20 08:15	recording end	Recording stopped. Could be due to power outage but not clear.
PS122/5_58-86 SSMI_radiometer_SN002	15.09.20 08:27	recording start	restart scan after power outage. Elevation 40° to 70°; delta 5°
PS122/5_58-86 SSMI_radiometer_SN002	16.09.20 08:48	recording end	End of recording due to power outage.
PS122/5_58-86 SSMI_radiometer_SN002	16.09.20 12:13	recording start	restart scan measurements 40° to 70° after power outage.
PS122/5_58-86 SSMI_radiometer_SN002	18.09.20 04:20	recording end	End of measurements during MOSAiC leg 5. For unknown reasons no photos were recorded. Radiometer data looks okay.

Microwave radiometer Balamis ARIEL

- List of stationary lead and melt pond measurements, and calibrations in Table 4.12.8 and for transects in Table 4.12.9
- L-band (1.413 GHz), dual-polarisation (H+V)
- Bandwidth 20 MHz, 0.7 K radiometric accuracy at 1 Hz
- Beamwidth (FOV): 36.1º x 56.3º
- Radiometer inclination on frame: 41.3°
- Manufacturer: Balamis
- Operated on a sledge to be pulled along transects; sledge parked at remote sensing site
- Institut de Ciències del Mar - CSIC
- DSHIP/SensorWeb: BALAMIS_Radiometer (BALAMIS_Rad)
- Project: “Improving emission models for sea ice low-frequency microwaves” supported by Spanish MOSAiC funding (MINECO)
- Corresponding satellite observations: SMOS, SMAP, Aquarius

More details about ARIEL can be found in the PS122/1 and PS122/2 cruise reports.

The Balamis ARIEL radiometer was operated several times looking at the lead near the remote sensing site formed in the beginning of Leg 5. Also the melt pond experiment at the remote sensing site was part of the measurements. We also did a parallel measurement with ELBARA with a similar field of view at the remote sensing site since they are measuring in the same frequency. We did several transects in the CO, as well transects during the ice stations on our transit back. During transect work several stops were made during the transects to avoid noise from the movement. The (main) RS transect had 10 stops (see Figure 4.12.1 for transect location). These stops are marked with time and supported by a

picture of the FOV and surface description. The transects line was also covered by the GEM2 and Magna-Probe, as well as snow and surface properties measurements. On regular basis, absorber and sky calibrations were performed. We lowered the internal temperature to 20°C to have longer power supply by the battery. For the ice station the internal temperature had to be increased to 25°C to get stabilized.

We positioned Ariel a lot of times at the lead to observe thin ice growth. The evolution of the ice in the lead was rather complex due to dynamics, melting and wind open up parts of the thin ice cover or pushing thicker ice in the footprint. There was most of the time some variation of ice types within the footprint.

The ice thickness, especially during the first two ice station, were on average below one meter which is very interesting for the L-band signal which is sensitive for the smaller ice thickness. The ice station transect was covered additionally by the IR-Camera, surface temperature measurements, thickness measurements, salinity measurements, snow and surface measurements, and the Flux sled from the atmospheric team.

For the further information about the other transect activities see also in Section 4.4 and snow in Section 4.2.

Fig. 4.12.9: Balamis ARIEL microwave radiometer (photo: Gunnar Spreen)

Tab. 4.12.8: List of stationary lead and melt pond measurements, and calibrations of the Balamis microwave radiometer ARIEL.

Activity - Device Operation	*Timestamp*	*Action*	*Comments*
PS122/5_59-246 BALAMIS_Rad	2020-08-22 08:51:00	calibration	
PS122/5_59-500 BALAMIS_Rad	2020-08-22 11:29:39	recording start	RS site
PS122/5_59-501 BALAMIS_Rad	2020-08-22 13:50:08	recording start	melt pond
PS122/5_59-248 BALAMIS_Rad	2020-08-23 08:58:00	recording start	melt pond
PS122/5_59-499 BALAMIS_Rad	2020-08-23 11:51:08	recording start	RS site

PS122/5_59-253 BALAMIS_Rad	2020-08-24 13:47:00	recording start	RS site
PS122/5_59-270 BALAMIS_Rad	2020-08-25 06:36:00	recording start	melt pond
PS122/5_59-271 BALAMIS_Rad	2020-08-25 09:47:00	recording start	lead
PS122/5_59-288 BALAMIS_Rad	2020-08-26 05:27:00	recording start	Lead-
PS122/5_59-324 BALAMIS_Rad	2020-08-27 09:32:00	calibration	
PS122/5_59-503 BALAMIS_Rad	2020-08-27 09:47:00	recording start	lead
PS122/5_59-339 BALAMIS_Rad	2020-08-28 05:09:00	recording start	lead
PS122/5_59-362 BALAMIS_Rad	2020-08-29 08:18:00	recording start	lead
PS122/5_59-377 BALAMIS_Rad	2020-08-30 10:16:00	calibration	
PS122/5_59-378 BALAMIS_Rad	2020-08-30 10:47:00	recording start	lead
PS122/5_60-8 BALAMIS_Rad	2020-08-31 10:07:00	recording start	lead
PS122/5_60-12 BALAMIS_Rad	2020-08-31 12:08:00	calibration	
PS122/5_60-13 BALAMIS_Rad	2020-08-31 12:25:00	recording start	lead
PS122/5_60-27 BALAMIS_Rad	2020-09-01 05:40:00	recording start	lead
PS122/5_60-44 BALAMIS_Rad	2020-09-02 05:16:00	recording start	lead
PS122/5_60-297 BALAMIS_Rad	2020-09-03 05:32:07	calibration	
PS122/5_60-114 BALAMIS_Rad	2020-09-03 05:55:00	recording start	lead
PS122/5_60-115 BALAMIS_Rad	2020-09-04 10:12:00	recording start	lead
PS122/5_60-138 BALAMIS_Rad	2020-09-05 10:54:00	calibration	
PS122/5_60-139 BALAMIS_Rad	2020-09-05 11:25:00	recording start	melt pond
PS122/5_61-59 BALAMIS_Rad	2020-09-07 12:06:00	recording start	melt pond
PS122/5_61-60 BALAMIS_Rad	2020-09-08 05:55:00	recording start	melt pond
PS122/5_61-143 BALAMIS_Rad	2020-09-09 08:48:00	calibration	

PS122/5_61-144 BALAMIS_Rad	2020-09-09 09:05:00	recording start	lead
PS122/5_61-146 BALAMIS_Rad	2020-09-10 05:25:00	calibration	
PS122/5_61-150 BALAMIS_Rad	2020-09-10 06:28:00	recording start	lead
PS122/5_61-151 BALAMIS_Rad	2020-09-10 10:13:00	recording start	melt p-ond
PS122/5_61-152 BALAMIS_Rad	2020-09-10 11:23:00	recording start	lead
PS122/5_61-199 BALAMIS_Rad	2020-09-12 09:03:52	recording start	lead
PS122/5_62-286 BALAMIS_Rad	2020-09-14 11:08:28	calibration	
PS122/5_62-19 BALAMIS_Rad	2020-09-14 11:21:45	recording start	lead
PS122/5_62-62 BALAMIS_Rad	2020-09-15 04:15:56	recording start	RS site, ELBARA comparison
PS122/5_62-64 BALAMIS_Rad	2020-09-15 08:35:00	recording start	lead
PS122/5_62-87 BALAMIS_Rad	2020-09-16 04:17:10	recording start	lead
PS122/5_62-287 BALAMIS_Rad	2020-09-17 05:51:34	calibration	
PS122/5_62-105 BALAMIS_Rad	2020-09-17 06:08:00	recording start	lead
PS122/5_62-115 BALAMIS_Rad	2020-09-17 09:05:10	recording start	lead
PS122/5_62-122 BALAMIS_Rad	2020-09-18 05:05:16	recording start	lead
PS122/5_62-152 BALAMIS_Rad	2020-09-19 05:52:01	recording start	lead
PS122/5_62-153 BALAMIS_Rad	2020-09-19 08:51:33	calibration	

Tab. 4.12.9: List of transects with the Balamis microwave radiometer Ariel.

Activity - Device Operation	*Timestamp*	*Transect name*	*Additional transect sensors*
PS122/5_59-378 BALAMIS_Rad	2020-08-30 10:47:00	RS transect	GEM-2, Magna-Probe
PS122/5_60-9 BALAMIS_Rad	2020-08-31 11:07:00	RS transect	N/A
PS122/5_60-79 BALAMIS_Rad	2020-09-03 04:36:00	RS transect	GEM-2, Magna-Probe

PS122/5_61-57 BALAMIS_Rad	2020-09-07 10:44:00	Radar transect	GEM-2, Magna-Probe, Ku/Ka-Radar
PS122/5_61-58 BALAMIS_Rad	2020-09-07 11:14:00	RS transect	GEM-2, Magna-Probe
PS122/5_61-145 BALAMIS_Rad	2020-09-10 04:36:00	Radar transect	GEM-2, Magna-Probe, Ku/Ka-Radar
PS122/5_61-147 BALAMIS_Rad	2020-09-10 06:04:00	RS transect	GEM-2, Magna-Probe
PS122/5_62-13 BALAMIS_Rad	2020-09-14 09:58:21	Radar transect	N/A
PS122/5_62-14 BALAMIS_Rad	2020-09-14 10:19:00	RS transect	Magna-Probe
PS122/5_62-104 BALAMIS_Rad	2020-09-17 04:30:43	RS transect	GEM-2, Magna-Probe
PS122/5_62-114 BALAMIS_Rad	2020-09-17 08:47:11	Radar transect	GEM-2, Magna-Probe, Ku/Ka-Radar
PS122/5_63-38 BALAMIS_Rad	2020-09-24 06:42:00	Ice Station 1: short transect	GEM-2, Magna-Probe, IR_Variocam_01, AARI Thermometer
PS122/5_63-70 BALAMIS_Rad	2020-09-26 06:30:53	Ice Station 2: short transect	GEM-2, Magna-Probe, IR_Variocam_01, AARI Thermometer
PS122/5_63-242 BALAMIS_Rad	2020-09-30 09:31:00	Ice Station 3: short transect	GEM-2, Magna-Probe, IR_Variocam_01, AARI Thermometer

Microwave radiometer EMIRAD2 (ONBOARD)

- Picture in Figure 4.12.3
- Location: upper Peil deck, port side
- L-band (1.400–1427 GHz)
- Full polarimetric
- Retrieved geophysical variables: ice thickness up to 1 m
- Technical University of Denmark
- DSHIP/SensorWeb: Microwave Radiometer L-band EMIRAD2 (EMIRAD2)
- Project: ESA MOSAiC remote sensing
- Corresponding satellite observations: SMOS, SMAP, Aquarius
- Output: Calibrated microwave brightness temperature data at L-band frequency

More details can be found in the PS122/1 and PS122/2 cruise reports.

EMIRAD was operated continuously at 45° incidence angle during the whole leg and will run until the end of leg 5 under the device operation PS122/5_58-5. The sky calibration at 150° was performed two to three times per week (21 in total). There are no or incomplete data from Sep 10 to Sep 14 due to unknown reasons. The data recording started again without further action. There are no data between Oct 02 04:00 UTC and Oct 04 17:00 UTC since *Polarstern*

was in the Svalbard area. For the observation of the footprint, pictures were taken during the calibration. For a more detailed coverage a GoPro time laps with 60 s frequency was done between Aug 30 and Oct 01. On Oct 01 we were out of the ice and in open water only. During the stay at the floe, the footprint was often open water only since there was a lead on port side.

GNSS reflectometry on ice

- List of measurement periods in Table 4.12.10-
- DSHIP/SensorWeb: GNSS Reflectometry equipment on MOSAiC Sea Ice Floe (GNSS-R_IceFloe)
- Sub-device: GNSS Reflectometer at dual linear polarizations on MOSAiC sea ice floe (GNSS-R_LinPol)
- Sub-device: GNSS Reflectometry receiver on the sea ice floe at two circular polarizations (GNSS-R_CircPol)
- Instituto de Ciencias del Espacio (ICE-CSIC/IEEC) and Universitat Politecnica de Catalunya (UPC)
- Project: ESA MOSAiC remote sensing (ESA FSSCat Validation in MOSAiC)
- Corresponding satellite observations: ESA FSSCat, UK TDS-1, future: ESA PRETTY, China FY-3E and Taiwan FS-7R

More details can be found in the PS122/1 and PS122/2 cruise reports.

The three GNSS antennas are installed on a tripod and a wooden pallet for more stability. Before the power line setup the instrument was powered by batteries. In between there were some interruptions due to unknown reasons. Icing of the instruments happened from time to time. It might have to be taken into account for the data analysis. During the setup of the instrument we found water in the down-looking antenna. After drying of the antenna we sealed the possible leaks. The antenna distances above ground were: down-looking (30 cm), horizontal (153 cm) and upper (201 cm).

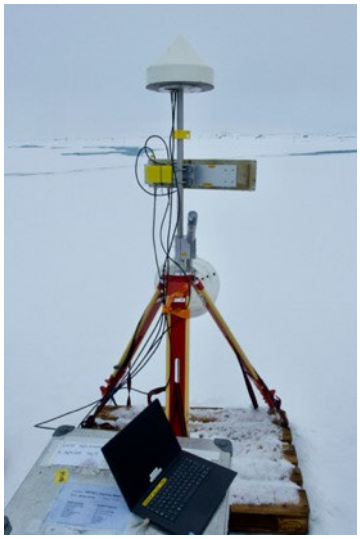

Fig. 4.12.10: GNSS reflectometry instrument (photo: Gunnar Spreen)

Tab. 4.12.10: List of measurement periods of the GNSS-R on ice instrument.

Activity - Device Operation	*Timestamp*	*Action*	*Comment*

PS122/5_58-49 GNSS-R_IceFloe	2020-08-22 14:00:00	recording start	not exact time stamp
PS122/5_58-49 GNSS-R_IceFloe	2020-08-23 08:40:00	information	Battery exchange: Interruption for some minutes. (no power connection yet)
PS122/5_58-49 GNSS-R_IceFloe	2020-08-24 13:30:00	information	Battery exchange
PS122/5_58-49 GNSS-R_IceFloe	2020-09-01 05:25:00	information	Antenna cleaning from snow and ice
PS122/5_58-49 GNSS-R_IceFloe	2020-09-05 04:43:00	information	De-icing until 5:00 UTC Movement because of mooring the instrument from 11:10 to 11:20 UTC.
PS122/5_58-49 GNSS-R_IceFloe	2020-09-12 08:54:24	information	End of data in MCS (still on GNSS-R computer)
PS122/5_58-49 GNSS-R_IceFloe	2020-09-12 09:08:00	information	De-icing from 09:08 to 09:12 UTC. restart from linear, stopped recording on Sep 04 for unknown reasons
PS122/5_58-49 GNSS-R_IceFloe	2020-09-16 12:00:00	recording end	End of measurements

GNSS atmosphere and sea ice reflectrometry (ONBOARD)

- Picture in Figure 4.12.3
- List of measurement periods in Table 4.12.11
- Location: upper Peil deck, port side
- Retrieved geophysical variables: atmospheric water vapour, sea ice properties like thin ice thickness
- Helmholtz Centre Potsdam GFZ, German Research Centre for Geosciences
- DSHIP/SensorWeb:
- GNSS-receiver for multi-GNSS observations (GNSS-receiver-TINY)
- GNSS-receiver for Occultation Reflectometry and Scatterometry measurements (GNSS-receiver-GORS)
- Corresponding satellite observations: ESA FSSCat, UK TDS-1, future: ESA PRETTY, China FY-3E and Taiwan FS-7R

The GNSS system to observe reflected GNSS signals from the snow and ice and measure atmospheric water vapor from GNSS delay is a fully automatic system. No user interaction is needed. Only a regular weekly check if the data is recorded was performed. The system daily sends an email with a data report back to GFZ on land.

Scientific Objectives:

- The refractive delay of GNSS signals can be measured to estimate atmospheric parameters, for example, the atmospheric water vapor content.
- Reflected GNSS signals can be used to sense surface parameters including, for example, water or ice surface heights or the permittivity or amount of sea ice.
- Collect data of GNSS reflections over the Arctic ocean and sea ice. Delay and amplitude of these signals are used to investigate L-band reflectivity and penetration depth for different sea ice conditions. Dependencies on sea ice thickness, conductivity (brine content) and concentration will be in focus.

Output from measurements:

- Precipitable water vapor with accuracy of about 1 mm
- Reflected GNSS data from the sea ice

Tab. 4.12.11: List of measurement periods of the onboard atmosphere and sea ice GNSS.

Activity - Device Operation	*Timestamp*	*Action*	*Comment*
PS122/5_58-129 GNSS-receiver-GORS	12.08.20 10:00	information	Continuation of measurements during leg 5.
PS122/5_58-128 GNSS-receiver-TINY	12.08.20 10:00	information	Continuation of measurements during leg 5.
PS122/5_58-129 GNSS-receiver-GORS	02.10.20 04:00	recording end	Stop of all measurements when entering Svalbard area.
PS122/5_58-128 GNSS-receiver-TINY	02.10.20 04:00	recording end	Stop of all measurements when entering Svalbard area.

GNSS ionospheric scintillation (ONBOARD)

- Picture in Figure 4.12.3
- List of measurement periods in Table 4.12.12
- Location antenna: lower Peil deck, port side
- Location processing unit: observation alley, in front of meteorologist's office
- Global Satellite Navigation Systems (GNSS) recording
- DLR, Germany
- DSHIP/SensorWeb:
- GNSS_NTlab_FE (GNSS_NTlab_FE)
- GNSS_JAVADd3 (GNSS_JAVADd3)

The GNSS ionospheric scintillation installation is an autonomous instrument that does not require operator interaction. The operation and data acquisition were checked on a weekly basis. The system daily sends an email with a data report back to DLR on land.

Scientific Objectives:

- Different distortions can severely degrade the GNSS accuracy and availability. One of these distortions are ionospheric scintillations, which occur mainly in equatorial and polar regions.
- The goal of this research is to record pre- and post-correlation samples of polar ionospheric scintillations to evaluate the impact of scintillations on GNSS and to develop new signal processing algorithms to mitigate scintillation from the received signal.

Tab. 4.12.12: List of measurement periods of the ionospheric scintillation GNSS.

Activity - Device Operation	*Timestamp*	*Action*	*Comment*

PS122/5_58-130 GNSS_JAVADd3	12.08.20 10:00	information	Continuation of measurements from previous legs. All data is stored under the "gnss_javadd3/exdata/" folder.
PS122/5_58-131 GNSS_NTlab_FE	12.08.20 10:00	information	Continuation of measurements from previous legs. All data is stored under the "gnss_ntlab_fe/exdata/" folder.
PS122/5_58-130 GNSS_JAVADd3	02.10.20 04:00	recording end	Stop of all measurements when entering Svalbard area.
PS122/5_58-131 GNSS_NTlab_FE	02.10.20 04:00	recording end	Stop of all measurements when entering Svalbard area.
PS122/5_58-130 GNSS_JAVADd3	04.10.20 17:00	recording start	Started recording again after leaving Svalbard 12nm zone.
PS122/5_58-131 GNSS_NTlab_FE	04.10.20 17:00	recording start	Started recording again after leaving Svalbard 12nm zone.
PS122/5_58-130 GNSS_JAVADd3	10.10.20 12:00	recording end	End of measurements during MOSAiC.
PS122/5_58-131 GNSS_NTlab_FE	10.10.20 12:00	recording end	End of measurements during MOSAiC.

Infrared thermography system and visual camera

- List of measurement periods in Table 4.12.13 and for transect in Table 4.12.14
- VarioCAM HDx head 625
- Manufacturer: Infratec
- 7.5-14 µm, 640x480 pixel
- In addition to the IR camera a visual camera is installed for monitoring purposes
- DSHIP/SensorWeb: Infrared VarioCAM HDx head 625 (IR_VarioCAM_01)
- DSHIP/SensorWeb: Camera VIS_INFRALAN_01 (VIS_INFRALAN_01)
- University of Bremen
- Project: Satellite Remote Sensing – Germany and MOSAiCmicrowaveRS supported by DFG
- Sampling frequency is 5 minutes

More details can be found in the PS122/1 and PS122/2 cruise reports.

The list of actions during Leg 5 can be found in Table 4.12.13. The infrared and visual cameras are installed together on one tripod, which is accompanied by one Peli case with a battery and an ebox PC for operation. Thus, the system is mobile and can be moved to different sites. The IR-Camera was mainly positioned at the remote sensing site. In between we had problems with icing on the lens. The IR-Camera was also positioned at the melt pond during the melt pond experiments to monitor the thermal surface conditions. In the beginning of the Leg, we did a lead observation in parallel to the Balamis Radiometer measurement. On Sep 18, we did an emissivity experiment for a more detailed investigation of the surface energy budget. It was performed at Met City close to the radiation station to have direct comparable data. Additionally, the actual surface temperature was measured on different points which we marked in the images of the IR-Camera. Afterwards we did an angle variation of the IR-Camera to investigate the dependency of emissivity from incidence angle.

During the ice stations the IR-Camera was installed on the sled of the Balamis Radiometer Ariel for measurements along the transect. The transect line for the 'short transect' was done from the ships position to the 3 or 4 o'clock position of the flow which was characterized by a lead with slush or thin ice cover. In parallel to the Radiometer and Camera measurements, the surface temperature was measured. Also, the thickness transect, the Flux Sled by the atmospheric team, and the snow team went along the same transect. The transect actions during the ice station are listed in Table 4.12.14. The description of the surface temperature measurements can be found in Section 4.2.-

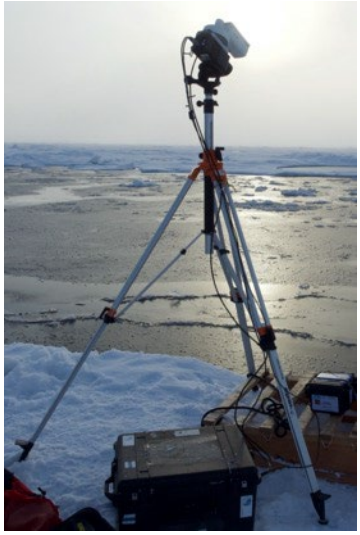

Fig. 4.12.15: Infrared and visual camera systems (photo: Gunnar Spreen)

Tab. 4.12.13: List of measurement periods of the infrared camera system. The measurement periods of the visual camera are similar.

Activity - Device Operation	*Timestamp*	*Action*	*Comment*
PS122/5_58-39 IR_VarioCAM_01	2020-08-22 12:30:00	deployed	Deployment at the remote sensing site; Camera height: 217 cm; Camera angle: 63° (relative to Nadir)
PS122/5_58-39 IR_VarioCAM_01	2020-08-22 13:02:00	recording	RS site; frame rate: 5 minutes
PS122/5_58-39 IR_VarioCAM_01	2020-08-22 14:27:00	information	Turned to melt pond
PS122/5_58-39 IR_VarioCAM_01	2020-08-24 13:37:00	information	Turned to RS site; no GPS data
PS122/5_58-39 IR_VarioCAM_01	2020-08-24 13:49:00	information	angle change to 74° relative to Nadir
PS122/5_58-39 IR_VarioCAM_01	2020-08-25 05:52:00	information	Stopped recording for GPS exchange. At 06:02 UTC start of new recording.
PS122/5_58-39 IR_VarioCAM_01	2020-08-25 10:16:00	information	Lead event observation; height: 220 cm +- 5cm (to lead surface); angle: 62° relative to Nadir.
PS122/5_58-39 IR_VarioCAM_01	2020-08-26 20:10:00	recording end	out pf power at lead in the evening

PS122/5_58-39 IR_VarioCAM_01	2020-08-28 05:19:50	recording start	Restart of Camera at the remote sensing site with view to the remote sensing site at 5:20 UTC
PS122/5_58-39 IR_VarioCAM_01	2020-09-04 09:00:00	information	height: 230 cm; angle: 61° relative to Nadir
PS122/5_58-39 IR_VarioCAM_01	2020-09-08 05:11:00	information	Repositioning at remote sensing site; increased Camera angle to 72.6° so the sky is part of the image
PS122/5_58-39 IR_VarioCAM_01	2020-09-09 19:27:00	recording end	Out of power
PS122/5_58-39 IR_VarioCAM_01	2020-09-10 05:47:39	recording start	Restart of camera after power failure. Lens has icing.
PS122/5_58-39 IR_VarioCAM_01	2020-09-10 08:29:00	information	Icing on lens removed
PS122/5_58-39 IR_VarioCAM_01	2020-09-10 09:10:00	information	Moved to melt pond (parallel with other instruments)
PS122/5_58-39 IR_VarioCAM_01	2020-09-10 11:59:00	information	Back to RS site
PS122/5_58-39 IR_VarioCAM_01	2020-09-15 05:22:00	information	Moved IR cam to melt pond at RS site. 05:25 start of MP measurements 06:15 end of MP measurements moved back to RS site
PS122/5_58-39 IR_VarioCAM_01	2020-09-18 09:05:26	recording end	no data recording; unknown reason
PS122/5_62-270 IR_VarioCAM_01	2020-09-18 08:15:00	station start	Emissivity experiment at Met City
PS122/5_62-270 IR_VarioCAM_01	2020-09-18 10:15:00	station end	Emissivity experiment at Met City

Tab. 4.12.14: List of transects with IR-Camera during the ice stations

Activity - Device Operation	*Timestamp*	*Action*	*Comment*
PS122-5_63-50 IR_VarioCAM_01	2020-09-24 06:20:29	Ice Station 1: short transect	GEM-2, Magna-Probe, Balamis Radiometer, AARI thermometer
PS122-5_63-71 IR_VarioCAM_01	2020-09-26 06:14:00	Ice Station 2: short transect	GEM-2, Magna-Probe, Balamis Radiometer, AARI thermometer
PS122-5_63-243 IR_VarioCAM_01	2020-09-30 09:30:00	Ice Station 3: short transect	GEM-2, Magna-Probe, Balamis Radiometer, AARI thermometer

Supporting snow and ice measurements

The measurements listed in Table 4.12.1 will be combined with detailed measurements of the snow and ice thickness and water salinity and temperature at our measurement sites. From the snow task (Section 4.2) snow pits and snow transects were done at the remote sensing site and also for the RS transect and Radar transect (Balamis ARIEL radiometer, Ku/Ka-band radar). In addition, the GEM-2 ice thickness and Magna-Probe snow depth transects covered most times the remote sensing transects. For continues ice and snow thickness measurements a DTC thermistor chain (Section 4.3) was deployed at the remote sensing site (see Figure 4.12.1). At the start as well as in the end of the leg, ice thickness measurements were

performed at the remote sensing site (see Table 4.12.15). Additional measurements were performed at the remote sensing melt pond to support the melt pond experiment (see Table 4.12.16) and at the lead complementary to the Balamis radiometer measurements (see Table 4.12.17). More additional measurements were done: During the ice station short transect at each stop snow and ice thickness, and at some stops water salinity and temperature measurements taken and listed in Table 4.12.18. When there was slush on the ice during our ice station transects, also slush samples were taken for salinity measurement.

Many measurements from the ICE and other teams are relevant for interpreting the RS measurements. Here a none exclusive list of supplementary measurements:

Important supplementary measurements for the remote sensing program

- Meteorological data acquired on the ship and at MET city (Chapter 3)
- Helicopter (Section 4.11): laser scanning, visual and hyperspectral imaging for characterizing the snow, ridge, lead, melt pond, and thin ice distributions of the CO and for regional upscaling.
- Terrestrial laser scanning (Section 4.2): snow distribution and redistribution by wind for the RS sites and CO
- Snow (Section 4.2): surface scattering layer properties, snow depth, density, grain size, moisture, salinity, snow structure CT
- Ice cores (Section 4.5): density & salinity profiles; thick sections, and CT for air bubble, brine channel distributions and ice structure
- Autonomous observation in the CO and DN (Section 4.3): snow and IMB buoys, and DTC thermistor chains (CO)
- Ice dynamics (Section 4.6): position data from all buoys of the distributed network; ship radar; ice strength

Tab. 4.12.15: List of additional ice measurements at remote sensing site

Activity - Device Operation	*Timestamp*	*Station name*	*Co-deployments*
PS122/5_59-497 ice_gauge	22.08.2020 11:45	deployed	at remote sensing site, close to instruments
PS122/5_59-498 ice_gauge	24.08.2020 14:00	deployed	at remote sensing site, close to instruments
PS122/5_62-285 ice_gauge	19.09.2020 11:40	deployed	in the middle of the remote sensing site, after camp take down

Tab. 4.12.16: List of additional snow and ice measurements of melt pond at remote sensing site

Activity - Device Operation	*Timestamp*	*Action*	*Co-deployments*
PS122/5_59-490 ice_gauge	2020-08-23 09:00:00	deployed	sali_ubremen_1
PS122/5_59-491 ice_gauge	2020-08-24 09:00:00	deployed	sali_ubremen_1
PS122/5_60-288 ice_gauge	2020-09-04 09:00:00	deployed	snow-stick

PS122/5_60-289 ice_gauge	2020-09-05 09:00:00	deployed	snow-stick
PS122/5_61-326 ice_gauge	2020-09-10 09:00:00	deployed	snow-stick
PS122/5_62-279 ice_gauge	2020-09-15 09:00:00	deployed	snow-stick; sali_ubremen_1
PS122/5_62-280 ice_gauge	2020-09-19 09:00:00	deployed	snow-stick; sali_ubremen_1

Tab. 4.12.17: List of additional snow and ice measurements in lead near remote sensing

Activity - Device Operation	*Timestamp*	*Action*	*Co-deployments*
PS122/5_60-287 ice_gauge	2020-09-05 09:00:00	deployed	snow-stick
PS122/5_61-324 ice_gauge	2020-09-09 09:00:00	deployed	snow-stick; sali_ubremen_1
PS122/5_61-325 ice_gauge	2020-09-10 09:00:00	deployed	snow-stick; sali_ubremen_1
PS122/5_62-276 ice_gauge	2020-09-15 05:45:00	deployed	snow-stick; sali_ubremen_1
PS122/5_62-277 ice_gauge	2020-09-17 09:00:00	deployed	snow-stick; sali_ubremen_1
PS122/5_62-278 ice_gauge	2020-09-19 09:00:00	deployed	snow-stick; sali_ubremen_1

Tab. 4.12.18: List of additional snow and ice measurements taken during the ice station

Activity - Device Operation	*Timestamp*	*Station name*	*Co-deployments*
PS122/5_63-124 ice_gauge	2020-09-24 06:43:00	Ice station 1	snow-stick, sali_ubremen_1
PS122/5_63-133 ice_gauge	2020-09-26 06:31:00	Ice station 2	snow-stick, sali_ubremen_1
PS122/5_63-247 ice_gauge	2020-09-30 09:30:00	Ice station 3	snow-stick, sali_ubremen_1

Preliminary (expected) results

All RS instruments (Table 4.12.1) are providing a time series of the temporal development of their measured parameters during the one-month MOSAiC leg 5 ice floe visit, i.e., microwave brightness temperature and backscatter at different frequencies, reflected GNSS signals, infrared temperatures and visual images. Their variability and changes will depend on the atmospheric conditions, e.g., melt and refreeze, and snow accumulation. The combination of on-ice remote sensing measurements together with the comprehensive snow and ice measurements will allow to improve microwave emission and scattering models of snow and ice, which in turn will lead to improved satellite remote sensing datasets.

Data recorded and stored in the MCS during leg 5 are primarily raw, uncalibrated measurements like backscatter power from the radars and voltages from the radiometers. We here show a few exemplary early results.

SSMI Microwave Radiometer 19-37-89-GHz

Figure 4.12.11 shows the uncalibrated microwave brightness temperatures (TB) measured by the SSMI microwave radiometer for the full leg 5 measurement period from 8th to 18th September 2020. TB values are uncalibrated and will change significantly after calibration, even the order of H and V (H should be higher than V) will change. Thus, no quantitative conclusions can be drawn from these time series. The radiometer was scanning between 40° to 70° incidence angle. Here as an example the 55° incidence angle time series is shown together with the air temperatures measured at about 30 m height at the *Polarstern* weather station.

The TBs follow at first order the air temperature development. The 89 GHz more directly and more pronounced, which is likely due to the lower penetration depth at 89 GHz and thus a more direct temperature response. However, during the warm air intrusion and rain on snow event on 13-14 September, TBs at both 19 and 89 GHz change rapidly and much stronger one can expect from the air temperature change alone. This is likely due to a strong change in emissivity caused by the rain on snow even with the following refreezing, which changes the snow properties and surface roughness and thus emissivity strongly.

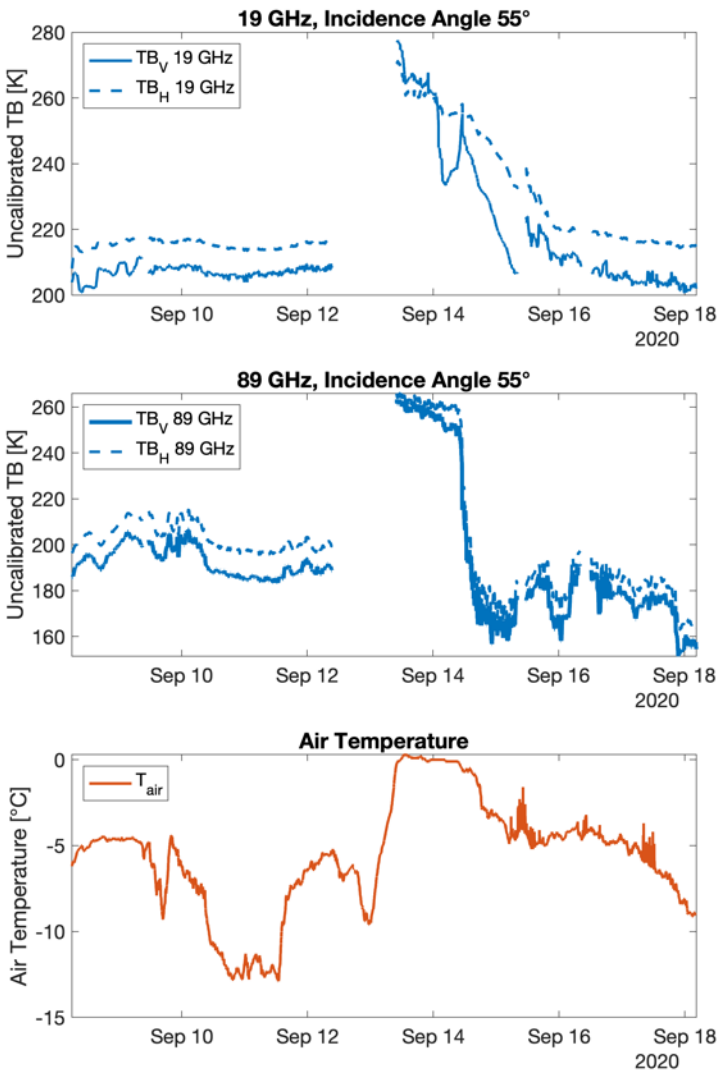

Fig. 4.12.11: Exemplary, uncalibrated microwave brightness temperatures (TB) from the SSMI radiometer for the full leg 5 measurement period from 8th to 18th September 2020. Measurements at 55° incidence angle are shown. TB values are uncalibrated and will change significantly after calibration, even the order of H and V (H should be higher than V) will change. Thus, no quantitative conclusions can be drawn from these plots. Top: time series at 19 GHz V and H. Middle: time series at 89 GHz V and H. Bottom: air temperature from the Polarstern weather station.

HUTRAD microwave radiometer

For HUTRAD the raw data in horizontal and vertical polarization for the 10.65 GHz and 18.70 GHz frequencies is shown in Figure 4.12.12. The 6.85 GHz frequency is left out for simplicity since it shows in both cases similar signals.

Figure 4.12.12 shows the time series from Aug 25 to Aug 27. During this time a warm event happened, which can be seen in the air temperature increasing above 0°C in the early morning of Aug 26. During this warming there is a strong signal, which dampens after some hours. This change in the raw data might be caused by the melting and the wet surface.

In Figure 4.12.13, the time series during one of our melt pond experiment is shown. The melt pond was frozen over and also covered with snow. Before and after the melt pond experiment, HUTRAD was measuring at the remote sensing site. For the duration of the melt pond experiment there is a strong change in the signal, even if both surfaces were defined by solid ice cover and snow on top.

The strong changes in the HUTRAD data can be used to test the sea ice concentration algorithms for these different cases of ice and surface characteristics. It has to be noted that this data are not calibrated yet. Therefore the interpretation is preliminary.

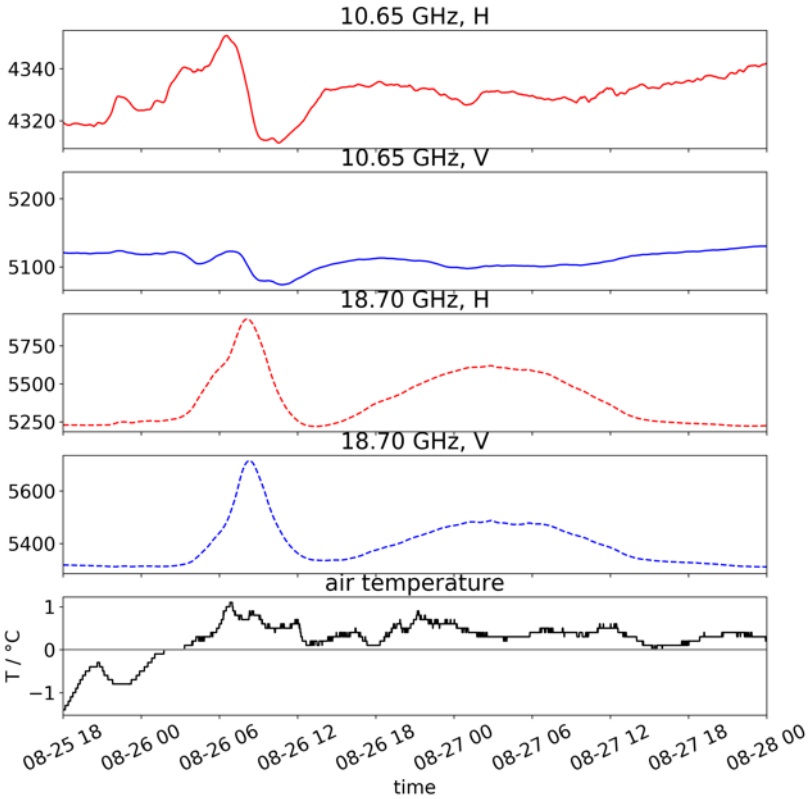

-

Fig. 4.12.12: Time series of HUTRAD raw data for the warm even from Aug 25 to Aug 27. Here average values over 60 seconds with a 20 minutes rolling mean are shown. Two of three frequencies with its horizontal and vertical polarisation are displayed. The 6.85 GHz frequency is left out, but shows similar signal. The last panel shows the air temperature from the Polarstern weather station as indication for the warm event.

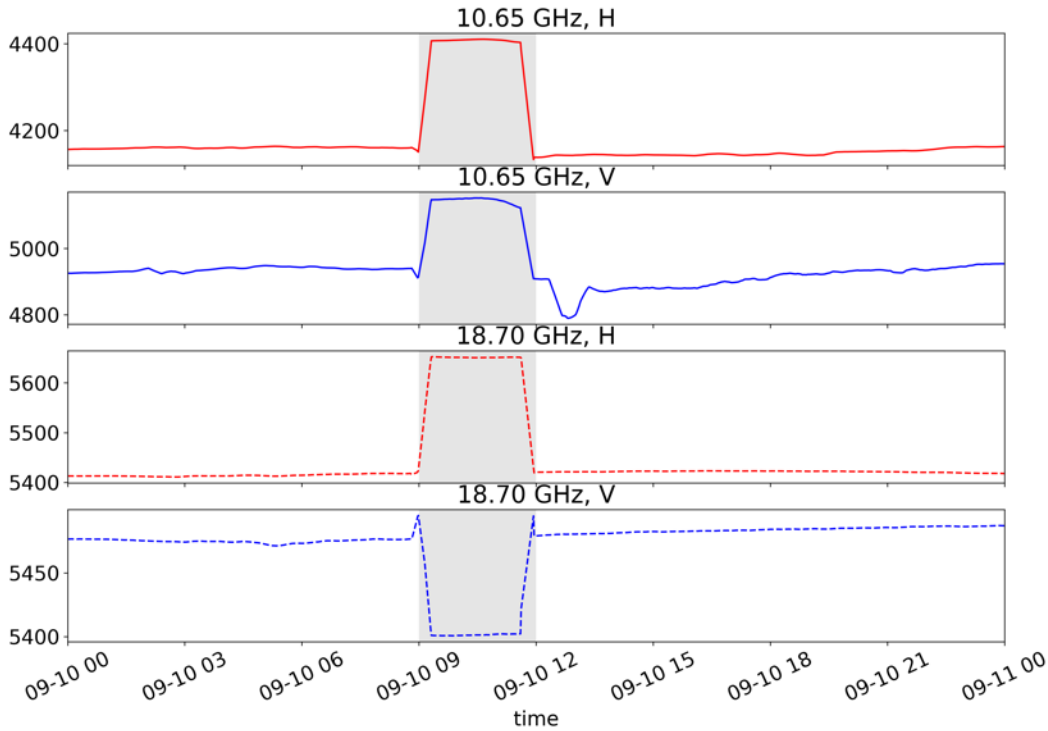

Fig. 4.12.13: Time series of HUTRAD raw data for Sep 10, 2020. Here average values over 60 seconds with a 20 minutes rolling mean are shown. Two of three frequencies with its horizontal and vertical polarisation are displayed. The 6.85 GHz frequency is left out, but shows similar signal. The grey shaded area indicates the duration of the melt pond experiment.

Balamis Microwave Radiometer Ariel

With the Balamis Microwave Radiometer Ariel we covered several times the RS transect in the CO. Along the transect line, 10 stops with different surface characteristics were defined. An example of the processed brightness temperature for both polarizations (horizontal: TBH, vertical: TBV) for two stops is shown in Figure 4.12.14. For a better overview about the surface conditions, pictures of the specific stops are displayed in Figure 4.12.15. This example is from Aug 30 where we had no snow cover. Therefore the ice surface characteristics were very good visible for us (ridged, melt pond, flat and homogeneous or others). Later during the leg this characteristics were not obvious anymore. In Figure 4.12.14, the part between the black and green vertical line shows the stop where there was a darker surface scattering layer than in the surroundings. There might be also an influence by the melt pond surface which depends on the size of the footprint. The next stop (between the blue and yellow line) was at a brighter scattering layer. For the darker surface the brightness temperature is lower, especially in horizontal polarization. In between the stops there is more noise which shows the advantage of the stops to get a characteristic brightness temperature for each stop.

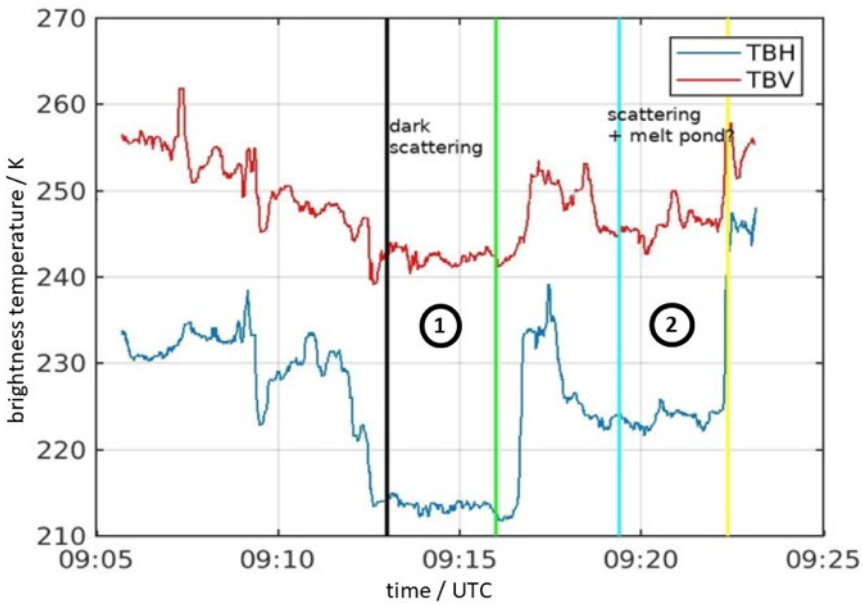

Fig. 4.12.14: Time series of the processed brightness temperature for both polarizations for two different stops during the RS transect on Aug 30 (plot by Carolina Gabarro, here slightly modified).

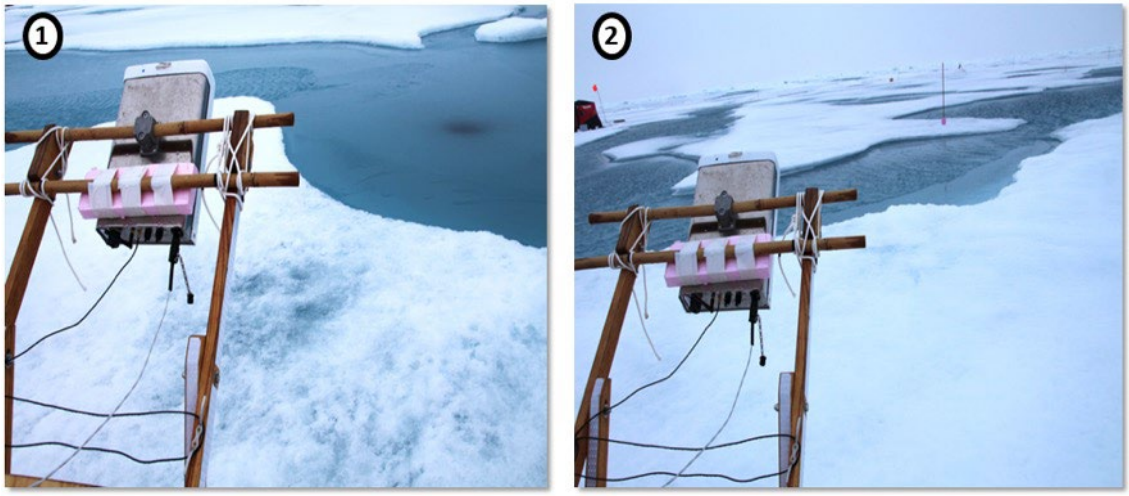

Fig. 4.12.15: Pictures of the footprint of Ariel during the stops as in Figure 4.12.14.

Data management

All data are handled, documented, archived and published following the MOSAiC data policy (see APPENDIX). All final data of all on-ice and onboard remote sensing instruments will be stored at the MOSAiC Central Storage (MCS) and at PANGAEA (World Data Center PANGAEA Data Publisher for Earth & Environmental Science (www.pangaea.de)) after post-processing and quality checks. Storage and release of data follow the MOSAiC data policy.

References

No references